DIRECT NUMERICAL SIMULATION OF TURBULENT CHANNEL FLOW WITH V-SHAPE TURBULATORS

By

Jaime A. Toro Medina

A thesis submitted in partial fulfillment of the requirements for the degree of

MASTER OF SCIENCE

in

THERMAL SCIENCES

UNIVERSITY OF PUERTO RICO
MAYAGÜEZ CAMPUS

May, 2010

Approved by:

Vikram R. Pandya, Ph.D Member, Graduate Committee	Date
Gustavo Gutierez, Ph.D Member, Graduate Committee	Date
Stefano Leonardi, Ph.D President, Graduate Committee	Date
Silvestre Colón, Ph.D Representative of Graduate Studies	Date
Gustavo Gutierez, Ph.D Chairperson of the Department	Date

Abstract of Dissertation Presented to the Graduate School
of the University of Puerto Rico in Partial Fulfillment of the
Requirements for the Degree of Master of Science

DIRECT NUMERICAL SIMULATION OF TURBULENT CHANNEL FLOW WITH V-SHAPE TURBULATORS

By

Jaime A. Toro Medina

May 2010

Chair: Stefano Leonardi
Major Department: Mechanical Engineering

Direct Numerical Simulations (DNS) are carried out to study the channel flow V-shaped roughness on both wall. The roughness is modeled by the immerse boundary method for passive heat transport in a turbulent channel flow with V-shape square ribs for $w/k = 3, 8, 10, 15$ (w being the pitch, k the height of the ribs turbulators) with a $k/h = 0.25, 0.1$ (h being the mid-height of the channel). The angle of inclination of the V-shape turbulators is 45 degrees. Numerical results show that V-shape square ribs are more efficient than square ribs in maximizing the heat transfer. The configuration with $w/k = 3$, $k/h = 0.25$ presents the largest heat flux. The increase in the heat transfer is due to a secondary motion which is generated by the V-shape turbulators. Secondary motions at the location of the sidewalls transport the heat out of the cavity of the turbulators to the crest pane.

Resumen de Disertación Presentado a Escuela Graduada
de la Universidad de Puerto Rico como requisito parcial de los
Requerimientos para el grado de Maestría en Ciencias

SIMULACIONES NUMERICAL DIRECTORS EN EL CANAL DE UN FLUJO TURBULENTO CON SUPERFICIES EXTENDIDAS EN FORMA DE V

Por

Jaime A. Toro Medina

Mayo 2010

Consejero: Stefano Leonardi
Departamento: Ingeniería Mecánica

Simulaciones numericas directas han sido realizadas para estudianr el flujo en un canal con superficies extendidas en forma de V localizadas en ambas paredes. La rugosidad del canal es modelada por medio del método de frontera sumergida para el transporte pasivo de calor en un canal con flujo turbulento con superficies extendiadas cuadradas en forma de V. Los parametros a utilizar son $w/k = 3, 8, 10, 15$ (w es la separación, k es la altura de las superficies extendidas) con variación del parámetro $k/h = 0.25$ (h es la altura media del canal). El ángulo de inclinación de las geometría en forma de V es de 45 grados. Las simulaciones numericas muestran que las superficies extendidas cuadradas en forma de V son más eficientes maximizando la transferencia de calor que las superficies extendidas en forma de cuadrado. La configuración que presenta la más alta transferencia de calor es $w/k = 3$, $k/h = 0.25$. El incremento en la tansferencia de calor es debido a los motivientos secundarios del flujo que son generados por la geometría de las superficies extendidas en forma de V.

This thesis is dedicated to my family which always supports me and motivates me to continue pursuing my dreams. To my girlfriend which was always by my side giving me support, counseling me in hard situations and for her unconditional love.

ACKNOWLEDGMENTS

The author gratefully acknowledge The Puerto Rico NASA Space Grant and Pratt & Witney for granting a research fellowship.I am also grateful for the computational time provided by Tera Grid Texas Advance Computational Center. Thanks to Prof. Stefano Leonardi for being my adviser and providing me the experience to working by his side. I thanks Benjamin Cruz for being my inseparable and all time partner since I started in the University, for being my travel partner in all our adventures around the world and for being a great friend. I thanks Byron Zambrano for all his support, help and being the sparks that brings joy to the laboratory. Thanks to Juan Garcia for his help and support.Thanks to John Lucena for his help implementing new features to the code. Thanks to Amabel Reyes for her help and support. In general I want to talk everybody that in one way or another they provided their help during their research. Specially, I want to thank God for being my best adviser.

TABLE OF CONTENTS

page

ABSTRACT ENGLISH ii

ABSTRACT SPANISH iii

ACKNOWLEDGMENTS vi

LIST OF FIGURES ix

LIST OF ABBREVIATIONS xiii

LIST OF SYMBOLS xiv

1 INTRODUCTION 1

2 JUSTIFICATION 3

3 OBJECTIVE 4

4 LITERATURE REVIEW 5
- 4.0.1 Rough wall 6
- 4.0.2 V-Shape Turbulators 11
- 4.0.3 Wall Structures 13

5 METHODOLOGY 17

6 CHANNEL FLOW 20

7 SQUARE BARS 24

8 V-SHAPED TURBULATORS 29
- 8.1 FLOW CONFIGURATION 29
- 8.2 MEAN FLOW 30
  - 8.2.1 Results 30
  - 8.2.2 Mean Flow 30
- 8.3 FRICTIONAL and FORM DRAG 46
  - 8.3.1 Pressure Upstream 47
  - 8.3.2 Pressure Downstream 49
  - 8.3.3 Skin Friction Drag 50
  - 8.3.4 From Drag 57
  - 8.3.5 Total Drag 59
- 8.4 TURBULENT INTENSITIES 60

8.4.1 Turbulent intensities for $w/k = 3$ . . . 60
8.4.2 Turbulent intensities along the normal direction . . . 62
8.5 MEAN TEMPERATURE . . . 62
8.6 TEMPERATURE FLUCTUATIONS . . . 64
8.7 HEAT TRANSFER . . . 66
8.7.1 Molecular Heat Conduction . . . 67
8.7.2 Turbulent Heat Flux Along the Normal Direction . . . 68
8.7.3 Spanwise Turbulent Heat Flux Along the Normal Direction 74
8.7.4 Nusselt . . . 75
8.8 AUGMENTATION . . . 81

9 CONCLUSION . . . 85

APPENDICES . . . 88

A STATISTICAL CONVERGENCE . . . 89

A.1 Turbulent Heat Flux Convergence for k/h=0.25 . . . 89
A.2 Turbulent Heat Flux Convergence for k/h=0.1 . . . 89

LIST OF FIGURES

Figure page

1–1 Geometrical Configuration of the V-shape Roughness Element 2

2–1 a)Damaged Turbine Blade. b)Turbine Blade Cooling Mechanisms . . 3

4–1 Schematic of modern gas turbine blade with common cooling techniques. 6

5–1 Geometrical sketch of immersed boundary method. Arrows, velocity vectors as defined in a staggered grid $(- - -)$; , points inside the roughness element; , points nearest to the boundary of the roughness element. The solid line delineates part of the roughness element. 18

6–1 a) Mean streamwise velocity along the wall normal direction. b)Root mean square of the three velocity components 21

6–2 Horizontal view of color contour of velocity fluctuations along the streamwise direction. 22

6–3 Side view of color contour of velocity fluctuations along the wall normal direction 23

7–1 Velocity vectors superimpose to mean temperature color contour for $k/h = 0.1$, $w/k = 1, 3, 7, 15$. 25

7–2 Molecular heat conduction for square bars with $k/h = 0.1$ for $w/k = 1, 3, 7, 15$ 26

7–3 Total heat flux augmentation with respect to the channel flow for $k/h = 0.1$ for $w/k = 1, 3, 7, 15$ 26

7–4 Total heat flux for square bars with $k/h = 0.1$ for $w/k = 1, 3, 7, 15$ . . 27

8–1 Sketch of the flow configuration and three dimensional view of the channel. The definitions of k, w, h, λ area included. 29

8–2 Three dimensional view of the channel. 30

8–3 Top: Plane view of velocity vectors superimposed to color contours of wall normal velocity for $w/k = 3$. Bottom: Side view of velocity vectors superimposed to color contours of spanwise velocity for $w/k = 3$. 31

8–4 a).Mean Wall Normal Velocity contours projected on a cross sectional view with arrows showing the direction of velocity increase. b)Instantaneous view of velocity stream traces along the streamwise direction 32

8–5 a)Spanwise vortex core in the cavity of the turbulators. b)Streamwise large-scale vortex at the top of the crest plane 33

8–6 Top: Plane view of velocity vectors superimposed to color contours of wall normal velocity. Bottom: Side view of velocity vectors superimposed to color contours of spanwise velocity for $w/k = 8$, $k/h = 0.25$ 34

8–7 Top: Plane view of velocity vectors superimposed to color contours of wall normal velocity. Bottom: Side view of velocity vectors superimposed to color contours of spanwise velocity for $w/k = 10$, $k/h = 0.25$ 35

8–8 Top: Plane view of velocity vectors superimposed to color contours of wall normal velocity. Bottom: Side view of velocity vectors superimposed to color contours of spanwise velocity for $w/k = 15$, $k/h = 0.25$ 36

8–9 Top: Plane view of velocity vectors superimposed to color contours of wall normal velocity. Bottom: Side view of velocity vectors superimposed to color contours of spanwise velocity for $w/k = 8$, $k/h = 0.1$ 37

8–10 Top: Plane view of velocity vectors superimposed to color contours of wall normal velocity. Bottom: Side view of velocity vectors superimposed to color contours of spanwise velocity for $w/k = 10$, $k/h = 0.1$ 38

8–11 Top: Plane view of velocity vectors superimposed to color contours of wall normal velocity. Bottom: Side view of velocity vectors superimposed to color contours of spanwise velocity for $w/k = 15$, $k/h = 0.1$ 39

8–12 Streamwise velocity averaged in time and streamwise direction: right $k/h = 0.25$, left: $k/h = 0.1$ for $w/k = 3, 8, 10, 15$ 40

8–13 Cross sectional view of mean normal velocity for $k/h = 0.25$ 41

8–14 Cross sectional view of mean normal velocity for $k/h = 0.1$ 42

8–15 a)Instantaneous plane view of velocity stream traces along the streamwise and spanwise direction. b)Mean spanwise velocity contours projected on a cross sectional view for $k/h = 0.25$, $w/k = 3$ 43

8–16 Cross sectional view of mean spanwise velocity for $k/h = 0.25$ 44

8–17 Cross sectional view of mean spanwise velocity for $k/h = 0.1$ 45

8–18 Cross sectional view of mean streamwise velocity for $k/h = 0.25$ . . . 46

8–19 Cross sectional view of mean streamwise velocity for $k/h = 0.1$ 47

8–20 Pressure Upstream along the wall normal direction for $k/h = 0.25$ for $w/k = 3, 8, 10, 15$ 48

8–21 Pressure Downstream along the wall normal direction for $k/h = 0.25$ for $w/k = 3, 8, 10, 15$ 49

8–22 a)Skin frictional drag for $k/h = 0.25, 0.1$ and $w/k = 3, 8, 10, 15$. 50

8–23 Skin frictional drag distribution and streamwise velocity contours along streamwise direction for $k/h = 0.25$ and $w/k = 3$. 52

8–24 Skin frictional drag distribution and streamwise velocity contours along streamwise direction for $k/h = 0.25$ and $w/k = 8$. 54

8–25 Skin frictional drag distribution and streamwise velocity contours along streamwise direction for $k/h = 0.25$ and $w/k = 10$. 55

8–26 Skin frictional drag distribution and streamwise velocity contours along streamwise direction for $k/h = 0.25$ and $w/k = 10$. 57

8–27 a)Form drag along the wall normal direction for $k/h = 0.25, 0.1$ and $w/k = 3, 8, 10, 15$. 59

8–28 Total Drag along the wall normal direction for $k/h = 0.25, 0.1$ for $w/k = 3, 8, 10, 15$ 60

8–29 Total Drag along the wall normal direction for $k/h = 0.25, 0.1$ for $w/k = 3, 8, 10, 15$ 60

8–30 Turbulent intensities for three velocity components (u, v, w) for $k/h = 0.25$ and $k/h = 0.1$ for $w/k = 3, 8, 10, 15$ 61

8–31 Turbulent intensities along the normal direction for $k/h = 0.25$ and $k/h = 0.1$ for $w/k = 3, 8, 10, 15$ 62

8–32 Normal Velocity profile for $k/h = 0.25$ and $k/h = 0.1$ for $w/k = 3, 8, 10, 15$ 63

8–33 Cross sectional view of mean temperature for $k/h = 0.25$, $w/k = 3, 8, 10, 15$ 64

8–34 Cross sectional view of mean temperature for $k/h = 0.1$, $w/k = 3, 8, 10, 15$ 65

8–35 Temperature fluctuations for $k/h = 0.25$ and $k/h = 0.1$ for $w/k = 3, 8, 10, 15$ 66

8–36 Time averaged molecular heat conduction along the wall normal direction for $k/h = 0.25, 0.1$ for $w/k = 3, 8, 10, 15$ 66

8–37 Wall normal time averaged turbulent heat flux along the wall normal direction for $k/h = 0.25$ and $k/h = 0.1$ for $w/k = 3, 8, 10, 15$ 69

8–38 Cross Section contour of time averaged wall normal turbulent heat flux along the wall normal direction for $k/h = 0.25$ with $w/k = 3, 8, 10, 15$ 70

8–39 Cross section contour of time averaged wall normal turbulent heat flux along the wall normal direction for $k/h = 0.25$ with $w/k = 3, 8, 10, 15$ 72

8–40 Turbulent heat flux $k/h = 0.25$ and 0.1 with $w/k = 3, 8, 10, 15$ 73

8–41 Total heat flux $k/h = 0.25$ with $w/k = 3, 8, 10, 15$ 74

8–42 Spanwise time averaged turbulent heat flux along the wall normal direction for $k/h = 0.25$ and $k/h = 0.1$ for $w/k = 3, 8, 10, 15$ 75

8–43 Skin frictional drag distribution and streamwise velocity contours along streamwise direction for $k/h = 0.25$ and $w/k = 3$. 78

8–44 Skin frictional drag distribution and streamwise velocity contours along streamwise direction for $k/h = 0.25$ and $w/k = 8$. 80

8–45 Skin frictional drag distribution and streamwise velocity contours along streamwise direction for $k/h = 0.25$ and $w/k = 8$. 81

8–46 Skin frictional drag distribution and streamwise velocity contours along streamwise direction for $k/h = 0.25$ and $w/k = 8$. 82

8–47 Total heat flux augmentation with respect to the channel flow for $k/h = 0.25, 0.1$ for $w/k = 3, 8, 10, 15$ 83

8–48 Total heat flux augmentation with respect to the channel flow for $k/h = 0.25, 0.1$ for $w/k = 3, 8, 10, 15$ 83

8–49 Total heat flux augmentation with respect to the channel flow for Square bars and V-shaped turbulators 84

A–1 Turbulent Heat flux for all ratios of w/k all ratios of $k/h = 0.25$ . . . 90

A–2 Turbulent Heat flux for all ratios of w/k all ratios of $k/h = 0.1$ 91

LIST OF ABBREVIATIONS

MPI	Message Passing Interphase
DNS	Direct Numerical Simulation
CFD	Computational Fluid Dynamics
RANS	Reynolds Average Navier-Stokes
CFL	Courant, Frederich and Lewis
LES	Large Eddie Simulations
RMS	Root Mean Square

LIST OF SYMBOLS

α	Thermal diffusivity
C_D	Total Drag
P_d	Form Drag
C_f	Skin Frictional Drag
$C_{f\infty}$	Skin Frictional Drag
ΔP	Pressure difference
Δt	Time step
Δx_i	Mesh width in the i^{th} direction
h	Mid-channel Height
k	Turbulators Height
w	width
λ	Pitch
μ	Dynamic viscosity
Nu	Nusselt number
Nu_∞	Nusselt number for smooth
∇	Gradient operator
ν	Kinematic viscosity
P	Pressure
Pr	Prandlt number
Π	Body force
q	Heat flux
Re	Reynolds number
ρ	Density
T	Temperature
τ	Time constant
τ_w	Shear stress
u_i	Instantaneous velocity component in the i^{th} direction
$\bar{U}_i$	Average velocity component in the i^{th} direction
u_i'	Fluctuating velocity component in the i^{th} direction
x_i	Component of coordinate in the i^{th} direction
V	Velocity
S	Symmetric tensor of velocity gradient
Ω	Antisymmetric tensor of the velocity gradient
λ_2	Second Eigenvalue
u	Streamwise velocity
w	Spanwise velocity
v	Wall normal velocity
U_b	Bulk velocity

CHAPTER 1
INTRODUCTION

The study of turbulent heat or mass transport is of special interest in engineering, especially for heat exchangers. Kim & Moin (1989), Kasagi et al. (1992), Kawamura et al. (1999) studied the transport of a passive scalar in a turbulent channel flow with smooth walls. However, the surface of heat exchangers is deliberately rough. For instance, roughness elements (turbulators) are usually placed on the walls of the internal channels of a turbine blade to enhance the heat transfer (Han et al. 2000). Recently with the use of a cluster of computers, it has been possible to perform Direct Numerical Simulations (hereafter DNS) of the flow over a rough wall. Leonardi et al (2003) studied how the pitch to height ratio of a square bar roughness influences the frictional and form drag and their correlation with the roughness function. Ashrafian et al. (2004) have performed a DNS of the turbulent channel flow with a square bar roughness on both walls with a small k/h ratio where k is the roughness height and h is the channels width. Bhaganagar et al. (2004) considered an egg-carton roughness underlying the differences between 2D and a 3D roughness. Another kind of roughness has been recently studied by Ikeda & Durbin (2007) who considered square bar elements with different heights. Miyake et al. (2001) considered the transport of passive scalar over a rough wall. They studied the effect of square bars with $w/k = 6$ (w is the spacing between roughness elements) on the temperature field. Recently Leonardi et al. (2007) have studied the dependence of the heat transfer for several w/k ratios. They found that $w/k = 7$ consistently to what happen for the roughness function is the one which maximize

the heat transfer. In the present research, DNSs are carried out in a turbulent channel flow with V-shape square ribs for $w/k = 3, 8, 10, 15$ and an angle of 45°. This particular type of turbulators has practical application in the internal channels of turbine blades. Experimental results (Henn 2000) show that V-shape (see Figure 1–1) square ribs show are more efficient in maximizing the heat transfer.

In this preset work, DNS is performed in order to simulate the turbulent channel flow with V-shape turbulators in both walls. The objective of this study is to obtain the geometrical configuration that maximizes the heat transfer and obtain details of the friction loss with a parametric study based on the optimization of the geometrical configuration of the rib elements. In this case we consider the variation of the pitch-to-height ratio for a constant height of the rib k. A fixed Reynolds number and angle of attack is used on the simulations.

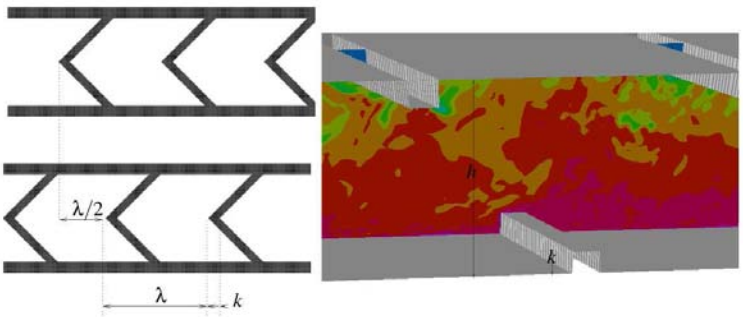

Figure 1–1: Geometrical Configuration of the V-shape Roughness Element

CHAPTER 2
JUSTIFICATION

Modern gas turbines are extensively used in the aerospace industry for aircraft propulsion. Turbine blades are designed to resist high temperatures to prevent damage of the blade (Figure 2–1.a). The cooling system of the gas turbine blades (see Figure 2–1.b) plays a critical role in increasing the thermal efficiency and power output of advanced gas turbine. In fact, by increasing the heat transfer, the turbine blade can resist to an imping fluid with higher temperature. Therefore the temperature in the combustor chamber can be increased thus improving the cycle efficiency. The aim of the present thesis is to find the geometrical configuration producing the largest heat tranfer.

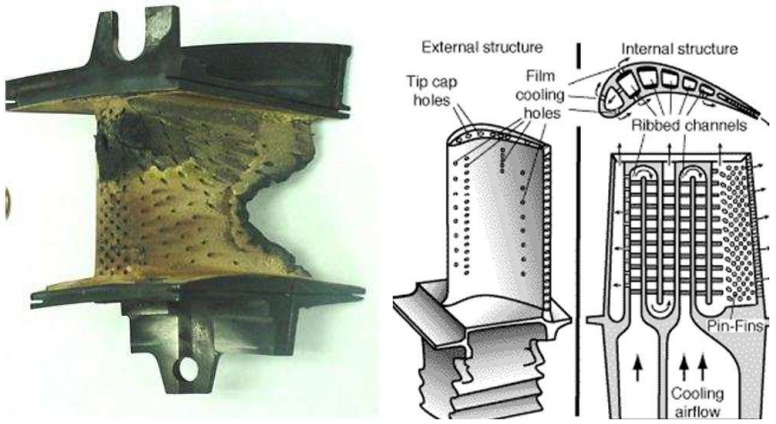

Figure 2–1: a)Damaged Turbine Blade. b)Turbine Blade Cooling Mechanisms

CHAPTER 3
OBJECTIVE

Through the development of the research, an alternate form of rib-tubulator called V-Shape was simulated for different scenarios which allowed us to determine the most efficient configuration that optimize the heat transfer. The heat transfer depends on the variation of aspect ratio, spacing between element, pitch over height ratio, width over height ratio and others. For the analysis of the configurations, Direct Numerical Simulation will be used as the primary tool of the research.

CHAPTER 4
LITERATURE REVIEW

In gas turbine engines, the turbine cooling technology plays a critical role in thermal efficiency and power output. It is found that high operation temperature (1200-1500 °C) increase the thermal efficiency and power output of the gas turbine engine. This ability to reach higher temperature is limited by design constraints of the turbine component in resisting flow impingement of high temperature which causes thermal stresses (J.L Han (2004) [1]). Therefore, more efficient cooling systems have been developed in order to increase operating temperatures.

Some of the cooling methods used are film cooling, turbulators and pin fins. Film cooling is based on an insulating blanket along the external surface of the turbine blade provided by a thin cool layer of air. This air is bled from the compressor stage, ducted to the internal chambers of the turbine blades, and discharged through small holes in the blade walls (see figure 4–1). In case of the turbulators, a coolant flow is passed through the in the middle portion of the internal channel of the turbine blade. At this location, rough elements or turbulators are place in order to enhance the heat transfer. The variation in the geometrical configuration optimizes the heat transfer by means of secondary motions along the channel. At the trailing edge of the turbine blade, small protruding cylinder are placed. The aspect ratio and spacing between cylinder are parameters that are optimized in order to enhance the heat transfer. In addition, pin fins provide structural support to the trailing edge of the turbine blade.This study is focused on internal cooling with turbulators.

Several studies have been performed in different types of turbulators to find the shape and configuration that maximizes the heat transfer. Experimental and numerical studies developed from rough wall to square ribs turbulators.

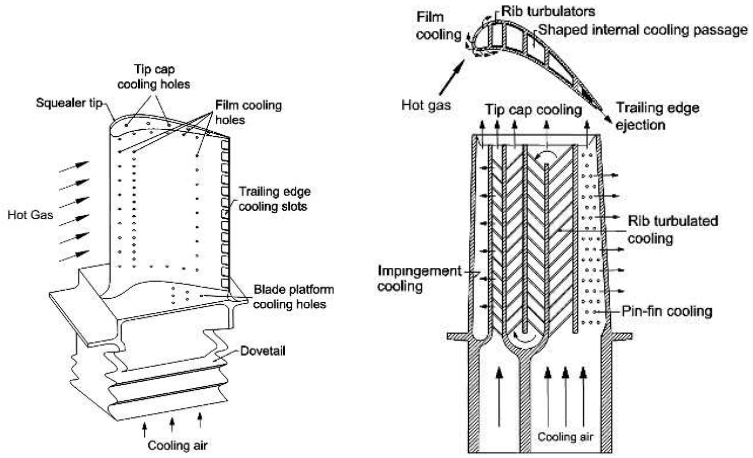

Figure 4–1: Schematic of modern gas turbine blade with common cooling techniques.

4.0.1 Rough wall

Experimental studies of rough surfaces have been performed by Furuya and Fujita (1967) [2]. Information on equivalent roughness size and drag coefficient have been measure on a wire-screen and sand plate plane. It has been accepted that in the wall the law the wall and the velocity defect law are valid and present through a linear logarithmic relation. The velocity profile in wall units, in fact, presents a downward shift with respect to that of a smooth wall. Their results showed that small discrepancy exits between the profile of the smooth wall and the rough wall.

Perry, Schofield and Joubert (1969) [3] described an experimental study with rough wall in boundary layer with zero and adverse pressure gradient over the rough walls. They observed two types of roughness. One of them depends on a Reynolds number which is based on the shear velocity and length of the channel. The other type consists of smooth wall containing a pattern of narrow cavities. This second type does not depends on the roughness scale, but it depends on the diameter of the pipe were they were tested. This indicates that exists a dependency on the flow

were at higher Reynolds number the flow becomes independent of the viscosity and became a function of k/d (k is roughness scale and d pipe diameter) only.

Dvorak (1969) [4] studied the boundary layer on rough surface with pressure gradient. The study extended the applications of the skin-friction law to a range of roughness shapes. This paper provides useful means in predicting the development of turbulent boundary layers over rough surfaces in pressure gradients.

The roughness density variation has an impact on the turbulent boundary layer. Roughness elements with the variation on spanwise aspect ratio has been compared with a smooth wall by Bandyopadhyay and Watson (1988) [5]. In the analysis of the kinetic energy it was found that the kinetic energy near the rough wall is low because the additional turbulence generated by the roughness elements does not contribute in proportion to the stress. In addition, the turbulent structure is independent of the wall conditions. In terms of the third moments $\bar{u}^3$ and $\bar{v}^3$ a positive fluctuation in u was found in the near-wall region, whereas negative values are found in the outer region. The change in sign take place in the near-wall region where the hairpin vortex forms. In this aspect, the rough wall behaves like a smooth wall in terms of the organized structure found in the smooth-wall boundary layer. In addition, a two dimensional roughness and shear stress over smooth walls can be modeled by hairpin vortices whereas, three-dimensional wall ward transport explain by a necklace vortex.

Numerical simulations of a channel flow with a rib roughened wall have been performed by Miyake *et al.* (2002) [6]. In terms of the flow structure, small recirculation zone is observed at the upstream vertical surface of the each rib which suggest separation of the flow in two streams, above and below the crest plane of the ribs. For the turbulent intensities, a peak of u^+_{rms} (where + indicates normalization with u_τ and u is the turbulent intensity in the streamwise direction) is found near the wall due to the effects of the streaks generation by quasi-stream vortices. In terms

of the fluctuation magnitude an increment is found in flat wall and low-rib cases. In the case of the components v_{rms} and w_{rms} the fluctuations are low because the ribs restrict the fluid motion close to the wall and obstruct the vortex generation preventing an increase the turbulent shear stress. The vorticity in the streamwise and wall normal direction are enhanced near the wall. The reason for this is because the no slip condition in the cavity of the wall elements is suppress by the vorticity form in this area. This effect produces that the diffusion of the vorticity decreases and the vortices generated on top of the roughness elements remains untouched by this viscous effect. Modeling of the evolution of a vortex by Miyake, Tsujimoto and Nagai (2002) [6] shows that close to the wall the flow is affected by the roughness, but away from the wall the flow is independent of the properties of the roughness element.

The separation process in closed and open cavities formed by the streamwise ribs in a square channel have been study by Wang *et al.* (2006) [7]. In their parametric study the pitch-to-height ratio is varied in order to identify closed and open cavities. In the closed cavity they found that the wall normal velocity $< V >$ shows strong momentum exchange between the separated shear layer and the mainstream and emphasizes that this motion enhances the heat transfer rate. They mentioned that one of the distinct features of cavity flow is the formation of separated shear layer. As a matter of fact, they compared results with Brown and Roshko (1974) and found good agreement in terms of the vorticity thickness. In terms of the turbulent kinetic energy, some fluctuations are due to the splashing effect as the flow encounters the vertical wall of the next roughness element as it moves in the streamwise direction. Maximum values of turbulent kinetic energy production has been observe at the crest plane of the roughness elements which may be outweigh by the pressure strain to maintain the turbulent energy at a positive level. As a summary, it can be indicated that a gradual increase in kinetic energy is obtained for open cavities due

to the splashing effect at the trailing edge and for close cavities the maximum kinetic energy occurs in the reattachment region where the velocity fluctuations reach their highest levels.

Orlandi & Leonardi (2006) [8] carried DNS for square bars in one wall of a channel in 2D and 3D configuration. Different configuration of the roughness with variation of the w/k ratio are compared (w is the width of the groves and k is the height of the roughness). The configuration variations are due to a search in the improvement of the overall heat transfer from one wall to the other. Here optimization was achieved when the ratio $w/k = 7$ the heat transfer is maximum and in addition the total drag increase to its maximum.

Similar DNS study of the turbulent flow in a rod-roughened channel have been performed by Ashrafian *et al.*(2004) citeAshrafian1. They showed that elongated streaky structures on top of the rods affect the mean flow and turbulence statistics. This effect indicate that the flow is in the transitional rough regime. Recently Leonardi *et al.*. (2007) [9] have studied the dependence of the heat transfer on w/k for a turbulent channel flow with square bars turbulators. They found that $w/k = 7$ is the geometry which maximizes the heat transfer and the effect rough wall on the total drag.

Extensive studies on boundary layer flow over rough surfaces continue to develop in order to understand this phenomenon. The difficulty that exists in experiments is to provide accurate results and reduce substantial errors when measuring high turbulent intensities near the wall. Direct numerical simulations (DNS) provide the detailed measurement of different quantities at a more detailed precision as compared to a laboratory albeit at lower Reynold number.

The first simulation of turbulent channel flow with roughness elements on both walls have been presented by Ashrafian *et al.* (2004) [10]. In their numerical simulation the high spatial resolution of 768 computation cells attempt to prevent spurious

oscillatory modes or wiggles which had been previous obtain LES investigations by Werner and Wengle (1993). Streamlines within the cavity of the square bars elements shows recirculation zones. A saddle point with in the cavity prevents reattachment of the flow in between the recirculation zones. These results agree with those obtained by Leonardi *et al.* (2003b) [11] for a higher roughness height. However, Leonardi *et al.* (2003b) [11] found a reattachment on the bottom wall for $w/k = 7$, which Ashrafian *et al.* (2004) [10] could not observe due to lack of resolution. Lower turbulent intensities downstream of the trailing corner of a roughness element are the reason prevention the reattachment of the flow in the bottom wall. In terms of the production of turbulent kinetic energy they found a variation at the crest plane of the roughness elements and a reduction in the Reynolds shear stress $- < uv >$ bellow $y^+ = 30$ which makes the production of kinetic energy small in this area. In addition, the alternation of sign and the enhancement of the secondary production term close to the roughness crest plane suggest that the effects of roughness on the turbulence field are confined to the roughness sublayer.

In term of coherent structures, Ashrafian (2004) [10] used the eigenvalue-value method of λ_2 from Jeong and Hussian (1995) to show elongated coherent structures formed in the streamwise direction which resembles streaky pattern. They found that the organizations of these structures are distorted by high turbulent intensities. Similar elongated structures near the wall where obtain by Leonardi (2003) [11] for flow over square cavity with λ/k=2 . As results of the mean flow and turbulence statistics the indication of transitionally rough regime is the presence of streamwise oriented streaks.

Direct numerical simulation is a numerical tool that have been vastly used by investigators in order to obtain accurate results without the necessity of conduction experiment. Several studies on rough surfaces have been the target of numerical simulation. DNS of turbulent channel flow with transverse square bars on one wall

have been performed be Leonardi *et al.*l. (2003) [11]. In this research a parametric study is taken into consideration with the variation of the w/k ratio (pith-to-height ration) to understand the flow physics around then. For this study the Navier-Stokes equations have been discretized and the geometry has been treated according to the immerse boundary method described by Fadlun *et al.* (2000). Mean flow present different flow structure around the roughness elements as it is for the vertical structures with in the cavity of the roughness. In this zones, separation and secondary motion have been observed by Leonardi *et al.*(2003) [11]. In terms of the drag, the effect of different w/k ratios has been study to understand their behavior along the cavity. Negative friction coefficient is observed at the leading edge of the square element and a positive peak is obtain at the crest plane. Values of pressure located on upstream face and crest plane present a maximum and minimum respectively which reflect that a strong pressure gradient is driving the flow through the channel. The effect on roughness can be observe by the shift of the mean velocity profile with respect to the law of the wall for a smooth surface. The estimation of the dependence on the w/k have been performed with the Jackson approach (1981). Since k has a significant variation, the value was set to $k = 0.2$ and the velocity profiles was estimate for several w/k. The minimum C_f and maximum P_d occurs when the reattachment on the bottom wall takes place after the upstream location of the next element. For lower ratio of $w/k < 2$ the frictional drag dominates the form drag and vice-versa for $w/k > 5$.

4.0.2 V-Shape Turbulators

Many studies have been performed to optimize the ribs design parameters which include the pitch-to-height ratio, height, angle of attack and arrangement configuration. V-shaped ribs have better efficiency at high Reynolds number in comparison to other roughness elements (Mittal *et al.* (2007) [12]). They observe that at low Reynolds number higher effective efficiency is obtained for high values of roughness

height. They found that the increase in fiction losses for lower Reynolds number is insignificant with the increase in relative roughness. In the contrary, the increase in heat transfer from roughened surface is high due to the increase of turbulence in the vicinity of roughened surface.

Numerical optimization procedures have used to define an objective function which maximize the performance of the turbulators combining the augmentation of heat transfer and reduction of pressure loss into a weighting factor (Kim & Lee (2007) [13]). Comparison in terms of the angle of attack of the V- and Λ-shaped ribs have been studied by Han *et al.* (1991) [14] showing that 60 degrees had higher heat transfer coefficient with higher friction loss for both cases. Measurements in heat/mass transfer on a square channel presorted by Choi *et al.* (2002) [15] showed that λ-shaped ribs had higher heat transfer rate than other ribs. The effect of secondary motion in rectangular channel with continues V-shaped ribs at an angle of attack of 60 degrees have been discussed by Lee *et al.* (2009) [16]. The results showed that maximum values of heat/mass transfer are located at the center of the channel and decrease along the ribs due to two pair of large-scaled counter-rotating secondary flows generated in the channel.

Several experiments of heat transfer enhancement have been performed showing the superior configuration of the V-shaped ribs over the square straight ribs. R. Jia *et al.* (2005) [17] performed Large Eddie simulation in other to evaluate the accuracy and reliability of the Reynolds-average Navier-Stokes (RANS) method. Their study showed that V-shape turbulators with the kink of the V-shape pointing downstream provided higher heat transfer on the rib side wall, while the ribs with the kink pointing to the upstream direction provided higher heat transfer coefficient on the smooth side wall.

A performance analysis was taken into consideration by S.W. Chang *et al.* (2007) [18]. Their studies showed heat transfer and pressure drop of compound V-shape roughness in a channel. In the variation of the Reynolds number, different Nusselt number and friction factors where calculated along the streamwise direction of the channel. The combination of the friction factor and Nusselt number with respect to the smooth channel is called the thermal performance. They mentioned that the methods of passive heat transfer enhancement (HTE) effects offer a heat transfer augmentations for an effective Reynolds number, but are accompanied by high pressure drop penalties. The HTE are significant in order to offset the pressure loss and elevate the thermal performance factors for V-shape ribs.

Temperature is correlated with the coherent structure in the flow. The increase in the intensity of the coherent structures in the flow increases the heat transfer. Therefore, an analysis of coherent structure is important to understand the mechanisms that enhance the heat transfer.

4.0.3 Wall Structures

Gavrilakis (1992) [19] studied the flow over a smooth square channel at low Reynolds number by performing numerical simulation. Secondary flows forms along the channel and two counter-rotating vortices symmetrically placed about the corner bisectors of the channel were observed. In addition, smaller and much weaker vortices are located in the wall bisectors. An average of all octant in the computational box indicates that the wall stress produce a peak due to large secondary flows near the corner of the channel and one at the middle of the duct. Streamwise velocity fluctuations at the center of the duct have their origin in events near any of the four walls, and on average each wall is of equal significance. The ejections that occur near the wall corner of the duct contribute to the normal velocity component, but its contribution is weak along the normal bisector. In terms of the vorticity, its value remains positive in the channel except for the wall bisectors. In addition,

the value of the wall maximum vorticity is more than twice the magnitude of the vorticity at the center of the channel.

Huser and Birigen (1993) [20] studied the same channel emphasizing the mechanism responsible for the generation of the stress-driven secondary flow. They studied the ejections generated near the corner and the interaction that exits between the two intersecting walls. A quadrant analysis has been performed where they assume that the same turbulent structures are present as in channel flow, and the average deviation of these structures accounts for the turbulence characteristic of the secondary flow; largest deviations are found in the corners where the anisotropies are more intense. The third quadrant was found to be the most significant and strength of the events found here are created by ejections at the vertical wall. It is interesting that their results indicate that there is stronger turbulence production along the walls away from the corner compared to channel and boundary layer flows. This effect produce positive and negative convection of the mean streamwise velocity at the respective location.

Experimental studies by Blackwelder and Kaplan (1976) [21] showed that the bursts are not necessarily larger in amplitude than the background turbulence, but are characterized by the high degree of coherence in the time and in the direction normal to the wall. In their study, conditional averages were computed to show that in regions of strong streamwise momentum deficit the normal velocity is directed outwards and when the streamwise velocity exceeds its mean value it is directed inwards. Also it was shown that the Reynolds shear stress that occurs during the bursting process is the most important contribution to the long-time average of the Reynolds stress. In addition, the study showed that the existence of a sequence earlier in time than the bursting suggest that the phenomenon is primarily driven by the outer turbulence.

Numerical studies of the turbulent channel flow indicate the formation of hairpin vortices. Moin and Kim (1985) [22] proposed a hairpin-like vortex as the dominant flow structure, which is formed from the deformation, stretching, and lifting of the transverse vortex. They indicated that the increase in an eddy diameter is consistent with the vortex-stretching mechanism. It should be noticed that the vorticity vectors of highest strength have a tendency of formation with respect to an angle and it has been found that this angle correspond in planes inclined at 45° from the wall. According to this study the production (stretching) of the vorticity due to mean strain is highest along the lines inclined along 45° and are most rapidly destroyed at the opposite angle (−45°) at an inclined wall. Streamwise vorticity (the legs of hairpin vortices) are responsible for producing the streaks.

These structures, produced at a high shear stress rate, are located in the sub-layer of wall bounded flows. The streaks are regions of high coherency in the streamwise direction. Lee, Kim, Moin (1990) found that high shear rate alone is sufficient for the generation of streaky structures, and that the presence of a solid boundary is not necessary. In fact, turbulent structures similar to the streaks are found even in homogeneous turbulence. A characteristic of the instantaneous turbulence structure is that since the low-speed and high-speed streaks alternate in the spanwise direction, the mean streak spacing is about twice the separation at which the minimum value of spanwise separation occurs. Some comparison with a turbulent channel flow has been made indicating that in homogeneous turbulent Reynolds number increases with shear, indicating a rapid growth of the 'large-eddy' timescale compare to the 'small-Eddie' timescale.

As part of the turbulence physics, the vortex dynamics plays an important role in the evolution and interaction of coherent structures. The identification of a vortex is a topic that brings considerable confusion in a turbulent flow. Different definitions of a vortex have been proposed. Jeong and Hussain (1995) [23] discussed different

identification schemes as a preliminary approach to present the faults of inadequacies of intuitive measurements and show a new approach in the identification of vortex. As a first inadequate measure, the identification of a local pressure minimum lies on the fact that pressure tends to have a local minimum at the axis of a circulatory or swirling motion. Is important to mention that this does not necessarily involve a vortex because this effect can exists in an unsteady irrotational motion. In addition, in a steady flow the centrifugal force is balanced not by the pressure force but by the Karman's viscous pump. As another inadequacy, Jeong and Hussain (1995) [23] criticized the use of closed or spiral path lines to detect vortices suggested by Lugt(1979). In fact, a particle may not complete a full revolution around the vortex center during the lifetime of a vortex. In terms of the vorticity magnitude $|\Omega|$ may be successfully on free shear flow, but is not satisfactory to identify vortex cores in a shear flow. A new approach has been proposed by Jeong and Hussain (1995) [23] where the eigenvalues of the $S^2 + \Omega^2$ are calculated in order to capture the pressure minimum due to vortical motion and define a vortex core. The results of the negative eigenvalue vales of $S^2+\Omega^2$ produces a symmetric second order tensor which defines a vortex as a connected region.

CHAPTER 5
METHODOLOGY

The incompressible non-dimensional NavierStokes and continuity equations may be written as

$$\frac{\partial U_i}{\partial t} + \frac{\partial U_i U_j}{\partial x_j} = -\frac{\partial P}{\partial x_i} + \frac{1}{Re}\,\frac{\partial^2 U_i}{\partial x_j^2} + \Pi\delta_{i1}\ , \qquad \nabla \cdot U = 0 \tag{5.1}$$

where Π is the pressure gradient required to maintain a constant flow rate, δ_{ij} is the Kronecker delta, U_i is the component of the velocity vector in the i direction and P is the pressure.

The energy equation is

$$\frac{\partial T}{\partial t} + \frac{\partial T U_j}{\partial x_j} = \frac{1}{Re\ Pr}\frac{\partial^2 T}{\partial x_j^2}\ , \tag{5.2}$$

where T is the temperature and $Pr = \nu/\alpha$ is the Prandtl number, with α the thermal diffusivity.

The NavierStokes and energy equations have been discretized in an orthogonal coordinate system using the staggered central second-order finite-difference approximation. Here we recall only the main features since details of the numerical method can be found in Orlandi (2000) [24]. The discretized system is advanced in time using a fractional-step method with viscous terms treated implicitly and convective terms explicitly. The large sparse matrix resulting from the implicit terms is inverted by an approximate factorization technique. At each time step, the momentum equations are advanced with the pressure at the previous step, yielding an intermediate

non-solenoidal velocity field. A scalar quantity Φ projects the non-solenoidal field onto a solenoidal one. A hybrid low- storage third-order RungeKutta scheme is used to advance the equations in time. The roughness is treated by the immersed boundary technique described in detail by Fadlun *et al.* (2000) [25]. This approach allows the solution of flows over complex geometries without the need of computational intensive body-fitted grids. It consists of imposing $U_i = 0$ on the body surface, which does not necessarily coincide with the grid (in figure 5–1). Another condition is required to avoid the geometry being described in a stepwise way. Fadlun *et al.* (2000) [25] showed that second-order accuracy is achieved by evaluating the velocities at the closest point to the boundary (in figure 5–1) using a linear interpolation. This accounts for the physical behavior of a linear mean velocity profile very near the boundary even for turbulent flows, albeit at the expense of clustering more points near the body. Fadlun *et al.* (2000) [25] showed that the velocity goes to zero where the boundary of the body is supposed to be, even if this location does not coincide with the grid.

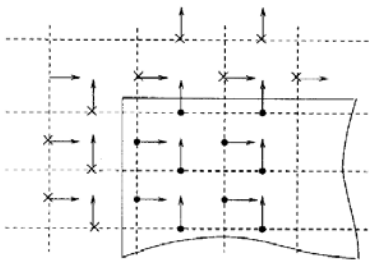

Figure 5–1: Geometrical sketch of immersed boundary method. Arrows, velocity vectors as defined in a staggered grid $(---)$; , points inside the roughness element; , points nearest to the boundary of the roughness element. The solid line delineates part of the roughness element.

The governing equations (5.1 and 5.2) are a set of partial differential equations which must be reduced to a set of ordinary differential equations, in time, for each mesh point throughout the domain. The system contains a range of linear and non-linear terms, which must be integrated differently with respect to time. The simplest manner is to treat all terms explicitly. It is not necessary to invert matrices, but

limiting conditions imposed for the stability of the solution have to be respected. The limit due to the explicit treatment of the nonlinear term

$$H_i = \frac{\partial U_i U_j}{\partial x_j}, \tag{5.3}$$

is known as the CFL condition, named after Courant, Friedrich and Lewis:

$$|\frac{U_i \Delta t}{\Delta x_i}| < 1, \tag{5.4}$$

This means that the distance traveled by a particle has to be less than the mesh width. It should be noted that this evaluation of the CFL condition is valid when only the non-linear terms are considered. Including also the linear terms acts to stabilize the solution, therefore expanding the limit of the condition. In fact in the present thesis all the simulations have been carried out at CFL=1.5.

The second condition, is a convergence criterion arising from the explicit treatment of the linear terms:

$$\frac{\Delta t}{\Delta x^2 Re} < \frac{1}{2n}, \tag{5.5}$$

where n is the number of dimensions of the simulation. Of the two conditions equation 5.5 is the most stringent in 3-dimensional simulations as n is at the denominator of equation 5.5. This condition is overcome by the implicit discretization of the linear terms.

CHAPTER 6
CHANNEL FLOW

As a preliminary study of the V-shape turbulators, a simulation of the turbulent channel flow in to understand the production of turbulence and find parameters that defines its behavior.

In general the instantaneous velocity field can be describe as:

$$u = u' + \bar{U} \tag{6.1}$$

where u is the instantaneous velocity field, u' is the velocity fluctuation and $\bar{U}$ is the mean velocity (F. White (1991) [26]). For a given velocity field which varies with time T the mean velocity can be compute as

$$\bar{U} = \frac{1}{T}\int u dt \tag{6.2}$$

where the overbar means the average of the instantaneous velocity over the period of time T.

The mean velocity profile was compute for the turbulent channel flow in 6–1.a. At the wall $y = -1$ and $y = 1$ a no-slip condition boundary condition can be observe where the velocity is zero. A comparison with an instantaneous velocity field showed the fluctuation of the mean velocity for one time. At the center of the channel the velocity reaches its maximum value. This plot represent the typical velocity profile for a turbulent channel flow.

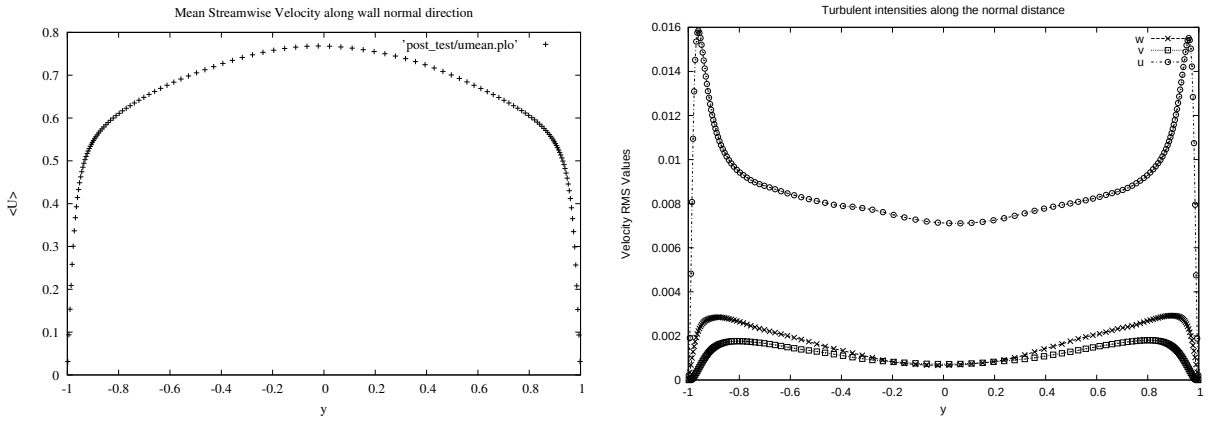

a) b)

Figure 6–1: a) Mean streamwise velocity along the wall normal direction. b)Root mean square of the three velocity components

Other aspect of study are the quantification of how much the instantaneous velocity field fluctuates from the mean velocity. This quantity is represented by the root mean square (RMS) of the velocity $\sqrt{u'^2}$. Figure 6–1 shows the turbulent intensities or RMS for the three velocity components (streamwise u, spanwise w red and wall-normal v). Near the rough wall, $y = -1$, the fluctuations are higher for the streamwise velocity due to the no-slip condition. Since the mean flow is the maximum value at the center of the channel, its fluctuation is minimum for the streamwise velocity. Spanwise and wall normal velocity have small fluctuations at the side walls since close to the wall turbulent structures are produced.At the center of the channel w and v are reduced to their minimum since the streamwise velocity dominates due to the mean stream flow.

A more interesting topic is to analyze the mechanism that generates the turbulence in the flow in which produces the fluctuation from the mean velocity. The study of the boundary layer is the study of a thin layer near a fixed surface in a moving stream in which shearing stresses are not negligible.The existence of organized structures near wall region of turbulent boundary layer flows have been vastly studied by several experimental and numerical investigators. The interaction of the different structures in the inner boundary layer with the outer flows has shown an

increase in the turbulence production. Studies near a smooth wall by Kim, Kline and Reynolds (1971) [27] states that essentially all the turbulent production occurs during busting times in the zone $0 \leq y^+ \leq 100$ ($y^+ = v^* y/\nu$ where v^* is the wall-friction velocity, ν is the kinematic viscosity and y is wall-normal direction). They describe the bursting process as a continuous chain of events leading from quiescent wall flow to the formation of relatively large and chaotic fluctuations. The bursting process of a streak produce an intermittent oscillations which remain organized for 3 to 10 cycles and after 10 cycles the motion becomes chaotic and the streaks breakup into the outer layer. The process is constantly moving low speed fluid particle from near the wall to the outer layer.

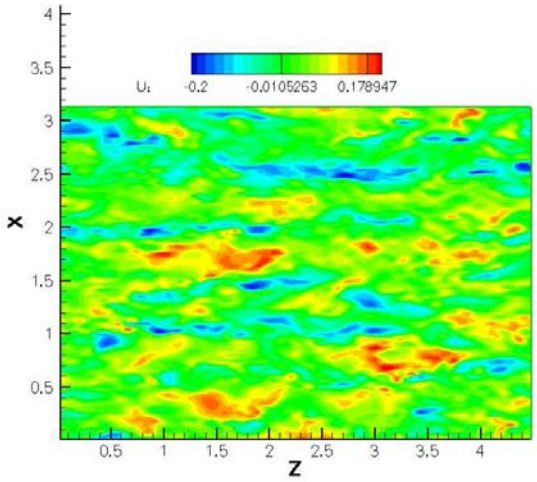

Figure 6–2: Horizontal view of color contour of velocity fluctuations along the streamwise direction.

Figure 6–2 shows the velocity contours of the fluctuations for the velocity. In this contours the streaks can be observe as high and low intensity colors traveling along the streamwise direction. These streaks increase the turbulence in the channel as it evolves up to the bursting process. As the streak raises from the lower wall to the outer layer, the fluctuation of the normal velocity allow us to visualize the streak the his bursting process in 6–3. Low and high intensity colors allows to see the intermittent oscillations as it increases the turbulence in the center of the channel and travels along the streamwise direction until the break up occurs. It is shown that

the frequencies of the bursting oscillations are in the center of the high energy range of the turbulent fluctuations and it reinforces the idea that the bursting process is the overall generator of the turbulence and the primary energy transfer occurs in the oscillatory growth stage.

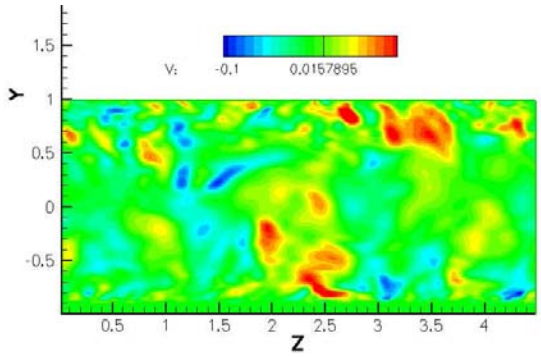

Figure 6–3: Side view of color contour of velocity fluctuations along the wall normal direction

CHAPTER 7
SQUARE BARS

As part of the preliminary studies of the V-shaped turbulators a Direct Numerical Simulation of square bars roughness on one wall was performed. After the study of the flow structure on the channel flow and the mechanisms that generates the turbulence, the addition of square bars roughness was a first step to understand channel flow with roughness.

Several values of w/k are considered ($w/k = 1, 3, 7, 15$, where w is the width of the cavity and k is the height of the turbulator). The square bars turbulators are located in the bottom wall the channel. The Reynolds number $Re = U_b h/\nu$ is 10400, while the Prandtl number Pr is set equal to 1; here,U_b is the bulk velocity and ν is the kinematic viscosity, h the channel half height. The computational box is $6h \times 2.1h \times 1h$ in z (streamwise), y (wall-normal) and x (spanwise direction) respectively. Periodic boundary conditions apply in the streamwise and spanwise direction. In the vertical direction a non uniform grid was used with 192 grid nodes. The additional $0.1h$ increase in channel half corresponds to the cavity height where the square elements are placed. The plane of the crests is at $y/h = -1$. The temperature T is set to $T = 1$ on the lower wall and to $T = -1$ on the upper wall.

Mean temperature contour superimpose with velocity vectors is showed in figure 7–1. For small ratios of w/k a recirculation of the flow is observe with in the cavity of the turbulators. This recirculated flow is maintain in the cavity reducing the interaction with external flow particles. As the w/k ratio increases the interaction of the mean stream flow and flow in the cavity increases. For $w/k = 7$ velocity

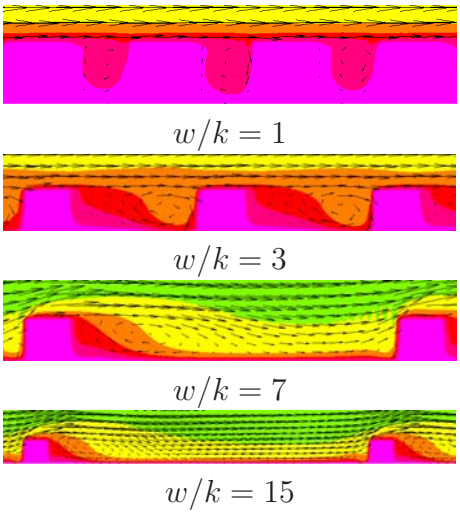

Figure 7–1: Velocity vectors superimpose to mean temperature color contour for $k/h = 0.1$, $w/k = 1, 3, 7, 15$.

contours shows that more fluid from the mean stream flow is injected into the cavity providing an increase in mixing of cold and hot flow particles. As a result of the injections, ejections at the leading edge of the following turbulators are observe for $w/k = 7$ which promotes the heat transfer from the hot wall to the cold wall. A characteristic of this square bar roughness geometry is the 2 recirculation zone along the cavity of the turbulator. One main recirculation is located at the trailing edge of the turbulator which is formed due to the injection of flow particles from the center of the channel into the cavity. The second recirculation is located at the leading edge of the next turbulator which is cause due to the ejecting flow. Similar flow structure is found in direct numerical simulations performed by Leonardi *et al* (2007) [9].

Heat transfer analysis is performed in order to compare the results with the V-shaped turbulators. The average molecular heat conduction is compute according to $(\frac{1}{RePr}\frac{\overline{dT}}{dy})$ along the channel. Figure 7–2 shows the distribution for $k/h = 0.1$ all the w/k ratios. Maximum molecular heat conduction can be observed at walls due to the no slip condition at the near wall region. Minimum values of heat conduction are found at the center of the channel where no surface for conductive heat transfer is available and the convective heat transfer dominates.

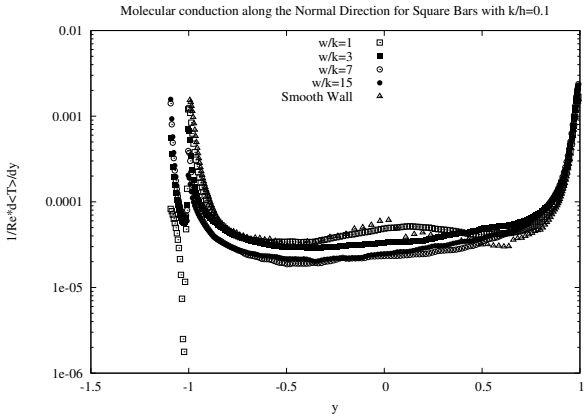

ht

Figure 7–2: Molecular heat conduction for square bars with $k/h = 0.1$ for $w/k = 1, 3, 7, 15$

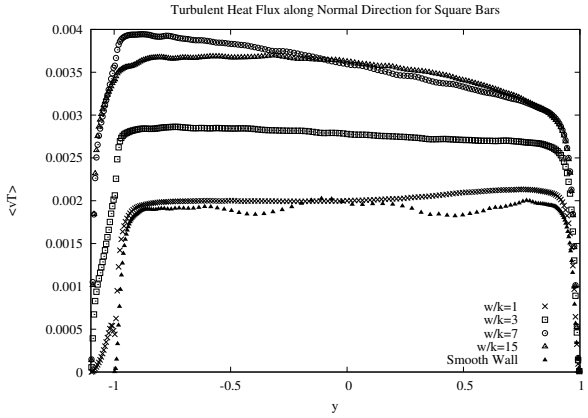

ht

Figure 7–3: Total heat flux augmentation with respect to the channel flow for $k/h = 0.1$ for $w/k = 1, 3, 7, 15$

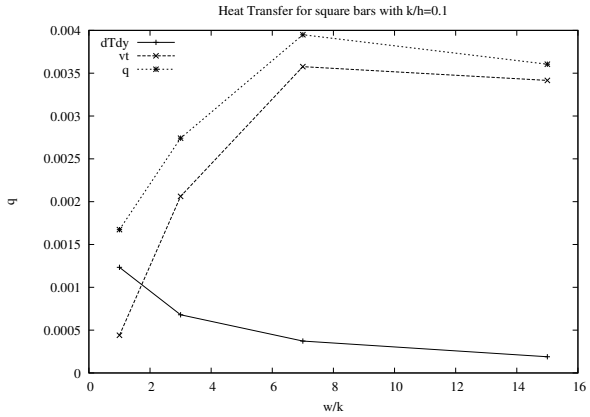

ht

Figure 7–4: Total heat flux for square bars with $k/h = 0.1$ for $w/k = 1, 3, 7, 15$

Figure 7–3 shows the turbulent heat flux $< Tv >$ distribution along the normal direction. At the bottom wall the turbulent heat flux is the minimum since the no-slip condition is present reducing the velocity to its minimum. At the crest plane of the turbulators, an increase in the turbulent heat flux is obtained due to the interactions of the cavity of the flow with the main stream flow in the center of the channel. As the wall normal distance increases, the turbulent heat flux increases until a constant value is obtained. At the center of the channel convective effects dominates over molecular conduction due to the absence of the geometry. At the top wall of the channel the turbulent heat flux decreases again due to the no-slip condition and the molecular heat conduction dominates. Maximum value for turbulent heat flux is obtain at $w/k = 7$ and reduces as the w/k distance increases. This is due to the increase in ejections and injections of the flow in the cavity of the turbulator. This configuration provides the necessary geometrical configuration for an optimum ejected flow. For lower ratios of w/k, the flow within the cavity remains trapped and recirculates around the cavity with minimum interaction with the mean stream flow. This results are in agreement with Leonardi *et al* (2007) [9].

The contribution of the molecular conduction and the turbulent heat flux to the heat transfer at the crest plane are presented in figure 7–4. The total heat flux

q is the sum of the molecular heat conduction $\frac{1}{RePr}\overline{\frac{dT}{dy}}$ and the turbulent heat flux $< Tv >$ (S. Pope (2000) [28]). The greater contribution for the total heat flux is due to the turbulent heat flux in the channel since the normal component of the velocity transport the heat out of the wall into the core of the flow. The total heat flux follows the tendency of the turbulent heat flux and molecular conduction in a descendant behavior as the w/k ratio increases for both k/h ratios. Since the $k/h = 0.25$ ratio shows a higher turbulent heat flux for all w/k ratios, the total heat flux is maximum for this ratio due to the mechanism previously mentioned. These results obtained agrees with direct numerical simulations performed by Leonardi *et al* (2007) [9].

CHAPTER 8
V-SHAPED TURBULATORS

8.1 FLOW CONFIGURATION

A sketch showing the channel, the flow orientation and roughness type is given in Figure 8–1. Several pitch to height ratio have been considered, $w/k = 3, 8, 10, 15$ where k is the height of the elements, w the width of the cavity ($w = \lambda$ - k) for $k/h = 0.25, 0.1$ (h is the channel half-height). The angle of inclination of the ribs is 45 degrees. A side wall of height h and thickness of $0.02h$ has been added at the end of the cavity of the turbulators (Figure 8–2). The temperature on the lower walls is $T = 1$ while on the upper wall is $T = 1$. Therefore heat is transported away from the lower wall and dissipated on the upper wall.

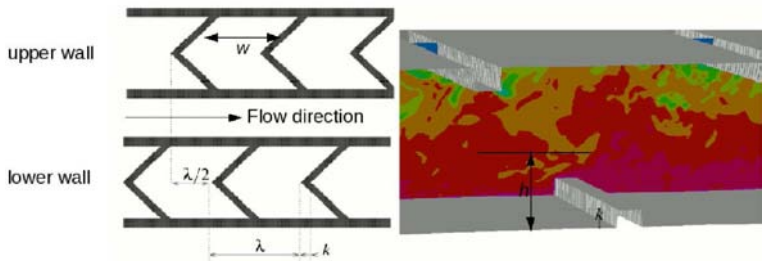

Figure 8–1: Sketch of the flow configuration and three dimensional view of the channel. The definitions of k, w, h, λ area included.

The Reynolds number $Re = U_b h/\nu$ is 10400, while the Prandtl number Pr is set equal to 1; here, U_b is the bulk velocity and ν is the kinematic viscosity, h the channel half height. The computational box is $6h \times 2h \times 2h$ in z (streamwise), y (wall-normal) and x (spanwise direction) respectively. Periodic boundary conditions apply in the streamwise and spanwise direction.In the vertical direction a non uniform grid was used with 192 grid nodes. Grid points are clustered near the rib turbulators where

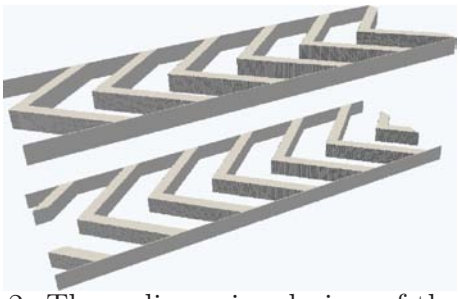

Figure 8–2: Three dimensional view of the channel.

the resolution is $k/50$ for $k/h = 0.25$ and $k/25$ for $k/h = 0.1$. Mesh sizes in the other two directions are uniform with 192 points in spanwise direction and 640 in streamwise direction, yielding typically about 24 million nodes within the domain.

8.2 MEAN FLOW

8.2.1 Results

The three-dimensional and time-dependent field outcome of the DNS have been statistical averaged in time for the three velocity components (U:streamwise, V:wall-normal, W:spanwise), pressure P and temperature T. Statistics are collected over 100 time independent data fields, where the separation between them is each $2 * t$, where t is a time unit defined as $t = h/U_b$. For the convergence of the solution in time the pressure gradient was taken in consideration until a constant value was obtained which reflects the fully develop flow.

8.2.2 Mean Flow

Velocity vectors averaged in time are shown in Fig. 8–3 superimposed to wall normal and spanwise velocity. Near the center of the channel in proximity of the crests plane, Sec. CC, the flow is driven inward, in the cavities between the two V-shaped turbulators. Two streams form and follow, to a good approximation, the direction of the V-shaped ribs. Therefore, the fluid entering in the cavity does not impinge on the following rib, as in 2D transverse ribs (Leonardi et al. 2003), but it is driven towards the side-walls of the channel. By observing the side view of Sec. CC, a strong recirculation can be observed at the trailing edge of the turbulator. For 2D transverse rib, the flow separates at the leading edge of the next rib, (Leonardi et

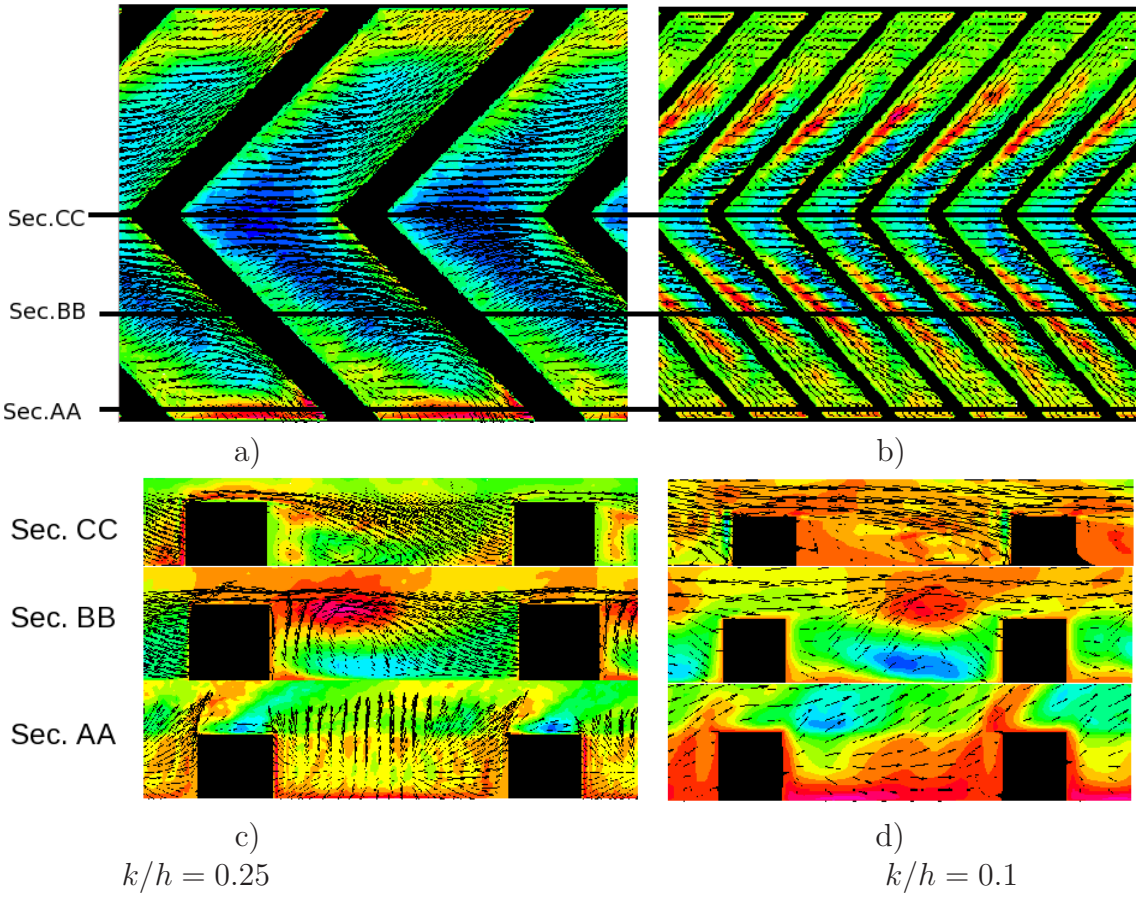

Figure 8–3: Top: Plane view of velocity vectors superimposed to color contours of wall normal velocity for $w/k = 3$. Bottom: Side view of velocity vectors superimposed to color contours of spanwise velocity for $w/k = 3$.

al. 2003). For V-shaped turbulators the flow does not separate because it is driven in the spanwise direction following the inclination of the ribs. Moving towards the side walls, the center of the vortex moves towards the leading edge of the next rib (see Sec. BB side view). Very near the side wall (Sec. AA) ejections are observed. In fact, a stream coming from the center of the channel (Sec. CC) is blocked by the side wall and the two ribs turbulators. Therefore for continuity ejections occur. In fact, in Sec. AA $\frac{\partial w}{\partial z}$ is large and negative since the spanwise velocity at the side wall is forced to be $w = 0$ by the impermeability condition. Therefore for continuity $\frac{\partial v}{\partial y}$ has to be large and positive. This determines a stream of fluid outward the cavity (ejection).

The fluid enters into the cavities in good approximation in an area centered on the kink of the V-shaped turbulators which extend to about half the spanwise length of the channel. The region of more intense inward wall normal velocity has the shape of a chevron with a curvature near the kink of the following rib. This shape resembles a boomerang. The vertical dimension of the square rib determines the flow rate entering into the cavities formed by the turbulators. The color contours of wall-normal velocity at the crest plane (Fig. 8–3) show that the larger k/h the larger the flow rate entering into the cavity. Since the ejections are due to a continuity mechanism, by decreasing the intensity of the stream coming from the center of the channel (Sec. CC), the ejection at the side wall decreases (see Sec.AAc-d). In particular, for $k/h = 0.1$ the angle of the velocity vectors is smaller than that for $k/h = 0.25$.

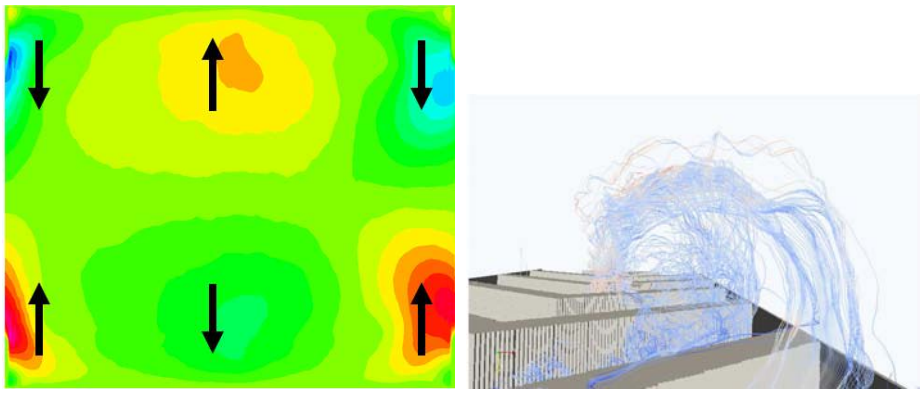

a) b)

Figure 8–4: a).Mean Wall Normal Velocity contours projected on a cross sectional view with arrows showing the direction of velocity increase. b)Instantaneous view of velocity stream traces along the streamwise direction

Further details of the motion inward and outward of the cavities delimited by the V-shaped turbulators can be appreciated in Fig. 8–4. Color contours of the mean wall normal velocity show that ejections out of the wall occur near the side walls of the channel. The fluid enters into the cavities at the center of the bottom and upper wall. So the fluid in the center of the channel is driven towards the cavities in the vertical direction, then after entering into the cavities two streams are formed which

goes towards the sidewalls where the ejections occur. Summarizing, the V-shaped turbulators induce a secondary motion made of 4 counter rotating vortices near the 4 corners of the channel. Similar large-scale counter-rotating secondary flows were observed by Lee *et. al.* (2009) [16]. Instantaneous visualizations of stream-traces (Fig. 8–4) show some helicoidal trajectories due to the superposition of the primary motion (the fluid flowing through the channel) and the secondary motion (the vorticity at the channel corner).

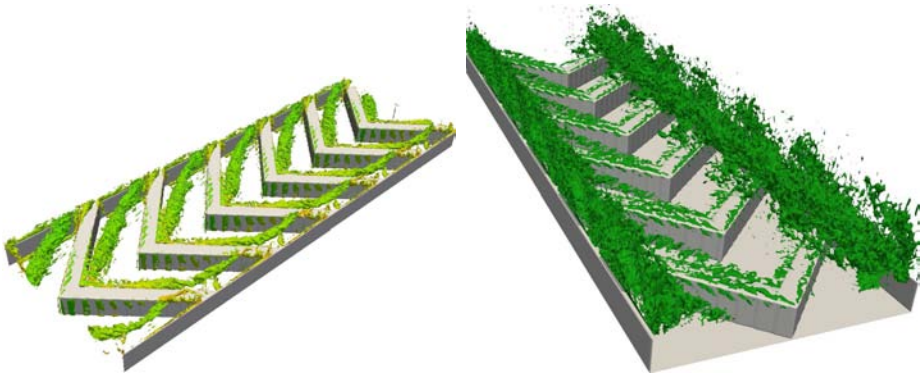

a) b)

Figure 8–5: a)Spanwise vortex core in the cavity of the turbulators. b)Streamwise large-scale vortex at the top of the crest plane

By discussing Fig. 8–3 and 8–4 , two main vortical structures were observed. From Fig.8–3, separated regions in sec. CC and BB denote the presence of a vortex oriented as the V-shaped turbulators (at 45 degrees); from Fig. 8–4 streamwise vortical structures are expected near the side walls of the channel, just above the crests plane.

In order to visualize properly these vortical structures, the second eigenvalue λ_2 technique was used from Jeong & Hussain (1995) [23]. The approach consists on calculate the eigenvalues of the $S^2+\Omega^2$ (S is the symmetry tensor and Ω is the antisymmetry tensor of the velocity gradient) in order to capture the pressure minimum due to vortical motion and define a vortex core. The results of negative eigenvalues of $S^2+\Omega^2$ produces a symmetric second order tensor which defines a

vortex as a connected region. Visualization of the vortex core can be observe in figure 8–5.a.

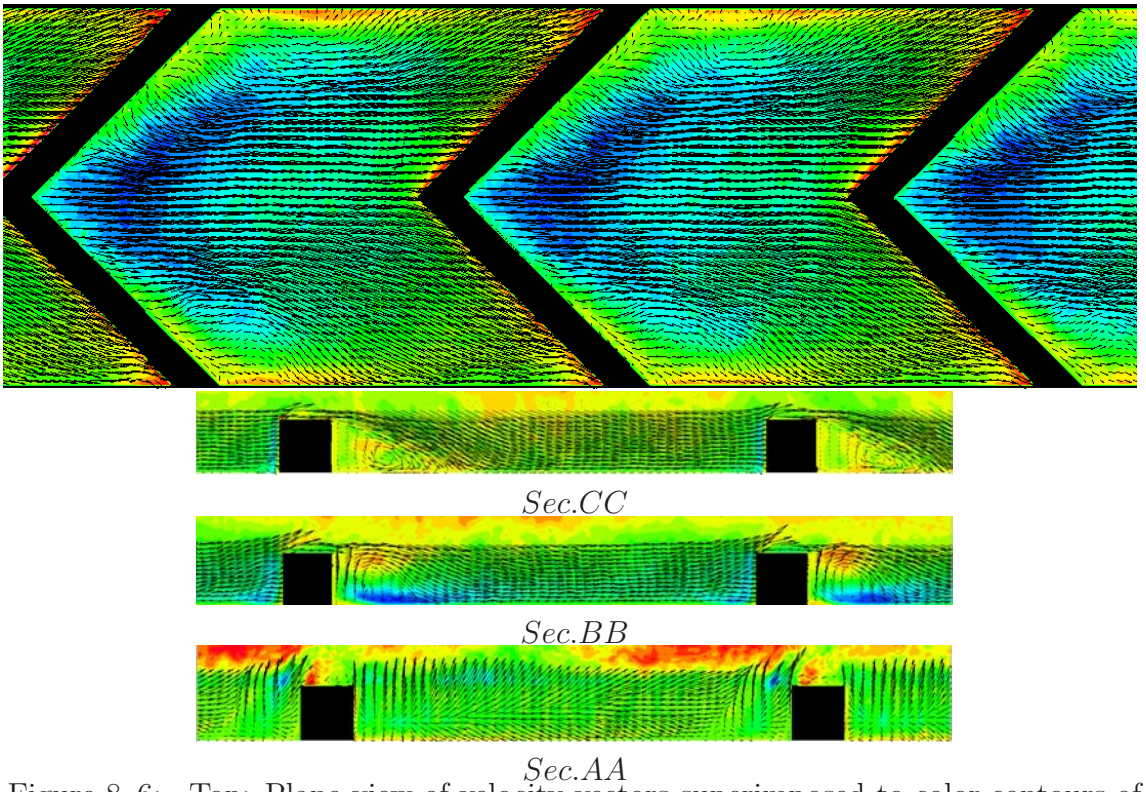

Figure 8–6: Top: Plane view of velocity vectors superimposed to color contours of wall normal velocity. Bottom: Side view of velocity vectors superimposed to color contours of spanwise velocity for $w/k = 8$, $k/h = 0.25$

By increasing the distance between the V-shaped turbulators, the intensity of the secondary motion decreases. In fact, the region where the flow enters inside the cavities is reduced with respect to that for $w/k = 3$. For the latter, the centerline portion of the channel presented an inward velocity for the entire length of the channel. For $w/k = 8$, the region where the wall normal velocity is negative is about one half of the cavity (fig.8–6). The other half of the cavity has a very weak vertical motion. In fact, a side view in proximity of the kink of the turbulators (Sec. CC Fig.8–6) shows reattachment on the bottom wall. The length of the recirculation region is much lower than that of a backward facing step or transverse turbulators (Leonardi *et al. 2003*). At the side walls ejections occur for a mechanism similar to that described before for $w/k = 3$. However, strong and vertical ejections are

observed only very close (about $1k$ upstream and downstream) to the turbulator. In the middle of the cavity (i.e. $1 < x/k < 7$ where the origin in x is at the trailing edge) the inclination of the velocity vector is reduced with respect to $w/k = 3$. This may indicate a reduced heat transfer and will be further corroborated in the next chapters. Since continuity must be satisfied, the reduction on the intensity of the upward flow due ejections at the side wall for $w/k = 8$ are complemented with an increase in the ejections at the leading edge of the next turbulator that the flow encounters. Instead of ejections at the side walls only the ejections are redistributed along the leading edge of the adjacent turbulator.

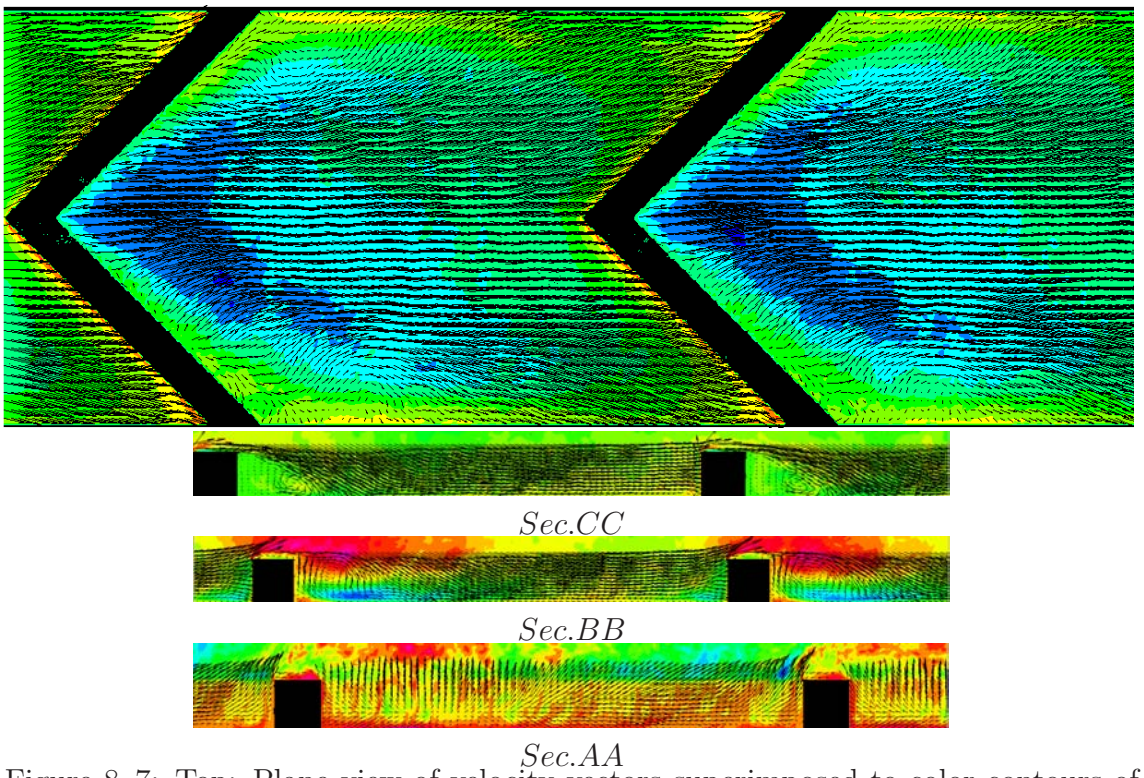

Figure 8–7: Top: Plane view of velocity vectors superimposed to color contours of wall normal velocity. Bottom: Side view of velocity vectors superimposed to color contours of spanwise velocity for $w/k = 10$, $k/h = 0.25$

By increasing further w/k ($w/k = 10, 15$) the secondary motion becomes weaker. In fact, the cavities are too wides to force the flow towards the sidewalls. Spanwise motion is intense only near the trailing edge of the turbulator, while velocity vectors near the leading edge of the following rib are to a close approximation aligned with

the direction of the overlying flow. The extent of what we called "boomerang" region at the center of the channel where the overlying flow enters into the cavity seems to be independent of w/k. Its extent increases slightly from $w/k = 3$ to $w/k = 8$, but it does not change significantly for a further increase of the width of the cavity.

Reattachment of the flow can be observed after the recirculation zone at trailing edge of the turbulator (see Fig. 8–7Sec. CC and Sec. BB). At the side walls (see Fig. 8–7 Sec. AA), ejections still occurs close to the trailing edge of the roughness element followed by a streamwise motion until the next turbulator is encountered.

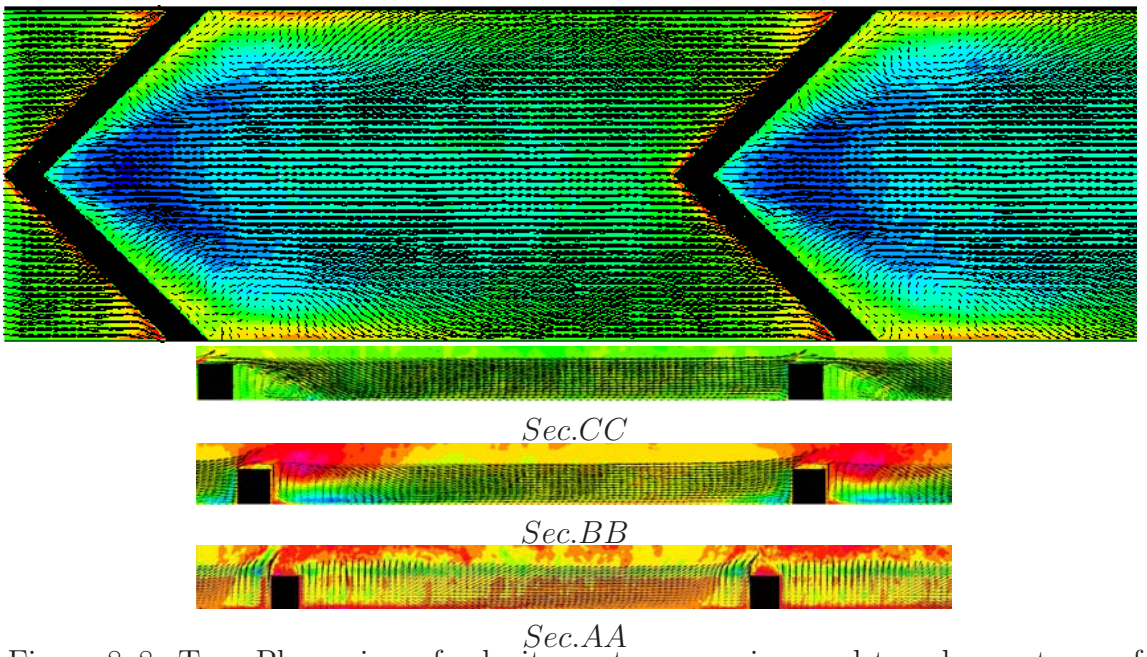

Figure 8–8: Top: Plane view of velocity vectors superimposed to color contours of wall normal velocity. Bottom: Side view of velocity vectors superimposed to color contours of spanwise velocity for $w/k = 15$, $k/h = 0.25$

The intensity of the streamwise velocity at the side wall increases (see Fig.8–7 Sec. AA and Fig. 8–8 Sec. AA). This indicates that part of the flow ejects due to its spanwise motion and the other part follows a streamwise trajectory. The reattached flow continues in the streamwise direction until new ejections occur at the leading edge of the next roughness element. Similar results were found in Leonardi *et al.* (2003) [11] for transverse ribs with high pitch to height ratio.

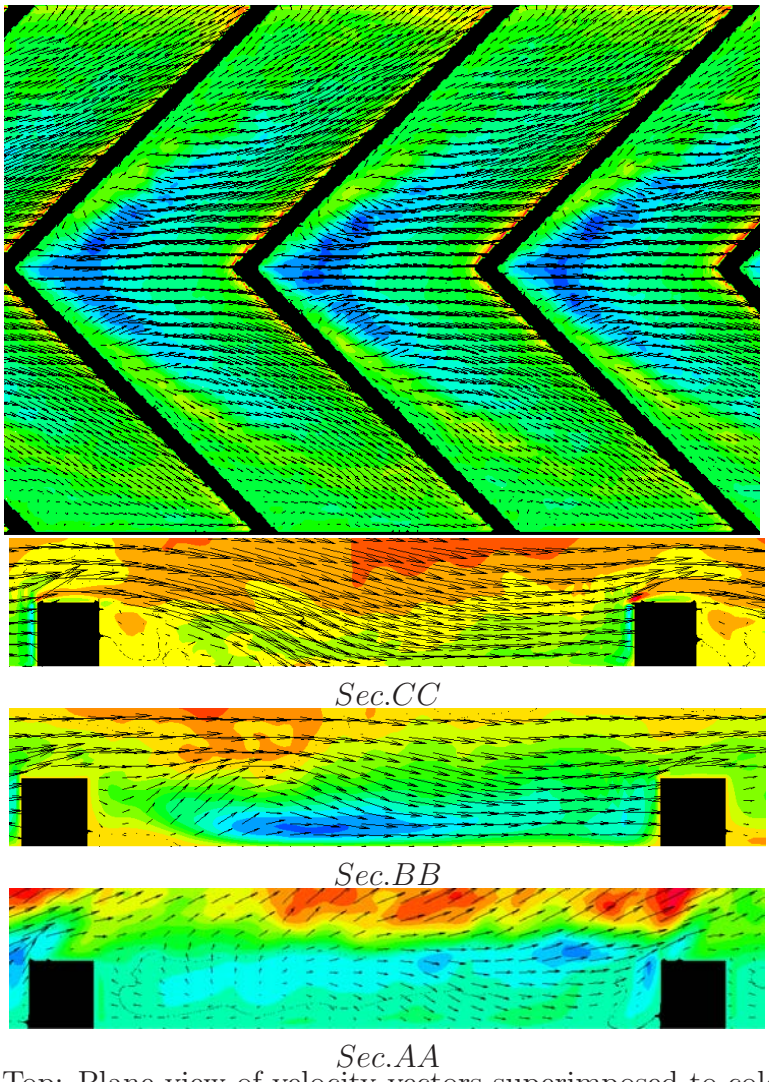

Figure 8–9: Top: Plane view of velocity vectors superimposed to color contours of wall normal velocity. Bottom: Side view of velocity vectors superimposed to color contours of spanwise velocity for $w/k = 8$, $k/h = 0.1$

For large w/k and small roughness elements $k/h = 0.1$, the flow structure has similarities with those relative to $k/h = 0.25$. In Fig. 8–9, the boomerang area, where the flow enters into the cavity, has a geometrical similarity with 8–6. However, the intensity of flow entering the cavity reduces. Sec.CC in Fig. 8–9 shows a recirculation zone at the trailing edge of the roughness element followed by a reattachment on the bottom wall. Side wall ejections decreases compared with lower w/k ratios which agrees with the reduction of inward flow into the cavity.

Sec.AA shows the ejections located at the trailing edge of the turbulators followed by a streamwise oriented flow until the next turbulators is reached.

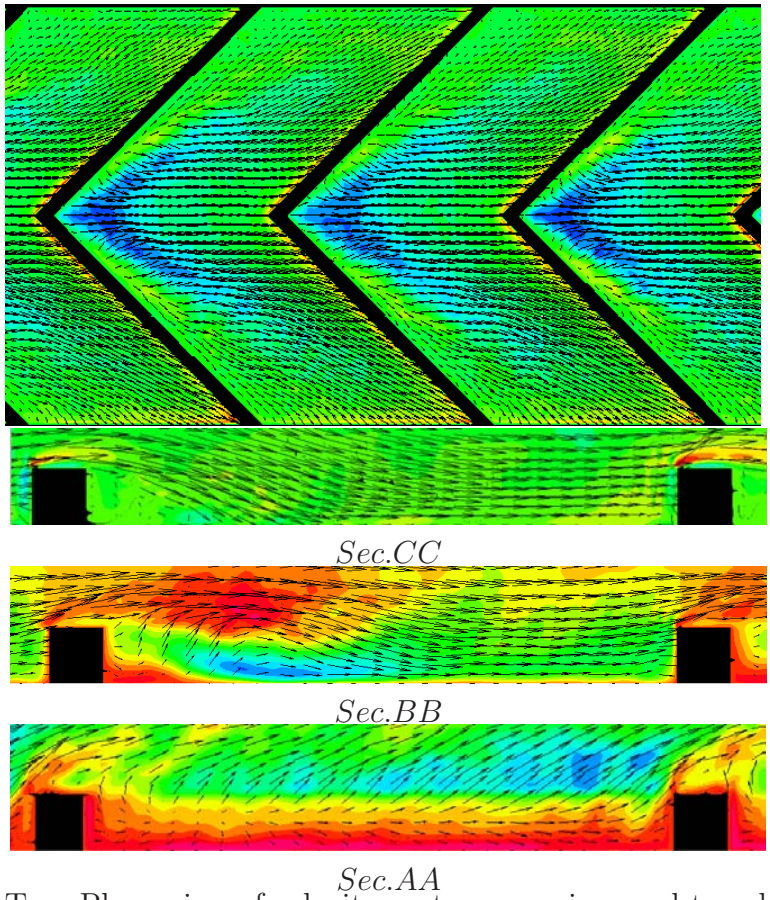

Figure 8–10: Top: Plane view of velocity vectors superimposed to color contours of wall normal velocity. Bottom: Side view of velocity vectors superimposed to color contours of spanwise velocity for $w/k = 10$, $k/h = 0.1$

An increase in the w/k ratio shows a noticeable reattachment of the flow to the wall for sec CC. Recirculation at the trailing edge still occurs for $w/k = 10$ and maintains almost constant for Fig. 8–11. An increase in the angle of the velocity vector to the upward direction is observed in sec.BB and it is maintained as the the w/k ratio increases (see Fig.8–11).

Figure 8–12 shows the streamwise velocity profiles along the normal direction of the channel. The lower and upper walls are respectively at $y = -1$ and $y = 1$. The crests plane is located at $y = +-0.75$ for $k/h = 0.25$, at $y = +-0.9$ for $k/h = 0.1$. With respect to a flat channel, the velocity profile presents inflection

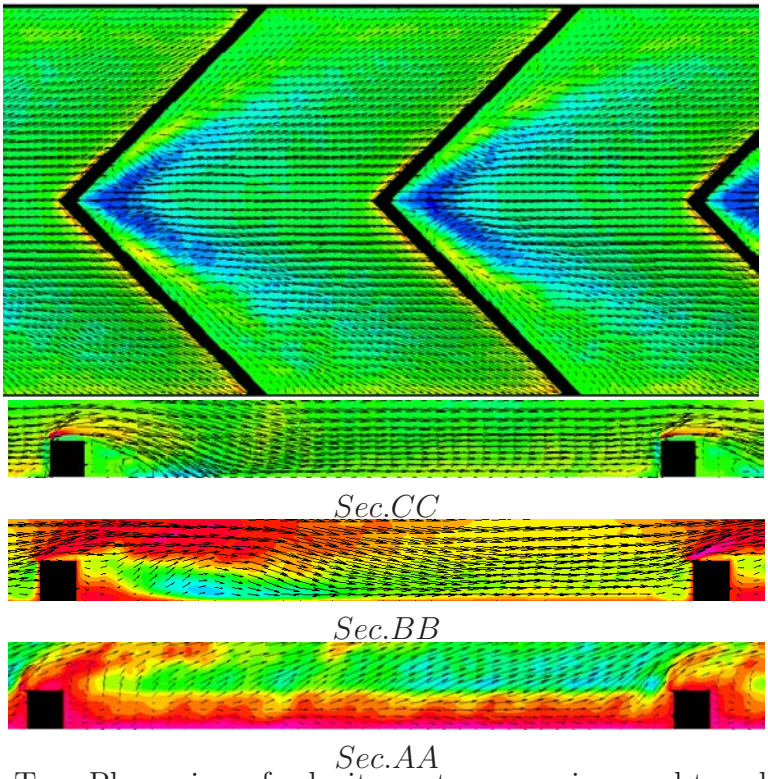

Figure 8–11: Top: Plane view of velocity vectors superimposed to color contours of wall normal velocity. Bottom: Side view of velocity vectors superimposed to color contours of spanwise velocity for $w/k = 15$, $k/h = 0.1$

points near the wall and changes of derivatives. Within the roughness layer (the region from the bottom wall to the crests plane) the momentum of the flow depends strongly on the width of the cavity. Not surprisingly, by increasing the width of the cavity (which means increasing w/k) the flow gradually enters into the cavity and the mean streamwise velocity increases. In fact, for $w/k = 8$ reattachment of the flow starts to increase which promotes the streamwise velocity near the turbulators as shown in Figure 8–12. Moreover, the increase in the separation between the turbulators allows the streamwise velocity to increase reducing the development of the secondary motion in the spanwise direction. At the centerline ($y = 0$) the velocity is maximum for all cases considered. For $w/k = 3$, the momentum is minimum in the roughness layer, therefore the velocity of the overlying flow has to be the largest (recall that velocities are normalized so as to have a constant flow rate regardless of w/k). As the w/k ratio increases, the streamwise velocity increases near

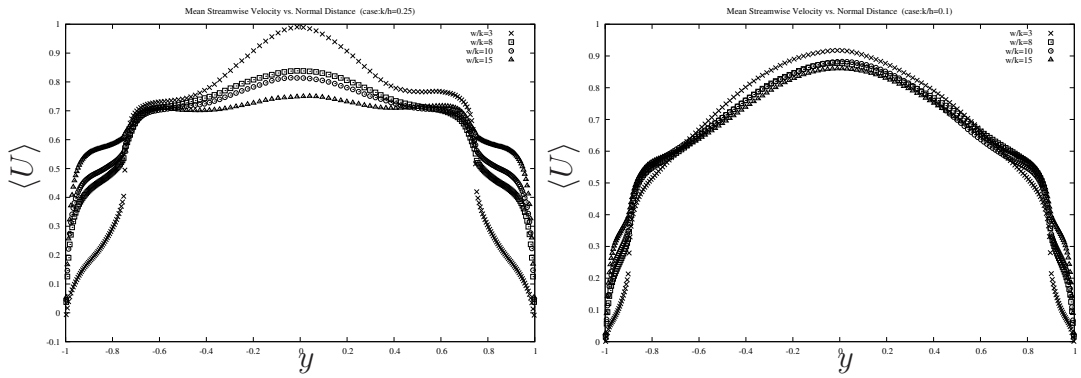

a) $k/h = 0.25$ b) $k/h = 0.1$

Figure 8–12: Streamwise velocity averaged in time and streamwise direction: right $k/h = 0.25$, left: $k/h = 0.1$ for $w/k = 3, 8, 10, 15$

the turbulators and reduces at the center of the channel because of continuity. This increase in the cavity width, increases the reattachment of the flow until it becomes independent of the width of the cavity. For the $w/k = 15$, the streamwise velocity near the turbulators is maximum and at the center of the channel is minimum. For this ratio the flow acts independent of the configuration array. Each turbulators is an independent obstacle and it is not affected by the array of turbulators. The effect of the reduction in the height of the turbulators can be observed in figure 8–12b ($k/h = 0.1$). The momentum within the roughness layer is smaller than that relative to $k/h = 0.25$. Being the turbulators smaller, the flow entering into the cavity is reduced as compared with large elements. A reduction in the height of the turbulators reduces the intensity of the spanwise vortex along the cavity inducing an increase in streamwise velocity. As w/k increases, the secondary motion within the cavity of the turbulators becomes weaker and the streamwise velocity increases.

Figure 8–13 presents the comparison of wall normal velocity color contour for different cavities width w/k and constant ribs height $k/h = 0.25$. By increasing w/k the intensity of the ejections is reduced. As seen in 8–3, the spanwise motion of the fluid particles bounded by the turbulators reduce as the w/k ration increase. This reduction has a direct impact on the intensity of the ejections at the side wall.

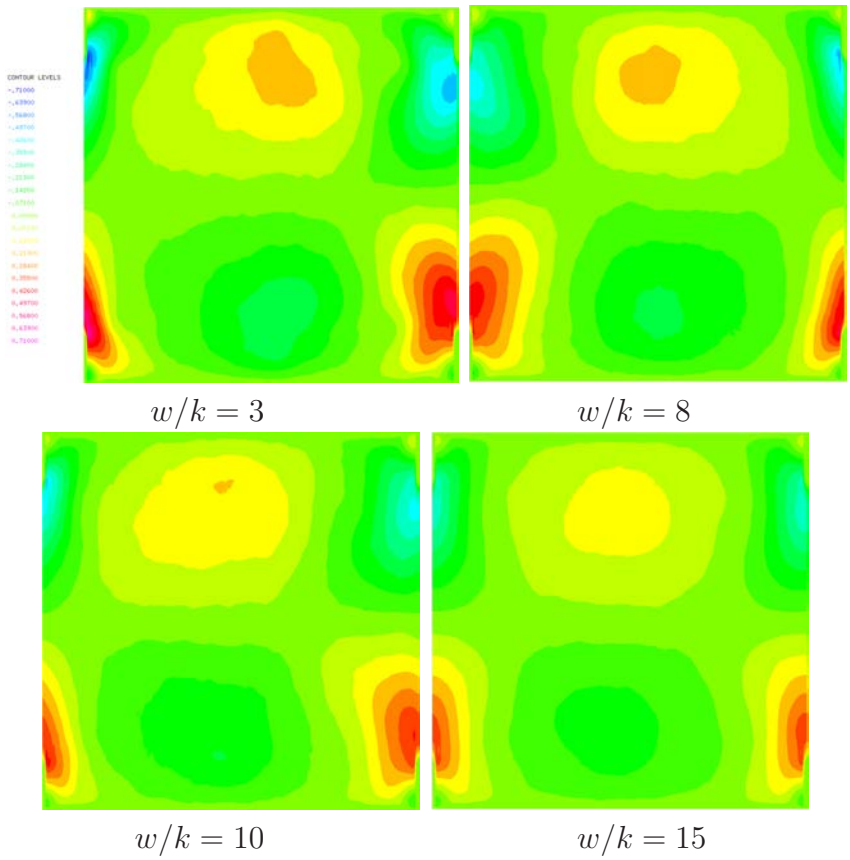

Figure 8–13: Cross sectional view of mean normal velocity for $k/h = 0.25$

Moreover as mentioned before, the ejections are redistributed along the leading edge of the next turbulator. This effect reduces the intensity of the side wall ejections. The increase in the downward velocity due to the flow entering the cavity at the kink of the V-shape becomes independent of the configuration and remains constant as the w/k ratio increases to $w/k = 15$. The case with $w/k = 15$ presents the lowest ejections intensity. This is directly related to the increase in streamwise velocity and reattachment of the flow on the bottom wall.

As k/h decreases, the height of the cavity decreases. This has a direct impact in the amount of flow particles entering the cavity of the turbulators. By decreasing k/h, the quantity of fluid entering into the cavity reduces and then the ejections on the side walls are less intense. For $w/k = 3$, at the kink of the turbulator, a normal-wall velocity smaller than that for $w/k = 3$ and $k/h = 0.25$ is observed (see

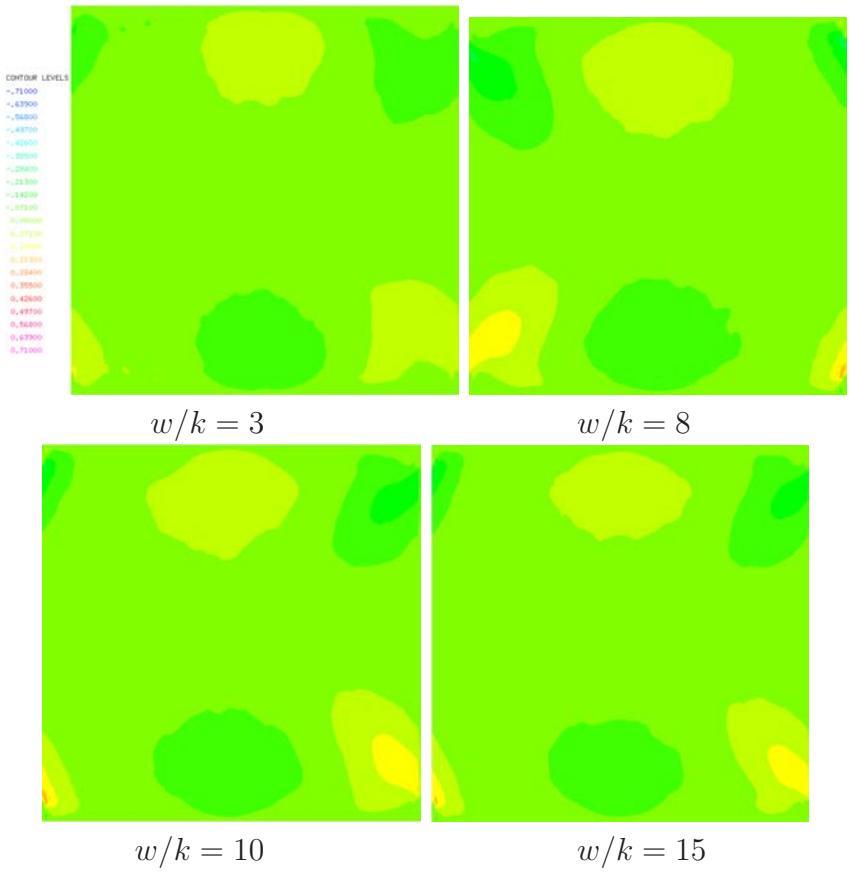

Figure 8–14: Cross sectional view of mean normal velocity for $k/h = 0.1$

Figure 8–13). which reduces the ejection of the flow. The structure of the secondary motion for $k/h = 0.1$ is similar to that for $k/h = 0.25$ with an inward motion at the kink of the turbulator, and an outward motion at the side walls.

The mass of fluid entering into the cavity is divided into two main streams redirected to the side walls (Fig. 8–15a) . Therefore, peaks of spanwise velocity are found near the bottom wall. This is further corroborated by color contours of spanwise velocity (figure 8–15b) Color difference in the figure represents opposite direction of the flow. At the side walls, after ejection occurs, the sign of the spanwise velocity changes. This is the signature of the large-scale counter rotating vortices at top of the crest plane.

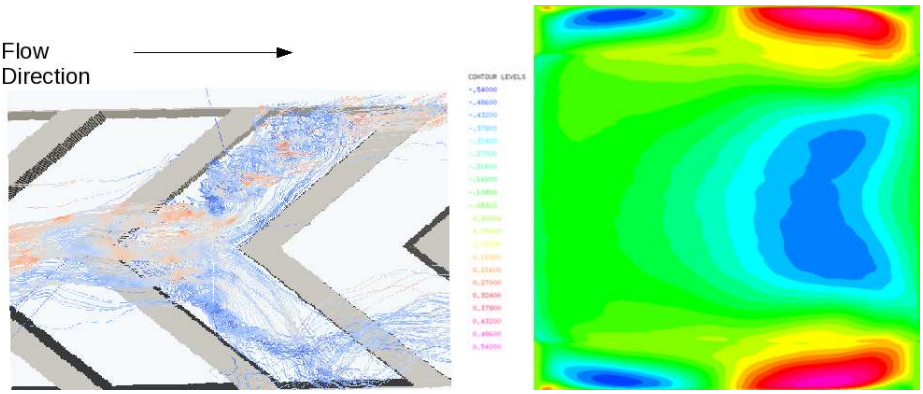

a) b)

Figure 8–15: a)Instantaneous plane view of velocity stream traces along the streamwise and spanwise direction. b)Mean spanwise velocity contours projected on a cross sectional view for $k/h = 0.25$, $w/k = 3$

As the w/k ratio increases, the secondary motion changes in intensity. The spanwise velocity decreases, while the streamwise velocity increases due to the reattachment of the flow into the bottom and top wall. Color contours indicates a change in the spanwise motion can be observe at the center of the channel from $w/k = 3$ to $w/k = 8$. This change is again reversed as the w/k ratio changes form 8 to 10. The intensity of the spanwise motion at the center of the channel oscillates as the w/k ratio increases until a symmetric flow is achieved for $w/k = 15$. This oscillation of the spanwise velocity at the center of the channel intensity shows that the system has stronger stability parameter as the separation between ribs increases. In addition, as the separation between turbulators increases, the mechanism that increases the spanwise velocity decreases. This separation reduces the effect of the incoming flow to the kink of the Vshape and separation of flow in two streams. This reduction can be observed for $w/k = 10, 15$.

A similar secondary motion is observed for $k/h = 0.1$ (smaller ribs height). The decrease in the k/h parameter produces a reduction in the amount of flow particles entering into the cavity of the turbulator. As a consequence of the smaller flow rate within the cavities, the spanwise velocity is less intense as compared with that for $k/h = 0.25$ (Fig.8–17). This effect increases the spanwise velocity and reduces the

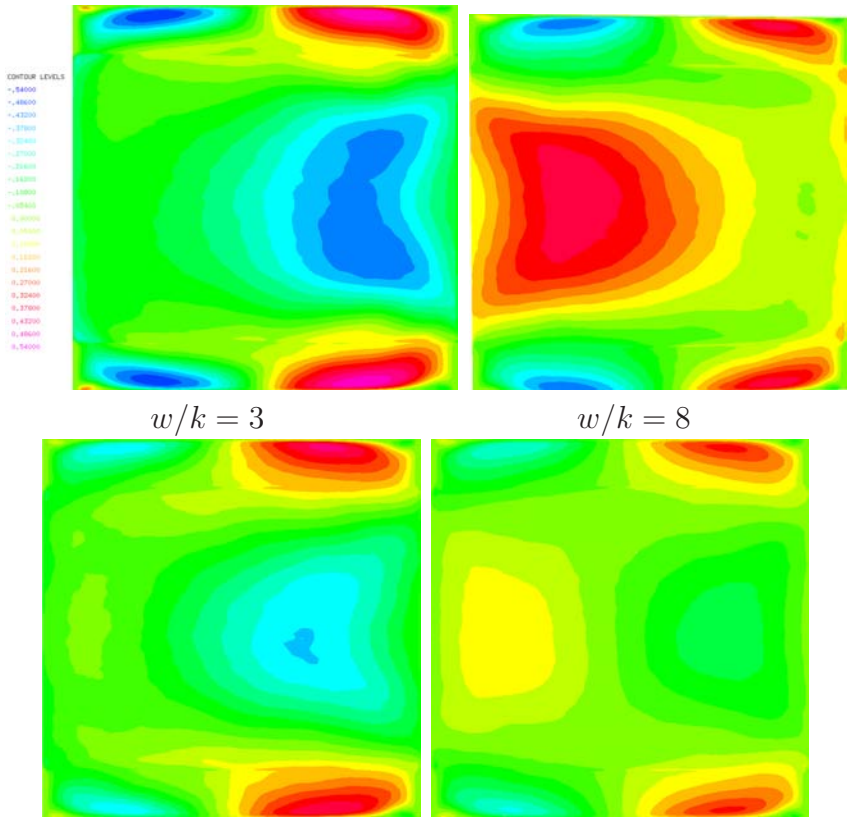

$w/k = 3$ $w/k = 8$

$w/k = 10$ $w/k = 15$

Figure 8–16: Cross sectional view of mean spanwise velocity for $k/h = 0.25$

streamwise velocity. Recirculation in the cavity for $w/k = 3$ promotes the stability of the spanwise vortex generated within the cavity. This spanwise vortex promotes the flow from the center of the cavity to the side walls. As the w/k ratio increases, the strength of the secondary motion reduces and the spanwise velocity decreases. This change can be observed as a color intensity reduction from $w/k = 3$ to $w/k = 15$.

Figure 8–18 shows the contour distribution of the streamwise velocity for $k/h = 0.25$. At the bottom and top wall of the channel the no slip condition is applied reducing the velocity to its minimum as show in Figure 8–18. For the $w/k = 3$ ratio, the streamwise velocity decreases at the location of the turbulators. Since the geometry of the turbulators divide the flow into two stream increasing the spanwise velocity, the streamwise velocity is reduce within the cavity of the turbulators. The maximum velocity is observe at the center of the channel. Due to the large scale vortex generated at the crest of the turbulators, the maximum velocity at the center

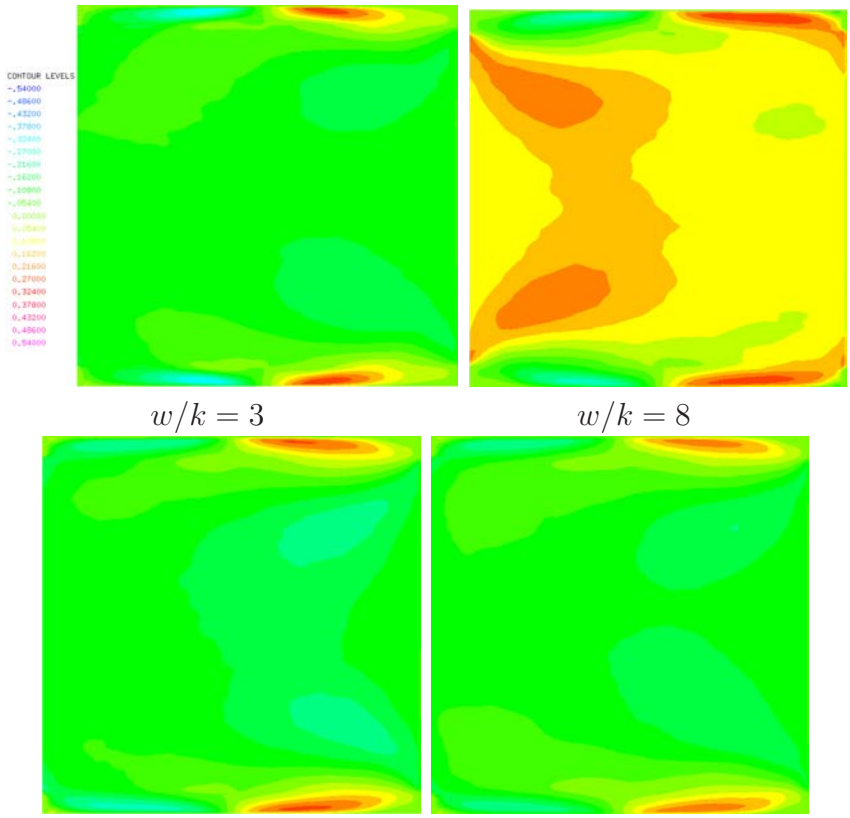

Figure 8–17: Cross sectional view of mean spanwise velocity for $k/h = 0.1$

of the channel reduces. For $w/k = 3$, this reduction can be observe at the right side wall where a vortex is formed at top of the crest plane in to bottom and top wall. As the w/k ratio increases the reduction in streamwise velocity due to the large scale vortex is shifted from side to side due to the effect previously mentioned. The $w/k = 8$ ratio shows the large scale vortex at the left side wall above the crest plane of the turbulators. For this ratio, the streamwise velocity in the center of the channel is reduce as compared with $w/k = 3$. As the distance between rib increases to the $w/k = 10, 15$, the streamwise velocity reduces and the oscillation of the large scale vortex is observed until a symmetric contour is observe for $w/k = 15$

Similar flow structure is presented in Figure 8–19 as compared with $k/h = 0.25$. Streamwise velocity is reduced as compared with $k/h = 0.25$. Oscillations of the large scale vortex follows the same pattern as $k/h = 0.25$which agree with the change in w/k ratio for both $k/h = 0.1, 0.25$. The reduction in the turbulators height

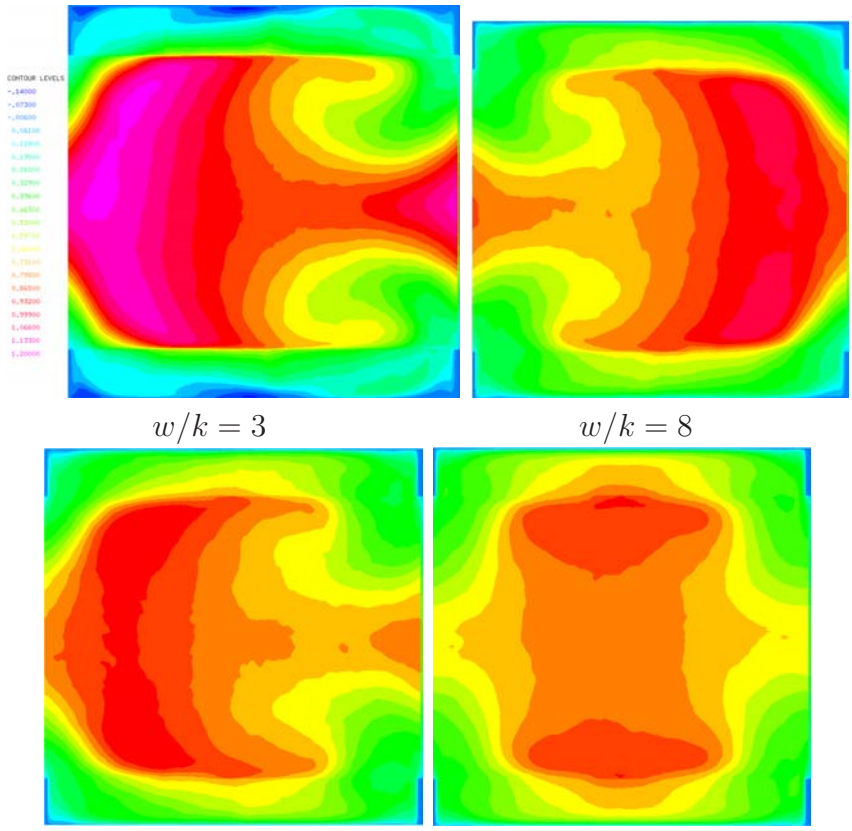

Figure 8–18: Cross sectional view of mean streamwise velocity for $k/h = 0.25$ produces an effect in the symmetry of the flow. As a result of this a difference can be observe in the comparison of the $w/k = 15$ for $k/h = 0.25$ and $k/h = 0.1$. In the case of $k/h = 0.1$ a symmetric structure is not observed which agrees with the antisymmetric flow structure in the spanwise and normal contour on Figure 8–17 and Figure 8–14 respectively.

8.3 FRICTIONAL and FORM DRAG

As well as the heat transfer, the drag plays an important role on the energy conservation along the channel. Due to the geometry of the turbulators changes in heat transfer are obtained which produces at the same time increase in the total drag. The conservation of energy on the entire system can be affected by the total drag produce by the secondary motion. The trade off of enhancing the heat transfer by changing the configuration of the turbulators is the pressure loss along the channel

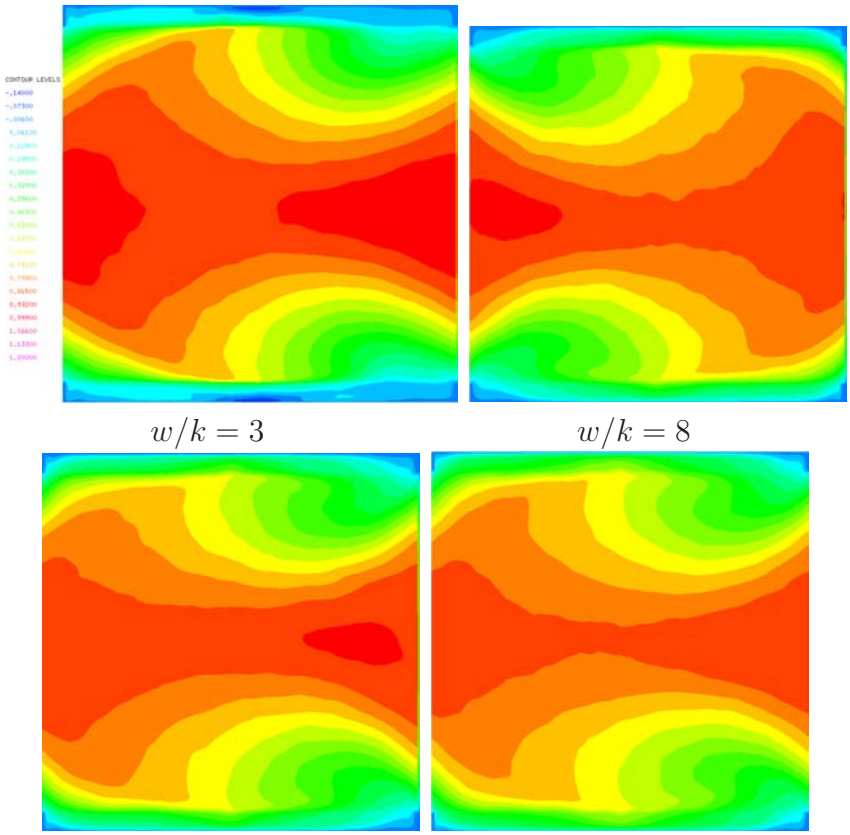

Figure 8–19: Cross sectional view of mean streamwise velocity for $k/h = 0.1$

produced by the drag due to the roughness. In this chapter a drag analysis is performed in order to understand the components of the drag in the system.

8.3.1 Pressure Upstream

First we analyze the pressure applied to the frontal surface of the turbulators. Pressure upstream is calculated at the front face opposing the direction of the mean stream flow. Figure 8–20 shows the pressure upstream distribution along channel in the normal direction. The upstream pressure calculation is considered at the frontal wall normal to the turbulator where the turbulators geometry is located. The highest pressure is obtained at the bottom wall within the cavity of the turbulators and decreases as it reaches the crest plane. Similar effect occurs at the upper wall where the pressure ranges from a minimum at the crest plane to a maximum at the top wall within the cavity of the turbulators. The turbulators represent an obstruction of the flow in the streamwise direction which generates a pressure gradient. At

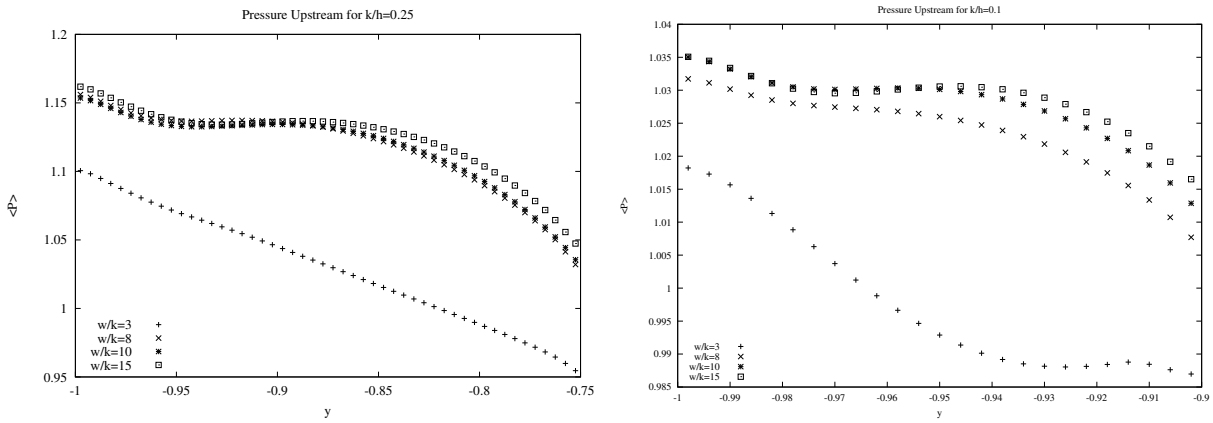

$k/h = 0.25$ $k/h = 0.1$

Figure 8–20: Pressure Upstream along the wall normal direction for $k/h = 0.25$ for $w/k = 3, 8, 10, 15$

the leading edge of the turbulators, an stagnation point is generated in which the streamwise velocity reduces and the normal velocity increases. Due to the angle of the V-shape, recirculation in this zone is not observe, but instead the spanwise vortex is produced. This spanwise vortex reduces the pressure at the frontal face of the roughness element. As the w/k ratio decreases, the upstream pressure decreases with a minimum at $w/k = 3$. Since for $w/k = 3$ shows the high intensity secondary motion as showed in previous chapter, the pressure for this ratio is the minimum. For the increase in w/k ratio, reattachment of the flow occurs and the spanwise vortex reduces which produces an increase in pressure at the normal face of the turbulator. As the normal direction increases the pressure is relief until a minimum is reach at the crest plane.At the middle portion of the turbulators an inflection point occurs showing a local increase in pressure followed by a continuous decay until the minimum is achieved. This effect is due to the redirection flow particles to the spanwise direction in the mid-height of the turbulator due to the angle of contact.Maximum upstream pressure is achieved for $w/k = 15$. This maximum is due to the effect previously mentioned in which for higher cavities the turbulators behaves as independent obstacles and not as an array of turbulators.

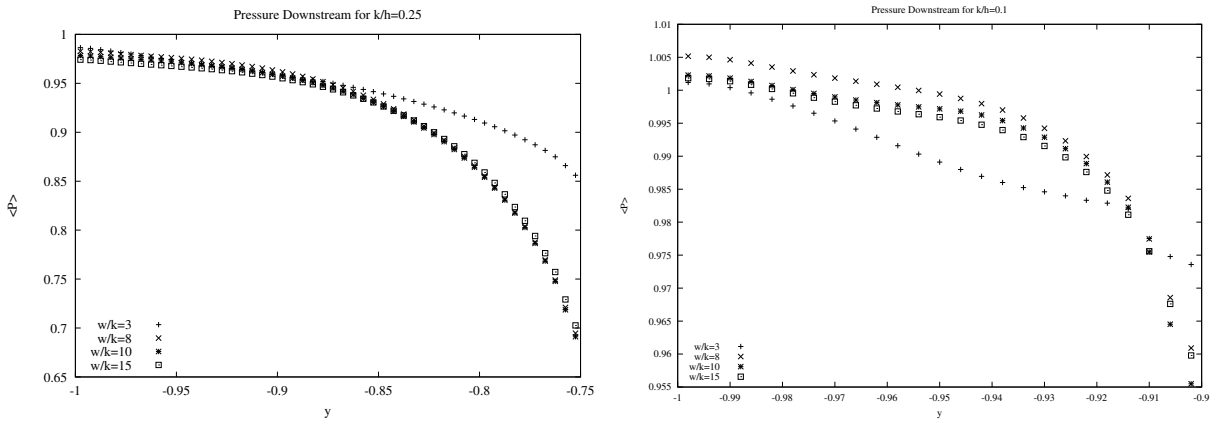

$k/h = 0.25$ $k/h = 0.1$

Figure 8–21: Pressure Downstream along the wall normal direction for $k/h = 0.25$ for $w/k = 3, 8, 10, 15$

8.3.2 Pressure Downstream

As well as the pressure upstream, the pressure downstream is calculated in figure 8–21 at the back face of the turbulator with the normal direction parallel to the mean stream flow. The downstream pressure is considered only where the geometry is located. As compared with figure 8–20 similar effect in reduction of pressure is observed from the cavity to crest of the turbulators. At the bottom of the cavity the pressure downstream is the highest and it reduces as the normal distance increase towards the crest plane. The decrease in the height of the turbulators reduces the area of contact in which the fluid impinges to produce a pressure gradient. This effect reduces the pressure in overall.As the w/k ratio decreases, the upstream pressure decreases because of the flow structure effects similar to $k/h = 0.25$.For this pressure profile no inflection point is observed as compared with the pressure upstream. The reduction in the cavity reduces the recirculation zone at the leading edge of the turbulator which reduces the redirection of the flow in order to produce a inflection point. For $k/h = 0.1$ a continuous decay of the pressure can be observed in figure 8–21.

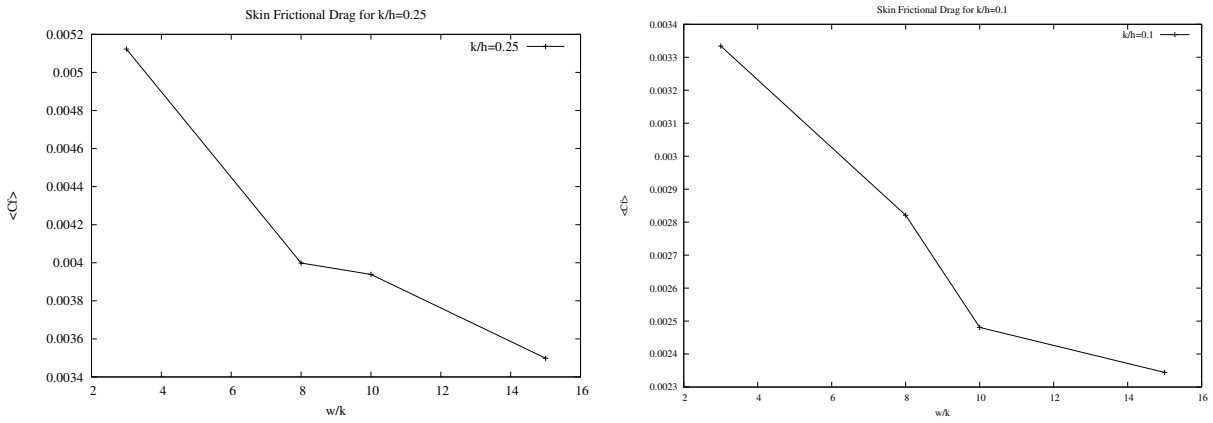

$k/h = 0.25$ $k/h = 0.1$

Figure 8–22: a)Skin frictional drag for $k/h = 0.25, 0.1$ and $w/k = 3, 8, 10, 15$.

8.3.3 Skin Friction Drag

Friction drag is the part of the drag that is due directly to the shear stress τ_w, on an object (see B. R. Munson (2002) [29]). In this case, the surface to be taken into consideration is the surface parallel to the upstream velocity. If the surface us perpendicular to the upstream velocity, the shear stress does not contribute to the frictional drag.

High shear stress $\frac{\partial u}{\partial y}$ can be found along the surface of the turbulators. This produces the skin frictional drag which is one of the components of the total drag on the system. The non-dimensional skin frictional is given by the formula:

$$C_f = \frac{1}{Re}\frac{1}{A}\int \frac{d < \overline{U} >}{dy} * da \tag{8.1}$$

where A is the total plane area and da is the infinitesimal area along the surface of the turbulators. The results in figure 8–22.a for several $w/k = 3, 8, 10, 15$ with $k/h = 0.25$ show the total skin friction in the channel. The contribution of the friction factor C_f was calculated over the surface of the entire set of turbulators including the wall. Maximum velocity gradient are observe for $w/k = 3$ due to the high intensity of the secondary motions for this ratio. The spanwise vortex that travels through the surface of the wall produces a high streamwise velocity gradient

which is reflected in high skin frictional drag. As the w/k parameter decreases the frictional drag decreases until it reach a minimum. For higher w/k ratios, the reattachment of the flow promotes the increase of streamwise velocity which reduces the high shear ratio.

For a decrease in height of the turbulators to the $k/h = 0.1$ a reduction in the skin friction is observe for all values of w/k. Reduction in secondary motion along the cavity of the turbulators are showed in 8–3. The spanwise vortex form for the $k/h = 0.25$ is altered for the present ratio, therefore the shear stress is reduce. The geometrical configuration of the cavity for a small rib height does not reduces the spanwise motion, therefore different flow structure is observe. The flow structure obtained for this ratio provides a lower shear stress than for the $k/h = 0.25$. As the w/k ratio increases these flow structures reduces increasing the streamwise velocity and promoting reattachment. Similar decedent behavior is observed for $k/h = 0.1, 0.25$

The drag distribution along spanwise direction is showed in fig.8–23. Different section are taken into consideration using as a reference the three sections on view on 8–3 from the mean chapter flow. For section CC the flow enters the cavity of the turbulators generating with velocity gradients at the crest plane of the turbulators. At the leading edge of the turbulators in the location of the crest plane high shear stress is observe due the interaction of the mean stream flow from the center of the channel with the to of the turbulators. This effect varies along the top surface of the turbulators due to the flow redirection. The at the top of the turbulator is redirected into a normal direction since it approaches the cavity of the turbulators. Once the flow reach the cavity of the turbulators the streamwise velocity reduces drastically increasing the normal velocity and reducing the shear stress at the trailing edge of the turbulator. Along the cavity of the turbulators negative values of the skin friction are observe due to the recirculation of the flow close to the trailing edge

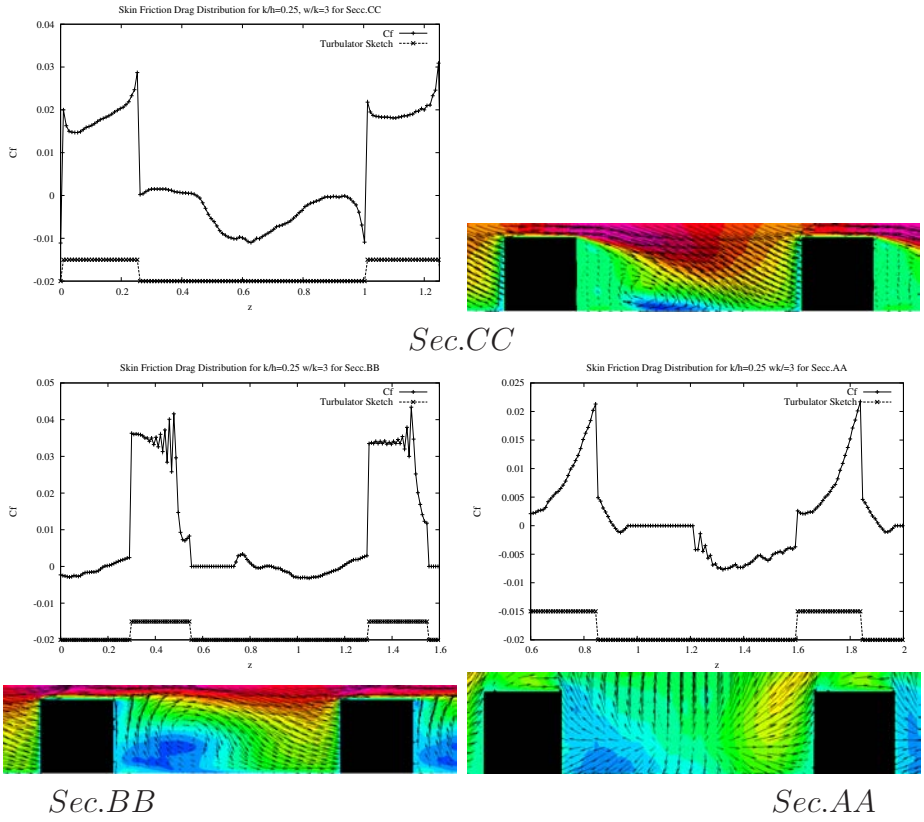

Figure 8–23: Skin frictional drag distribution and streamwise velocity contours along streamwise direction for $k/h = 0.25$ and $w/k = 3$.

of the turbulators. Streamwise velocity contour in section CC show a low intensity color at the location of the recirculation. As the flow approaches the leading edge of the next turbulator, the shear stress starts to increases from negative values to positive values because recirculation is no longer present. At the leading edge of the next turbulator a shear stress spike is observe due to the encounter of the flow with the turbulators. The behavior of the skin friction drag is similar in the consecutive roughness elements.

As the flow moves along the spanwise direction different skin friction distribution is observed ins section BB. At the crest plane location, close to the leading edge, velocity gradient are the highest due to the interaction of the mean stream flow at the center of the channel with the top of the turbulator. As the particle approaches the trailing edge of the turbulator an oscillatory behavior is observe. Since at this

section the spanwise motion dominates the transporter of particles in the cavity, a difference with respect with section CC is observed in terms of the skin friction is observed at the trailing edge. Instead of a sudden from of the skin friction, a transition occurs with the variation of the shear stress in an oscillatory motion until the variation of the streamwise velocity reduces to zero at the bottom wall. At the location of the spanwise vortex, a change from positive to negative skin friction is observe as the streamwise distance increases. At the location of the leading edge of the next turbulator, a skin friction spike is obtained due to the high variation in the streamwise velocity from bottom wall to crest plane.

Close to the side wall at section AA the skin friction reduces and a different behavior is observed in figure 8–23. Shear stress spikes still occurs at the crest plane of the turbulators without an uniform distribution. Ejections as the location of the sidewall increases the change in the streamwise velocity. The superimpose vectors on the velocity contour shows a redirection of the flow from the top of the turbulator close to the trailing edge. Velocity vectors change from streamwise direction to normal direction at the entrance of the cavity. This generates reduction in the streamwise velocity which reduces the skin friction drag. Along the cavity of the turbulators the streamwise velocity varies from negative to positive which is reflection in section AA of the skin friction. At the leading edge of the next turbulator, the shear stress starts to increase due to the interaction of the mean stream flow at the center of the channel.

As the w/k ratio increases similar effects are obtained. For $w/k = 8$ (see fig. 8–24) high shear rate is present at the crest plane of the turbulators. Section CC shows similar behavior in terms of the increase and decrease in the shear rate at the top of the turbulator. As the flow approaches the cavity, recirculation occurs and the gradient of the streamwise velocity decreases. The increase in the streamwise direction shows the development of the recirculation zone which produces high shear

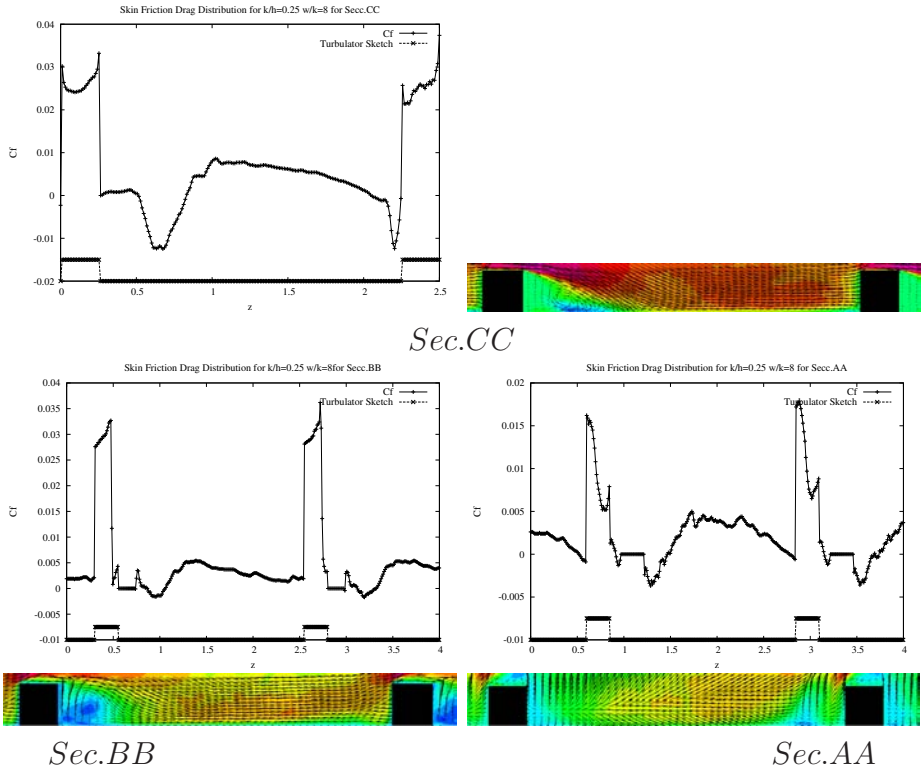

Figure 8–24: Skin frictional drag distribution and streamwise velocity contours along streamwise direction for $k/h = 0.25$ and $w/k = 8$.

rate at the trailing edge in the negative region. The reattachment of the flow after the recirculation zone produces a small decay of the skin friction. At the leading edge of the next turbulator high negative vales are followed by a raise in the velocity gradient. The negative values at this streamwise location are due to the reattachment and reduction of the streamwise velocity close to the leading edge of the next turbulators. The high increase in skin friction is due to the flow interaction with the mean stream flow from the center of the channel at the top of the turbulators. The effect of the peak value at the top of the turbulator is similar to the $w/k = 3$ ratio.

In terms of section BB, the effects of the dissipation of the spanwise vortex into ejections and injections of the flow is observed after the trailing edge of the turbulator. This effect produces positive and negative peaks as shown in section BB (see fig. 8–24). After ejections and injections passed a descended behavior of the

shear stress is observed until the flow reaches the next turbulator. The leading edge of the next turbulator present a increase of the velocity gradient until the maximum value is obtain.

As the flow particles moves to the side wall of the cavity (see see fig. 8–24 section AA) different effects are observed. An overall reduction of the skin friction values is obtain due to the secondary motions at this locations. The ejections at the side wall reduces the streamwise direction and increases the normal direction which produces a reduction in the velocity gradient close to the side walls. At the center of the cavity an increase in the streamwise velocity can be observed in the color velocity contour due to the reattachment of the flow. At the leading edge of the next turbulator an increase in the velocity gradient is obtained due to the interaction with mean stream flow. This interaction produces the highest value of skin friction for the configuration.

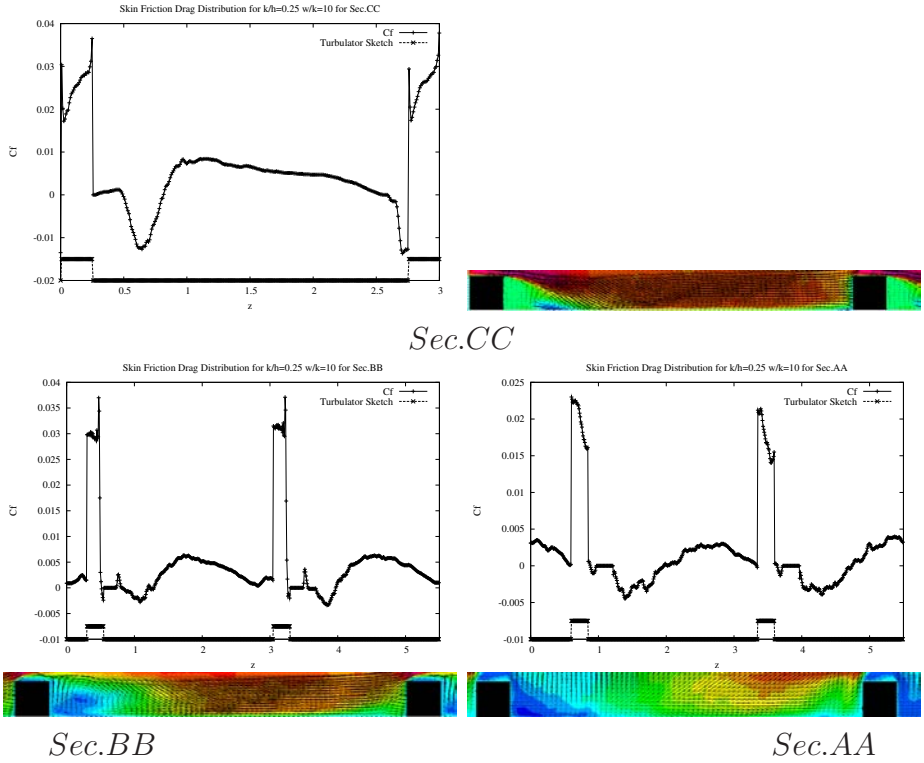

Figure 8–25: Skin frictional drag distribution and streamwise velocity contours along streamwise direction for $k/h = 0.25$ and $w/k = 10$.

As the w/k ratio increases to $w/k = 10, 15$ in figure 8–25 and 8–26 similar effects can be observe. In section CC, the recirculation zone becomes independent of the distance between the ribs and the reattachment form after the recirculation zone ends. In the skin friction plot can be observed that at the crest plane of the turbulators the highest values of streamwise velocity gradient are observed. After this location a drop to zero of the skin friction is observe due to the reduction of the streamwise velocity as a direct effect previous to recirculation. A negative values are obtained due to the negative direction of the velocity produces by the recirculation. After the recirculation velocity gradient begins to reduces until a minimum is reached at the leading edge of the next turbulator. Once again, a high peak of the shear stress is obtained at the crest plane due to the interaction between the mean stream flow and the top of the turbulators.

As the spanwise distance increase different effects are observed. Figure 8–25 and 8–26 section BB shows injections and ejections at the trailing edge of the turbulators which generates positive and negative values of shear stress. The secondary motion at the trailing edge of the turbulators becomes independent as the w/k distance increases. This effect produce similar skin friction profiles between $w/k = 10$ and $w/k = 10$. In the comparison between the roughness element of higher pitch distance the remarkable difference is showed on the over magnitude of their maximum values at the crest plane. This shows that for the section under study (section BB) the skin friction drag decreases as the w/k ratio increases. As the streamwise distance increases similar profiles is observed between the ratios in comparison. At the leading edge of the next turbulator an increase in the skin friction is obtained due to the interaction with the mean stream flow which has higher streamwise velocity than the flow particles in the cavity.

For the section AA in the figure 8–25 and 8–26 a decrease in the skin friction is observe for both $w/k = 10, 15$. At the leading edge of the turbulator a peak of

maximum value for shear stress is reached. This peak starts to decreases as the streamwise direction increases at top of the crest plane. At the trailing edge of the turbulator a drop of the velocity gradient is observed due to the backward velocity at this location. This backward velocity can be observed in the velocity color contour by the low intensity color in the leading edge of the turbulators. as the streamwise distance increases the velocity gradient increases from the negative values to positive values. As the streamwise distance reaches the leading edge of the next turbulator a increase to a maximum value is obtain due to the interaction of the crest plane with the mean stream flow. This effect is similar with the $w/k = 3, 8$ previously mentioned.

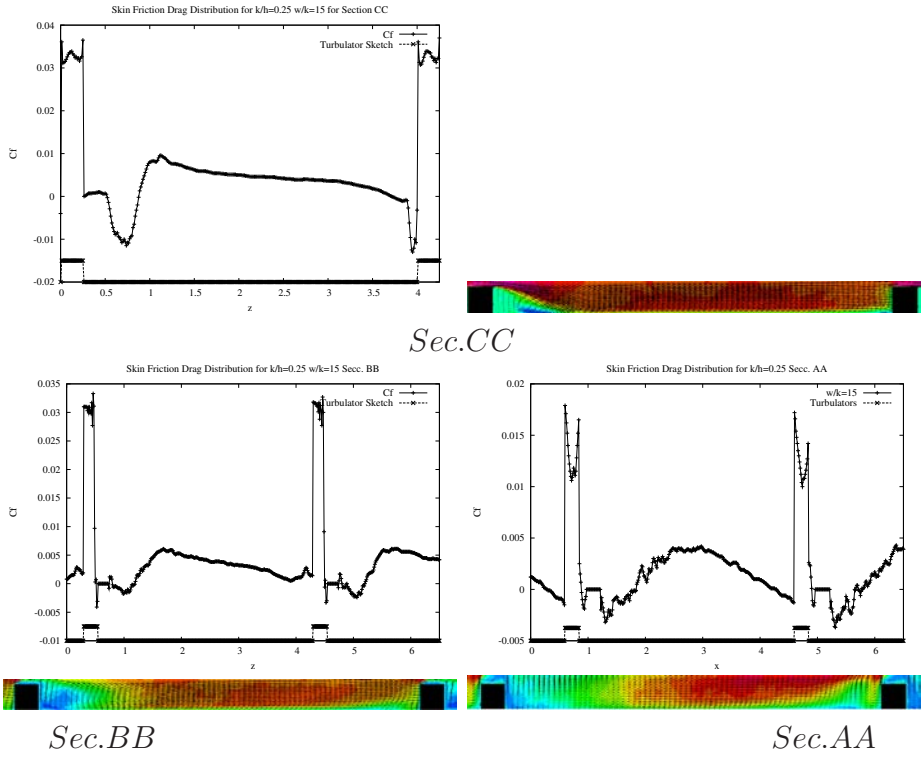

Figure 8–26: Skin frictional drag distribution and streamwise velocity contours along streamwise direction for $k/h = 0.25$ and $w/k = 10$.

8.3.4 From Drag

As well as the skin frictional drag, the form drag is the component of the drag that is due directly to the pressure on th turbulators. It is named form drag because

of its strong dependency of the shape or form of the turbulator (P. Kundu (1990) [30]).In this case the flow oriented in the perpendicular direction of the turbulator contributes to the form drag. In other words, the form drag is a function of the magnitude of the pressure and the orientation of the surface element on which the pressure force acts.

The non-dimensional form drag was calculated according to the formula:

$$P_d = \frac{\int (\overline{p_u} - \overline{p_d}) * ds}{A} \tag{8.2}$$

where A is the plane area along the streamwise direction, ds is the area normal to the surface of the turbulator, p_u and p_d are the pressure upstream and downstream respectively. The difference in upstream and downstream pressure results on the pressure gradient in each of the turbulators where the form drag is calculated.

Figure 8–27 shows the total pressure drag calculated along the channel. Since the form drag is highly dependent of the form or shape of the turbulator, we can observe that as higher the height of the rib, higher is the form drag. In terms of the separation between ribs, can be observe that the increase on w/k reduces the form drag. This effect is due to the flow structure and the impingement of the flow into the leading edge of the rib elements. As mentioned in the mean flow chapters, higher ejections are found close to the side walls for the $w/k = 3$ case. This means that due to the spanwise vortex that transport the flow particles to the side walls, the flow is prevented to impinge directly onto the leading edge of the turbulator after being injected into the cavity. The highest ejections of the flow are found for this case. The increase of w/k shows a decrease on the intensity of the ejections as showed in 8–4 which means that the fluid is impinging the leading edge of the turbulators with less pressure than for lower rib separation. This effect explain the descend of the form drag as the separation of the turbulators increase.

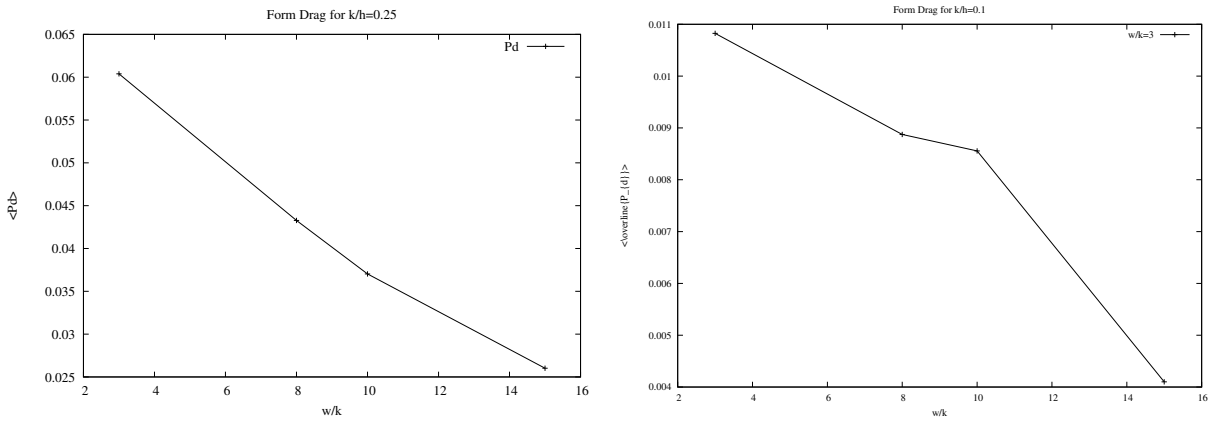

$k/h = 0.25$ $k/h = 0.1$

Figure 8–27: a)Form drag along the wall normal direction for $k/h = 0.25, 0.1$ and $w/k = 3, 8, 10, 15$.

8.3.5 Total Drag

The sum of the skin friction and form drag represents the total drag along the channel due to the geometrical configuration. As shown in figure 8–42 the greatest contribution to the total drag is represented by the form drag reaching a maximum for the $w/k = 3$ configuration. As the w/k decreases the total drag decreases following the same behavior as the skin friction and form drag. The combined effects that case the flow behavior for the skin and form drag previously mention are the product of the behavior on the total drag. In terms of the scale, the friction drag represent a small portion of the total drag as compared with the form drag shown in 8–42. For the parameter $w/k = 3$ the contribution of the geometry to the drag is of greater significance since a large portion of turbulators over the channel are obtained for the same streamwise distance. As the w/k ratio increases for the same horizontal area the quantity of turbulators decreases. This is proportional to the decrease in the form drag for the $w/k = 8, 10, 15$. The decrease in the turbulators high decreases the total drag due to the effects previously mentioned.

Fig. 8–29 summarizes the total drag for $k/h = 0.1, 0.25$ with all ratios. The configuration of $k/h = 0.25$ produces the higher total drag for all w/k ratios. A

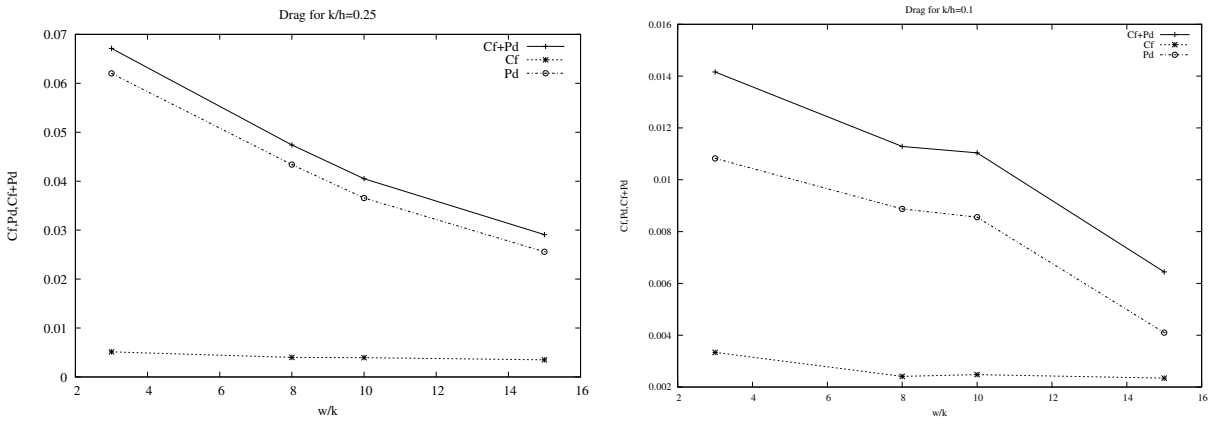

$k/h = 0.25$ $k/h = 0.1$

Figure 8–28: Total Drag along the wall normal direction for $k/h = 0.25, 0.1$ for $w/k = 3, 8, 10, 15$

peak is reaches for the $w/k = 3$ and its value decreases as the separation between ribs decreases which decreases the secondary motions in the flow.

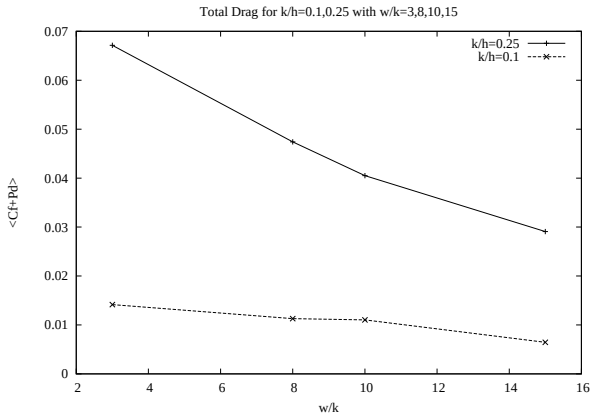

Figure 8–29: Total Drag along the wall normal direction for $k/h = 0.25, 0.1$ for $w/k = 3, 8, 10, 15$

8.4 TURBULENT INTENSITIES

8.4.1 Turbulent intensities for $w/k = 3$

Turbulent intensities for the $k/h = 0.25$ with $w/k = 3$ are presented in Figure 8–30. The relation that exists between the increases and decreases in the different velocities shows the variation of secondary motions along the normal direction. The increase in turbulent intensity of spanwise velocity along the cavity of the turbulators shows an increase due to the division of the turbulators into two streams. The

coherent structure within the cavity of the turbulators is due to a spanwise vortex which transports the flow particles from the center to the side walls. At the center of the channel the spanwise velocity reduces to its minimum since the flow at this location is mostly in the streamwise direction. In terms of the wall normal velocity, a peak is observed at the crest plane of the turbulators where ejections of flow particles from the cavity to the mean stream flow take place near the side walls. This increase is followed by a decrease in wall normal velocity at the center of the channel where the flow is mainly in the streamwise direction. In terms of the streamwise velocity, an increase is observed at top of the crest plane of the turbulators. This increase is due to the large scale vortex in the streamwise direction due to interaction of the ejected flow in the wall normal direction and mean stream flow in the streamwise direction. The core of the vortex at the crest plane of one turbulators present turbulators is connected to the core the next and previous set of turbulators which allows the large scale vortex structure to travels along the channel in the streamwise direction.

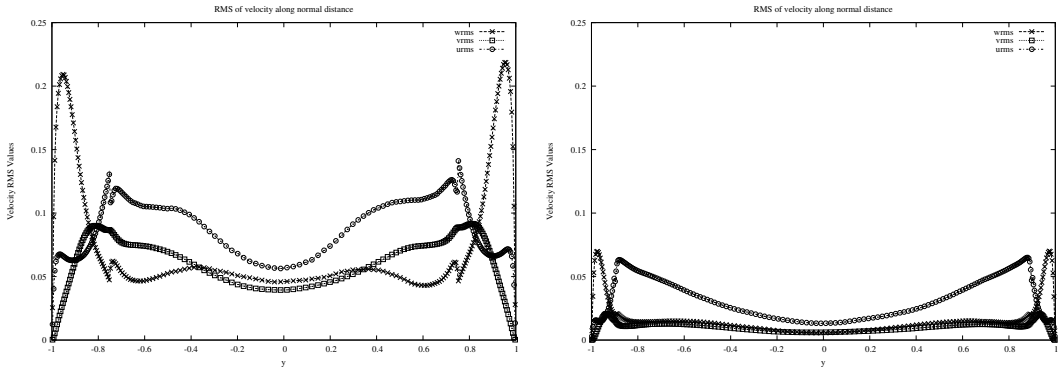

$k/h = 0.25$ $k/h = 0.1$

Figure 8–30: Turbulent intensities for three velocity components (u, v, w) for $k/h = 0.25$ and $k/h = 0.1$ for $w/k = 3, 8, 10, 15$

A reduction in the turbulators height reduces the turbulence intensities in overall as seen in 8–30 for $k/h = 0.1$. The spanwise velocity shows similar velocity profile in $k/h = 0.25$. Due to the spanwise vortex, the spanwise velocity increases in the cavity of the turbulators and decreases as it reaches the center of the channel where streamwise motion dominates. In case of the normal velocity, an increase in velocity

is observed due to the ejections located at the side walls of the cavity. The normal velocity reaches its minimum at the center of the channel. In the case of the streamwise velocity, a maximum is located at top of the crest plane where similar effect of the transverse vortex occurs as compared with $k/h = 0.25$. Since for $k/h = 0.1$ the geometrical configuration of the turbulators is less that the $k/h = 0.25$, similar coherent structures are presented in the channel with a reduced intensity.

8.4.2 Turbulent intensities along the normal direction

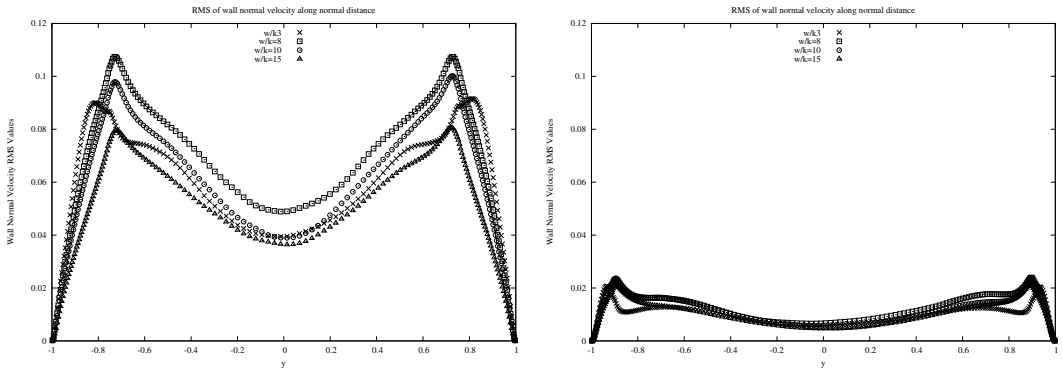

$k/h = 0.25$ $k/h = 0.1$

Figure 8–31: Turbulent intensities along the normal direction for $k/h = 0.25$ and $k/h = 0.1$ for $w/k = 3, 8, 10, 15$

Turbulent intensities for the wall normal velocity shows that at the location of the side walls, the variation from the average velocity is the highest due to the secondary motion. Ejections increases the normal velocity at the side walls as show in Figure 8–31. Wall normal turbulent intensities decrease to a minimum at the center of the channel where the flow is mainly in the streamwise direction.

8.5 MEAN TEMPERATURE

Figure 8–32 show the temperature distribution along the normal direction. The boundary condition for the bottom wall of the channel is set to be non-dimensional $T = 1$ which makes reference to the hot wall. The boundary condition for the top wall of the channel is $T = -1$ which makes reference to the cold wall. These boundary conditions allows the channel to present a temperature distribution in decedent behavior from bottom to top wall. The purpose of the boundary condition

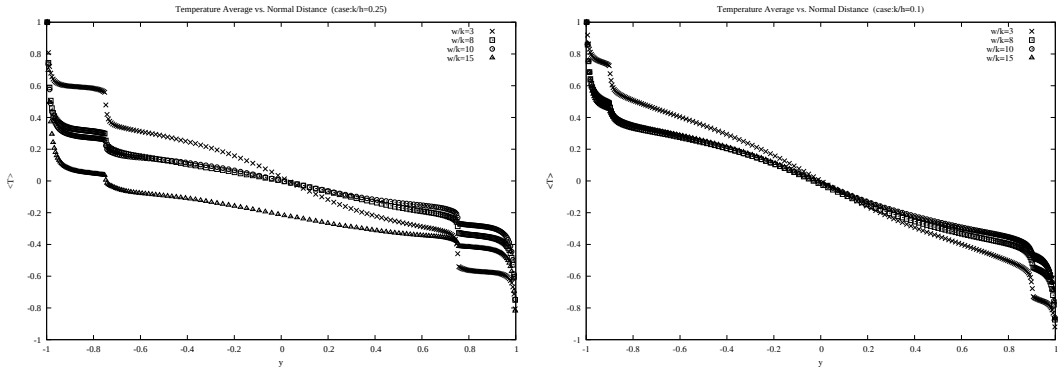

$k/h = 0.25$ $k/h = 0.1$

Figure 8–32: Normal Velocity profile for $k/h = 0.25$ and $k/h = 0.1$ for $w/k = 3, 8, 10, 15$

is to establish the temperature distribution in order to measure the heat transfer from the bottom to the top wall. In addition, for the turbulators located at the top wall temperature has an uniform distribution of $T = -1$. Opposite asseveration is done in the turbulators of the lower wall where the temperature is $T = 1$. These boundary conditions allows the study of the effect of the turbulators in the heat transfer analysis. For $k/h = 0.25, 0.1$ the effect of the turbulators in the temperature profile can be observe in the Figure 8–32 as a constant temperature profile along the k/h distance away from the wall.

Superimpose velocity vectors over the mean temperature contour is shown in figure 8–33. The direction of the velocity vectors shows a vortical pattern which makes reference to the large-scale vortex as a secondary motion at top of the crest plane as shown in figure 8–4.b. In case of the temperature, it can be observe that the area around the vortex is at higher temperature above the crest plane than everywhere else in the center of the channel. This indicate that a mixing of flow particles of high and low temperature are taking place at the location of this secondary motion.

In terms of the $k/h = 0.1$, velocity vectors over the mean temperature contour is shown in figure 8–34. Similar flow structure occurs for this case with a reduction in the intensity of the secondary motion. The direction of the velocity vectors shows a vortical pattern at the bottom and top wall similar to the $w/k = 0.25$, but with a

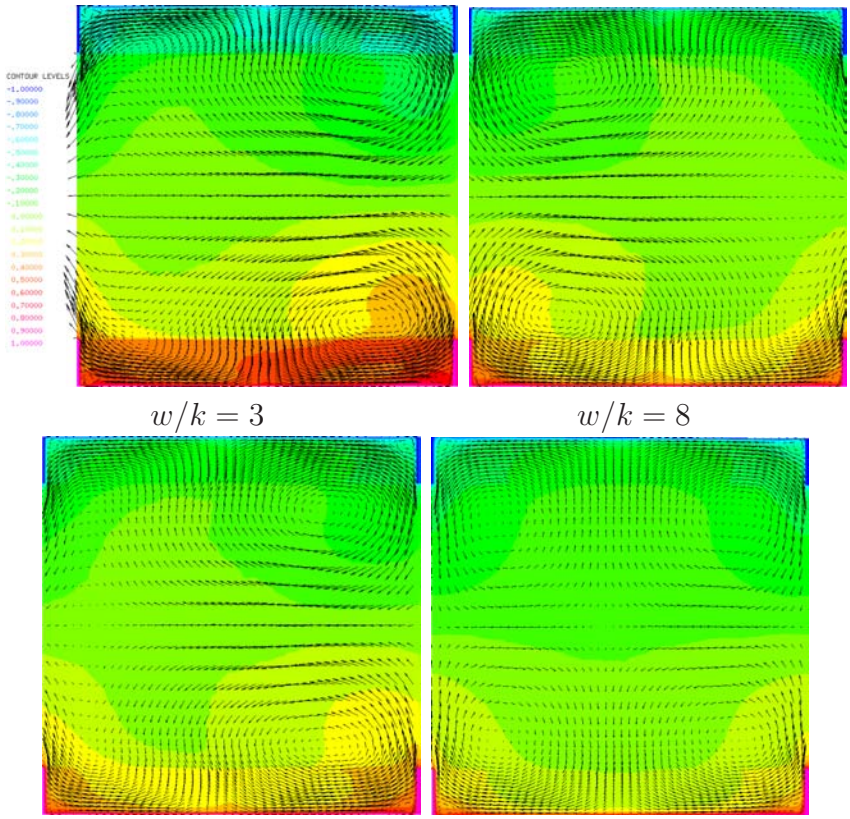

Figure 8–33: Cross sectional view of mean temperature for $k/h = 0.25$, $w/k = 3, 8, 10, 15$

reduction in the ejection intensity at the side walls. In case of the temperature, it can be observe that close to the wall higher temperature is found and are around he vortex is at higher temperature above the crest plane than everywhere else in the center of the channel. As well as in the $k/h = 0.25$, a mixing of flow particles of high and low temperature are taking place at the location of this secondary motion. As the w/k ratio increases, the secondary motion decreases and the temperature gradient reduces from the wall to the center of the channel.

8.6 TEMPERATURE FLUCTUATIONS

Figure 8–35 shows temperature fluctuations for $k/h = 0.25$ with $w/k = 3, 8, 10, 15$. At the bottom wall the temperature is set to be the hot wall and the top is set to be cold. The average of this temperature is located at the center of the channel. In 8–35 temperature fluctuation are the highest at the top and bottom wall due to

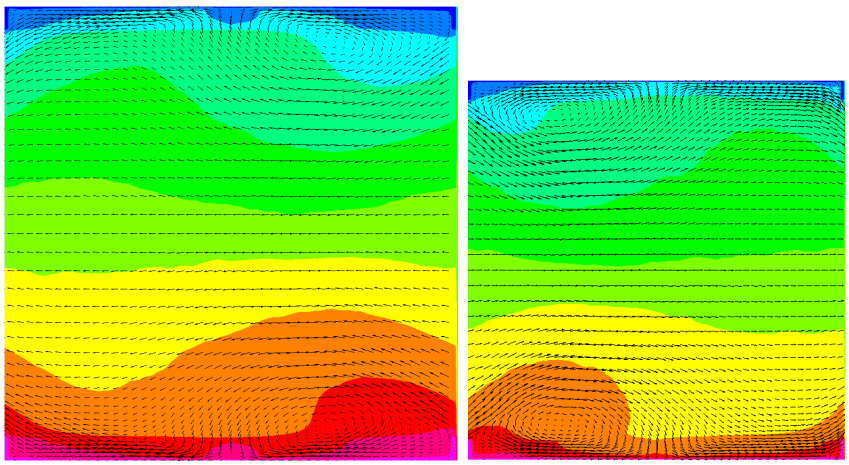

$w/k = 3$ $w/k = 8$

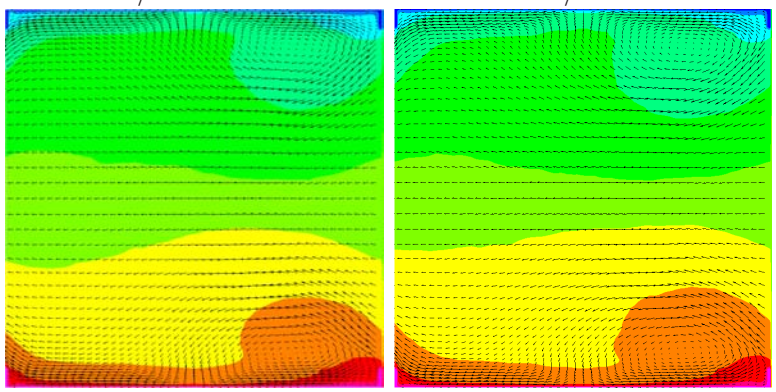

$w/k = 10$ $w/k = 15$

Figure 8–34: Cross sectional view of mean temperature for $k/h = 0.1$, $w/k = 3, 8, 10, 15$

the boundary condition mentioned previously. The center of the channel has the minimum fluctuation since at this location the average temperature can be found. The $w/k = 3$ has the highest temperature fluctuation which is analogous to the high turbulent intensities found for this ratio. At the center of the channel secondary motions reduces, therefore the mechanism that increases the fluctuations of the temperature reduces. As a result of this, the minimum temperature fluctuation is found at the center of the channel.

As the k/h ration reduces the variations of temperature from the average reduces. Figure 8–35 shows the temperature fluctuations for the $k/h = 0.1$ for different ratios of w/k. Similar to the $k/h = 0.25$, temperatures fluctuations have a similar

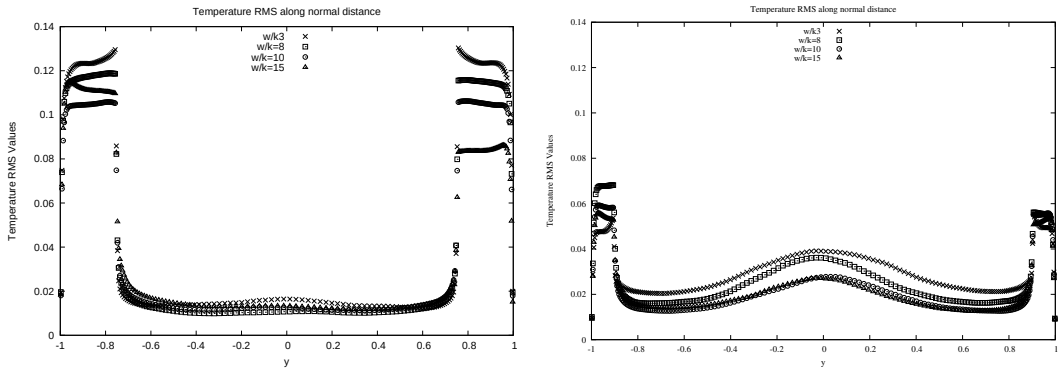

$k/h = 0.25$ $k/h = 0.1$

Figure 8–35: Temperature fluctuations for $k/h = 0.25$ and $k/h = 0.1$ for $w/k = 3, 8, 10, 15$

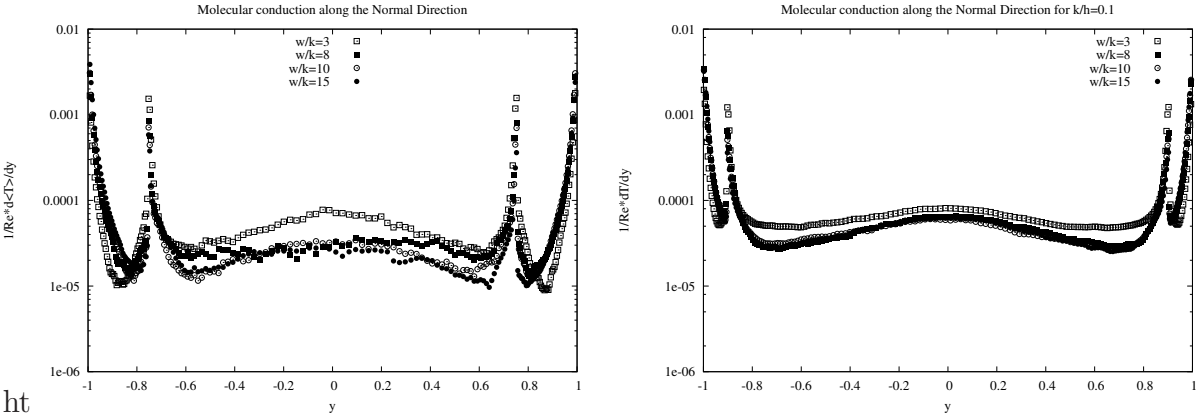

ht

$k/h = 0.25$ $k/h = 0.1$

Figure 8–36: Time averaged molecular heat conduction along the wall normal direction for $k/h = 0.25, 0.1$ for $w/k = 3, 8, 10, 15$

behavior with less intensity. Maximum temperature fluctuation are observed at the top and bottom wall and minimum values are obtained at the center of the channel.

8.7 HEAT TRANSFER

In the mean flow analysis it was observe that different flow transfer mechanism occur in the channel due to the geometrical configuration of the turbulators. The secondary motion have a direct impact over the heat transfer along the channel. This section will discuss the effect of the secondary motion on the convective and conductive elements of the heat transfer.

8.7.1 Molecular Heat Conduction

The average molecular heat conduction is compute according to $(\frac{1}{RePr}\frac{\overline{dT}}{dy})$ (see Incropera (2002) [31]) along the channel. Figure 8–36 shows the distribution for $k/h = 0.1$ and 0.25 for all the w/k ratios. Maximum molecular heat conduction can be observed at walls due to the no slip condition at the near wall region and the temperature gradient between the stagnant fluid and the wall. Minimum values of heat conduction are found at the center of the channel where no surface for conductive heat transfer is available and the convective heat transfer dominates, also at this zone the temperature gradients are small.

A minimum of heat conduction is located inside the cavity formed by the turbulators, between the end wall and the crest plane. This minimum is due to the high secondary motion that increases the convective heat transfer inside the cavity thus reducing the molecular conduction as the primary mean for heat transfer.

At the crest plane of the turbulators the molecular conduction tends to increase due to the no slip condition and high temperature gradient at the top of the turbulators with the mean stream fluid which is mainly in the streamwise direction. Once the distance increases away from the top of the turbulator, the mechanism of conduction reduces to its minimum and the convection dominates.

High conductive heat transfer is found for the $w/k = 3$. In this case for the same distance in the streamwise direction, more turbulators are found. The high surface area of contact with the flow increases the heat transfer in the conductive term. As the w/k ratio increases the molecular conduction decreases for the same Re. This is due to the reduction in the number of turbulators for the same streamwise distance. This reduction decrease the surface area available for conduction, therefore the molecular conduction reduces. In addition, as the w/k ratio increases the fluid that enters in the cavity generates reattachment and the temperature gradient decreases. The secondary motions of the flow with a lower w/k ratio induce high

temperature gradient and as the w/k ratio increases the secondary motion decreases as well as the temperature gradient. Similar results where found by Leonardi et al. (2003) for square bars turbulators, they found that the contribution of $\frac{1}{RePr}\frac{\overline{dT}}{dy}$ to the total heat transfer decreases as the w/k ratio increases.

Comparing $k/h = 0.25$ with $k/h = 0.1$, can be observed that as the turbulators height decreases the molecular conduction at the crest plane decreases due to the decrease in secondary motion as mentioned in previous chapter. The temperature gradient at the crest plane decreases due to the decrease in secondary motion in overall see Figure 8–36. At the location of the cavity higher temperature gradients can be observed. At this area the secondary motions are different for this $k/h = 0.1$ than for $k/h = 0.25$. As showed in the mean flow chapter, the combination of ejections and injections in the middle portion of the cavity (see 8–3Secc.BB) generates a higher temperature gradient for than $k/h = 0.1$ than the spanwise vortex for $k/h = 0.25$. Therefore, higher molecular conduction is obtain with the cavity for the $k/h = 0.1$ ratio. At higher w/k ratios, reattachment of the flow occurs and this reduces the molecular conduction similar to the $k/h = 0.25$.

For both k/h cases at the center of the channel a reduction in the molecular conduction is observed. At this area no geometrical boundaries are located and heat transfer is mainly due to the convection component. Symmetry in the conduction profile is observe due to the symmetry in the geometrical configuration.

8.7.2 Turbulent Heat Flux Along the Normal Direction

As part of the energy equation, the convective term called turbulent heat flux along the wall normal direction (see F. White (2002) [26]) was calculated according to $< Tv >$. Figure 8–37 shows the turbulent heat flux distribution for $k/h = 0.1, 0.25$ for all w/k ratios. For the case of $k/h = 0.25$ minimum values of turbulent heat flux are located at the walls where heat transfer is dominated by the molecular conduction as shown in figure 8–36. Within the cavity the direction of the flow is

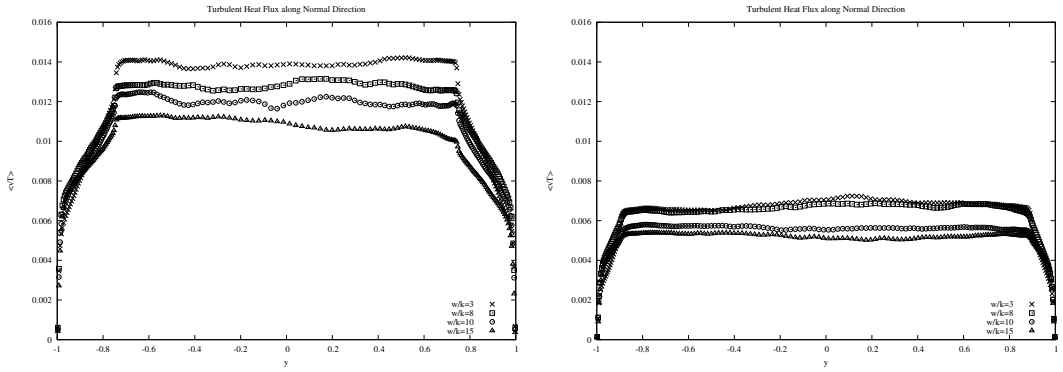

$k/h = 0.25$ $k/h = 0.1$

Figure 8–37: Wall normal time averaged turbulent heat flux along the wall normal direction for $k/h = 0.25$ and $k/h = 0.1$ for $w/k = 3, 8, 10, 15$

redirected into a spanwise motion as mention in the mean flow chapter which reduces the wall normal turbulent heat flux in this area. At the crest plane, an increase of turbulent heat flux begins due to the ejections that occurs at the side walls of the cavity which increases the normal velocity and temperature gradient in this area. Maximum values of turbulent heat flux are located at the center of the channel where molecular conduction is minimum and convection is the dominant component of the heat transfer. A symmetric profile is observed due to the symmetry of the geometrical configuration of the channel and the turbulators. In addition, as shown in the time convergence analysis, the symmetric profile indicates that the system has reached steady state for all w/k ratio. The effect of the separation between ribs shows that as the w/k ratio increases the turbulent heat flux in the normal direction decreases. This effect is related to the reduction in secondary motions due to the increase in the size of the cavity between the turbulators. As mentioned in previous chapter, the reattachment of the flow increases the streamwise velocity which decreases the velocity in other direction due to conservation of momentum. Therefore, wall normal velocity decreases which decreases the wall normal turbulent heat flux.

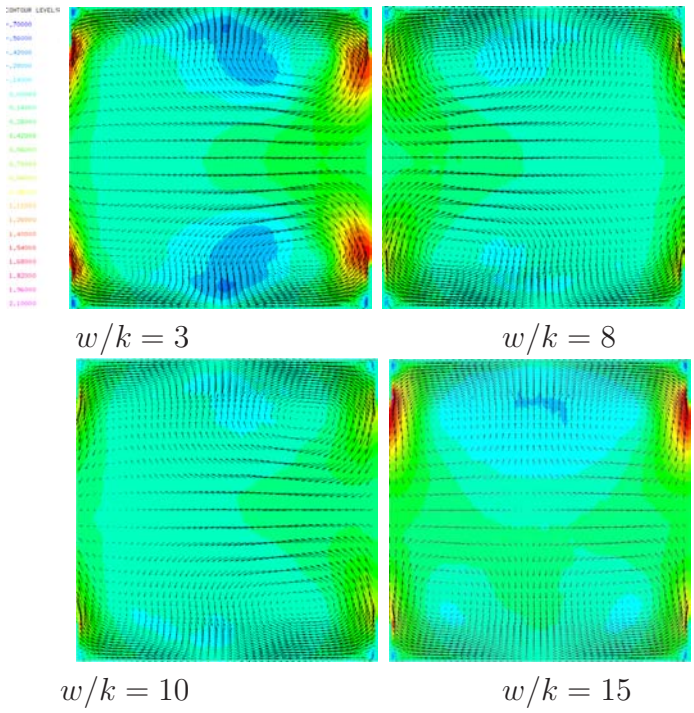

Figure 8–38: Cross Section contour of time averaged wall normal turbulent heat flux along the wall normal direction for $k/h = 0.25$ with $w/k = 3, 8, 10, 15$

A direct relation was found between the turbulent intensities due to secondary motions and the increase in the normal turbulent heat flux in the section. Ejections at the sidewalls generates an interaction of flow particles between the cavity of the turbulators and the streamwise bulk flow. This secondary motion promotes the generation of the large scale vortex (see 8–4 at top of the crest plane which is the mechanism that increase the mixing of flow particles along the streamwise direction.

As the height of the rib reduces to $k/h = 0.1$ a reduction in the turbulent heat flux is observed on figure 8–36. The intensity of the secondary motion reduces which has a direct impact on the turbaned heat flux. Similar profile to $k/h = 0.25$ is observed for this cases and the increase in turbulent heat flux from its minimum to the maximum is achieve at a lower distance normal to the wall as compared with $k/h = 0.25$ due to the reduction in the height of th turbulator. As well as $k/h = 0.25$, the increase in w/k reduces the turbulent heat flux due to the reduction in secondary motion.

This mixing of the flow is reflected in the increase in normal turbulent heat flux at the center of the channel as seen in figure 8–38. Similar secondary motion were found by S.W. Chang et.al (2008) where they state that the enhancements of turbulent and vortical activity and the string cross-stream secondary flow induce by the V-shaped turbulators generate a significant heat transfer augmentation. The increase in w/k reduces intensity of the ejections and large-scale vortices which directly reduces the turbulent heat flux. This mixing is reflected in the increase in turbulent heat flux at the center of the channel presented in figure 8–37. Ejections at the sidewalls present a high intensity value for the turbulent heat flux which indicates that heat transfer is promote by the secondary motion. At the the kink of the V-shape the low intensity color indicates the injection of the flow into the cavity of the turbulators which means that flow particle from the mean stream flow are mixing with high temperature particles enclosed by the cavity of the turbulators. The gradient of the turbulent heat flux in the side wall and at the kink of the V-shape shows that these are the mayor areas of heat transfer in the array of turbulators. Since the increase of w/k reduces the secondary motion in the flow and increases the streamwise velocity due to the reattachment, the wall normal turbulent heat flux reduces. The velocity vectors shows that the secondary motions are maintain for all ratios, but the color contours indicates that the injections and ejections at the mayor areas of the normal turbulent heat flux are reduce. In summary, the increase in the separation of the turbulators reduces the normal turbaned heat flux, but the large-scale vortices are maintain. This indicates that in order to use the large-scale vortices as a mixing tool of flow particles to enhance heat transfer, the ejections and injections must be strong at the side walls and kink of the V-shape.

As the height of the turbulators decreases to $k/h = 0.1$ in figure 8–39, turbulent intensities also decreases thus reducing the mixing of flow particles by means of the large scale vortices. This reduction is directly proportional to the decrease in

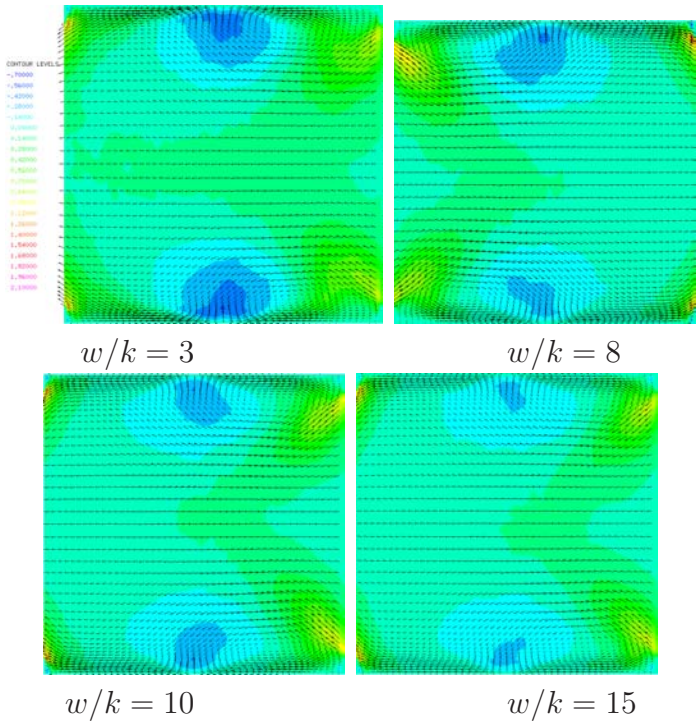

Figure 8–39: Cross section contour of time averaged wall normal turbulent heat flux along the wall normal direction for $k/h = 0.25$ with $w/k = 3, 8, 10, 15$

turbulent heat flux for all w/k ratios at this height. For all w/k ratios, $k/h = 0.25$ configuration produces more heat transfer than $k/h = 0.1$. Turbulent structures are the primarily responsible for the augmentation of the convective heat transfer. The configuration that generates the maximum turbulent heat flux is $w/k = 3$ and $k/h = 0.25$. As the w/k ratio increase the turbulent heat flux decreases for all k/h ratios.

Taking into consideration that at the crest plane of the turbulators is where ejected flow encounters the mean stream flow, the normal turbulent heat flux was calculated for $k/h = 0.25, 0.1$ with all w/k ratios as showed in 8–40. The $k/h = 0.25$ configuration produces more turbulent heat flux than the $k/h = 0.1$. The configuration that generates the maximum heat transfer in $k/h = 0.25$ is $w/k = 3$ due to the high injections and ejections produced. The cavity form by this configuration has the characteristics of enhancing the transference of particles from the center of the cavity to the side wall by a transverse vortex as previously mention in 8–3. The

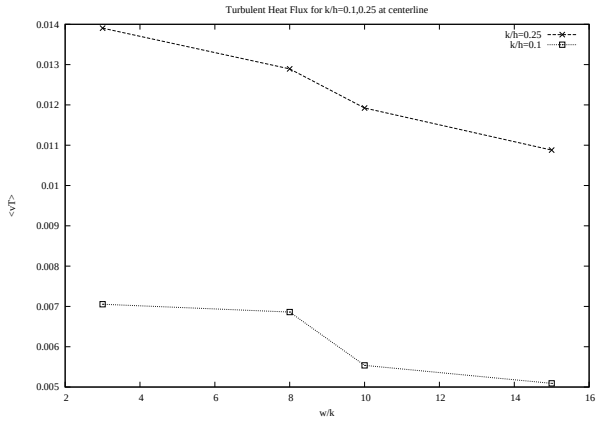

a) b)

Figure 8–40: Turbulent heat flux $k/h = 0.25$ and 0.1 with $w/k = 3, 8, 10, 15$

flow in this configuration is prevented from developing a reattachment and for this reason all the normal spanwise flow change directions only to outward and inward along the cavity. This conservation of momentum in spanwise and normal direction is optimum for producing strong ejections and injections. As the w/k ratio increases the turbulent heat flux decreases for all k/h ratios. In these cases the flow distributes in spanwise, streamwise and normal which reduces the normal velocity of the ejections and injections due to the conservation of momentum. As the w/k ratio increases to its maximum the reattachment of the flow reduces the mechanism that promotes the secondary motion and as a consequence of that the turbulent heat flux is reduced to its minimum.

As a summary of the heat transfer methods mentioned previously, the contribution of the molecular conduction and the turbulent heat flux to the heat transfer at the crest plane are presented in figure 8–41. The total heat flux q is the sum of the molecular heat conduction $\frac{1}{RePr}\frac{\overline{dT}}{dy}$ and the turbulent heat flux $< Tv >$ (S. Pope (2000) [28]). The greater contribution for the total heat flux is due to the turbulent heat flux in the channel since this is the component that promotes the secondary motions in the flow. The total heat flux follows the tendency of the turbulent heat flux and molecular conduction in a descendant behavior as the w/k ratio increases for both k/h ratios. Since the $k/h = 0.25$ ratio shows a higher turbulent heat flux

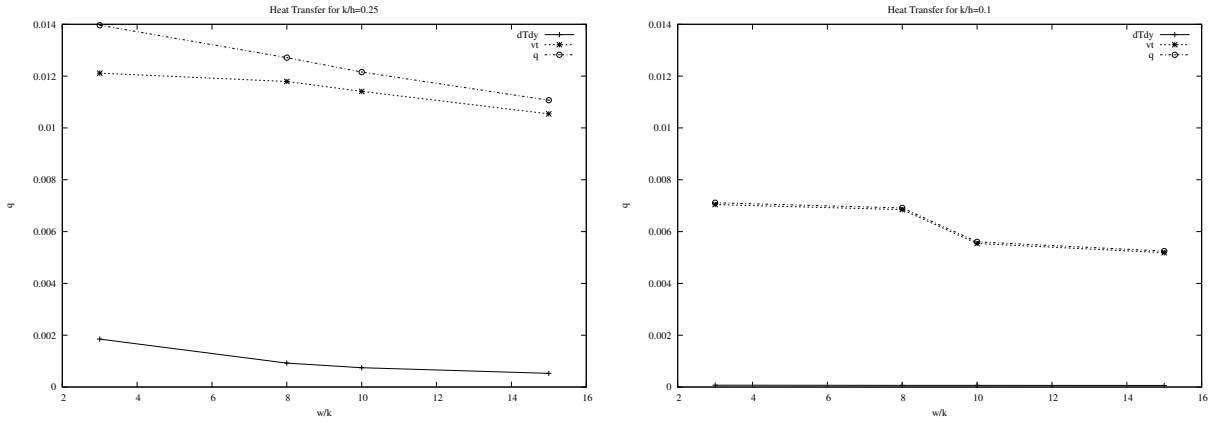

a) b)

Figure 8–41: Total heat flux $k/h = 0.25$ with $w/k = 3, 8, 10, 15$

for all w/k ratios, the total heat flux is maximum for this ratio due to the mechanism previously mentioned.

8.7.3 Spanwise Turbulent Heat Flux Along the Normal Direction

Since spanwise motion is important due to the secondary motions that occurs along the channel, the spanwise turbulent heat flux $< Tw >$ along direction was calculated in figure 8–42 for $k/h = 0.1$ and 0.25 for all w/k ratios. Spanwise vortex located at the cavity of the turbulator (see 8–5.a) increase the spanwise velocity reducing the streamwise velocity due to conservation of momentum. This secondary motion increases the spanwise turbulent heat flux at the cavity of the turbulators. As the w/k ratio increases the transverse vortex generated within the cavity of the turbulators dissipates and streamwise velocity start to increase. This dissipation of the secondary motion reduces the turbulent heat flux in the spanwise directions as shown in figure8–42. For the $k/h = 0.25$, high turbulent heat flux can be observed at the cavity of the turbulators. The height of the turbulators allows this spanwise vortex to develop along the cavity between the turbulators. As the w/k ratio increases the transverse vortex in the cavity of the turbulators reduces, increasing the streamwise velocity. This effects produces a reduction in the turbulent heat flux as the separation between ribs increases. At the center of the channel normal turbulent

heat flux dominates the heat transfer due to the interaction between the ejections at the side walls and the large-scale vortex at top of the crest plane.

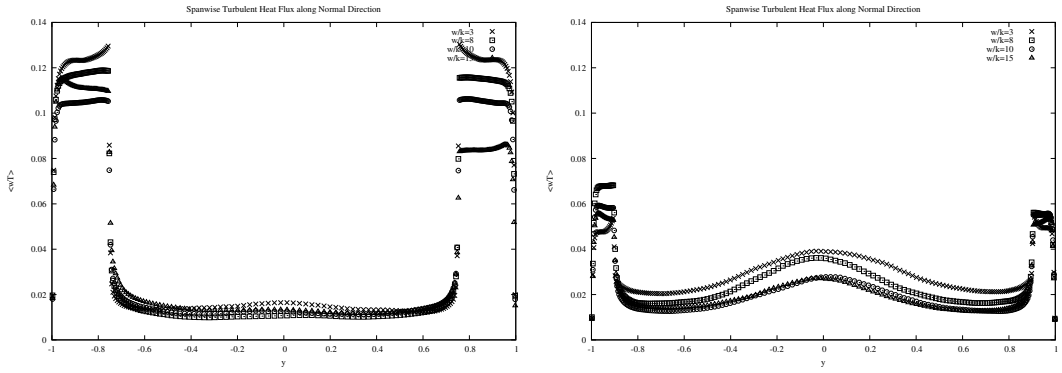

$k/h = 0.25$ $k/h = 0.1$

Figure 8–42: Spanwise time averaged turbulent heat flux along the wall normal direction for $k/h = 0.25$ and $k/h = 0.1$ for $w/k = 3, 8, 10, 15$

In the case of $k/h = 0.1$ in figure8–42, turbulent heat flux has similar behavior to $k/h = 0.25$. Maximum spanwise turbulent heat flux is obtained at the cavity of the turbulator due to the secondary motions. The reduction in the height of the turbulator reduces the intensity of the spanwise transverse vortex and increases the streamwise velocity until reattachment of the flow is obtain. At the center of the channel an increase in the spanwise turbulent heat flux is observed due to spanwise motion of the streamwise large scale transverse vortex. This increase in the spanwise turbulent heat flux reduces as the separation between turbulators is reduced.

8.7.4 Nusselt

The parameter that describes the temperature gradient and provides a measure of the convection heat transfer at the surface is the Nusselt number Nu. The Nusselt number can be describe by the following equation:

$$Nu = \frac{1}{A} \int \frac{d < \overline{T} >}{dy} * da|_{y=0}. \tag{8.3}$$

The Nusselt distribution is calculated along the streamwise direction for the $k/h = 0.25$ for $w/k = 3$ in figure 8–43. Temperature contour shows the variation of

temperature along a wavelength distance λ. The Nusselt number shows an increase at the leading edge of the turbulator. This effect is due to the variation of temperature of the crest plane with the mean stream flow temperature. This represents the maximum value of temperature gradient. As the streamwise direction increases, the Nusselt number decreases as shown in Secc CC where the decrease from the maximum value to the minimum is found in the transition of the crest plane and the trailing edge of the turbulator. The secondary motions previously discussed in the mean flow chapters shows a recirculation zone at the trailing edge of the turbulator. The vortex formed in this area maintains the temperature at the lower gradient possible which is the mechanism that decreases the Nusselt number. As the streamwise velocity starts to increase, the temperature gradient increases. The dissipation of the recirculation zone as the streamwise direction increases produces an increase in the temperature gradient which produces the increase in the Nusselt number. As the streamwise direction reaches the leading edge of the following turbulator the temperature gradient drops and raises to the maximum value. This drop in the Nusselt number is due to the stagnation point at the at the leading edge of the turbulator which produces a reduction in the temperature gradient. After the leading edge, a raise in the Nusselt number is obtain due to the interaction of the mean stream flow with the crest plane.

As the spanwise direction increases, different behavior in the Nusselt number is observe in section BB in figure 8–43. Similar effect is obtain at the crest plane of the turbulator with respect to section BB. At this location the maximum temperature gradient is observe due to the interaction with mean flow. At the cavity of the turbulator, the spanwise vortex mentioned in previous chapters maintains the temperature constant along the streamwise direction. As the streamwise direction increases, a higher temperature gradient is obtain which increases the value of the Nusselt number. For this ratio a sudden drop of the Nusselt number is not present.

This is due to the transport of fluid particles with different temperature from the center of the cavity to the side walls. This transport increases of the spanwise direction and this effect increases the Nusselt number. At the leading edge of the turbulator the temperature gradient increases due to the interaction with the mean flow.

At the location of the side wall in section AA, similar effect occurs at the crest plane of the turbulator with respect to BB and CC sections. The cavity of the turbulators shows different behavior in the temperature gradient. In the temperature contour for section AA, high intensity color increases around the turbulators. The ejections of flow particles into the main stream flow produces an increase in temperature gradient. As mentioned in the heat transfer chapter, ejections promote the heat transfer on the turbulators which has a direct effect in the temperature gradient at this location. An oscillatory motion shows the transition of the increment in temperature gradient until ejections occurs. The Nusselt number on the cavity of the turbulator is higher in section AA due to the effect of secondary motions. At the streamwise distance increase to the leading edge a constant behavior of Nusselt is obtained. At the crest plane of the turbulator the maximum value of Nusselt number is obtain due to the interaction with the mean stream flow.

The increase in the w/k ratio produces different effects in the Nusselt number distribution for 8–44. In section CC the increase in the Nusselt number is similar to the $w/k = 3$. At the cavity of the turbulators the dissipation of the spanwise vortex and the increase in the streamwise velocity due to reattachment of generates high temperature gradient at the wall as shown in section CC. At the trailing edge of the turbulator low temperature gradients are obtained due to the recirculation. As the streamwise direction increases, an increase in the temperature gradient is obtain due to the dissipation of the spanwise vortex producing a local maximum in the channel. This value at the center of the channel deceases as the streamwise

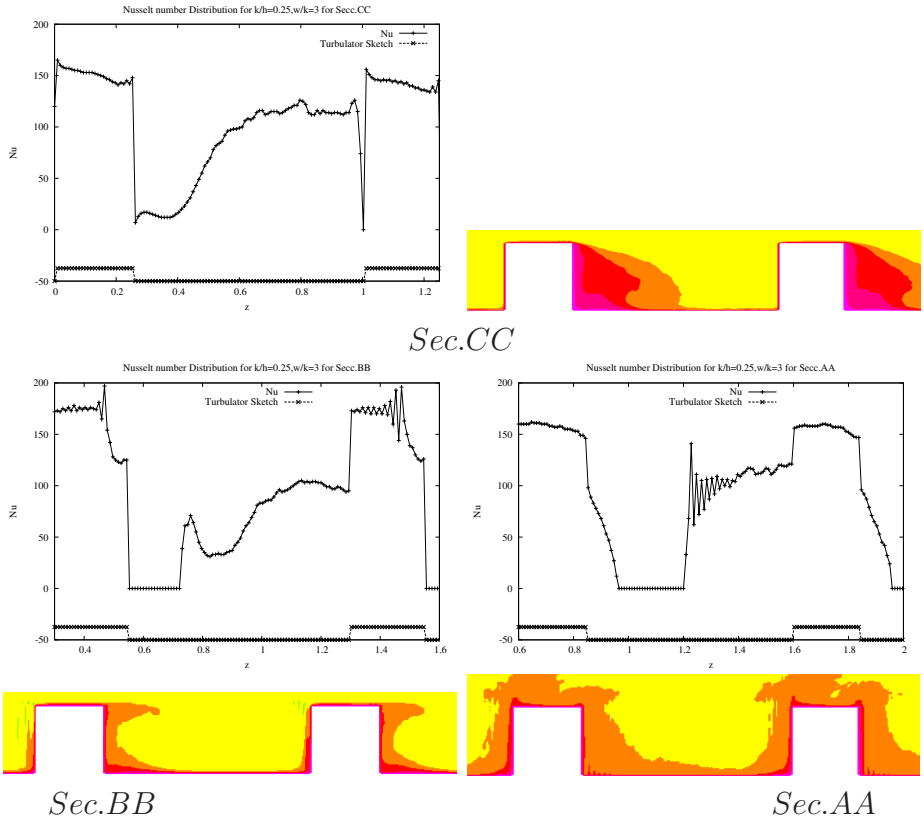

Figure 8–43: Skin frictional drag distribution and streamwise velocity contours along streamwise direction for $k/h = 0.25$ and $w/k = 3$.

distance increases. At the leading edge of the next turbulator an increase of the Nusselt number is obtain due to the interaction with mean stream flow. This effect is similar to the Nusselt number for the $w/k = 3$ ratio.

As the spanwise distance increases to section BB the Nusselt number within the cavity of the turbulators decreases. The temperature contour in section BB shows the effect of the recirculation at the trailing edge of the turbulator. At this area the temperature gradient decreases which decreases the Nusselt number. At the streamwise distance increases the variations in temperature increases which increases the Nusselt number. This increase in the variation of temperature is due to the reattachment of the flow within the cavity of the turbulators. After the increase in the Nusselt number, a continuous decrease is showed in section BB until the next turbulators appears. At the leading edge of the turbulators an increase in the

temperature gradient is obtain which increases the Nusselt number. This increase is due to the interaction with the mean stream flow similar to $w/k = 3$

The behavior in the Nusselt distribution for section AA is similar to section BB. At section AA ejections occurs at the side walls of the channel. This produces increases in the Nusselt number within the cavity after the trailing edge. Similar values of Nusselt number are obtain as compared with $w/k = 3$, but different distribution. In the case of $w/k = 8$, the increase in the w/k ratio produces a decrease in the intensity of the ejections as mentioned previously in the mean flow chapter. This decrease reduces the heat transfer in the cavity, but ejections still strong in order to generate a Nusselt number close to the $w/k = 3$ values. For the case of $w/k = 3$, an oscillatory transition was observe until a peak value was obtained within the cavity of the turbulator. In the case of $w/k = 8$, no oscillations are observed, but instead a more sudden increase in the Nusselt number. This peak in the cavity is followed by a continous decrease of the temperature gradient until the leading edge of the following turbulator is reached.

As the w/k ratio increases to $w/k = 10, 15$ in figure 8–45 and 8–46 similar behavior is observed with respect to $w/k = 8$. At the crest plane of the turbulators in section CC, $w/k = 10, 15$ present the same constant behavior due to the interactions with the means stream stream flow and its value reduces as the flow interns the cavity of the turbulators. As mentioned in the mean flow chapter, the injection of the flow into the cavity of the turbulator becomes independent of the w/k ratio as it increases. This effects produces similarities of the Nusselt number for this ratios since the secondary motions are the mechanism that enhance the heat transfer. The recirculate zone produces a reduction of the Nusselt number at the trailing edge of the turbulator. This effect is followed by an increase in the temperature gradient after the recirculation zone due to the reattachment of the flow.

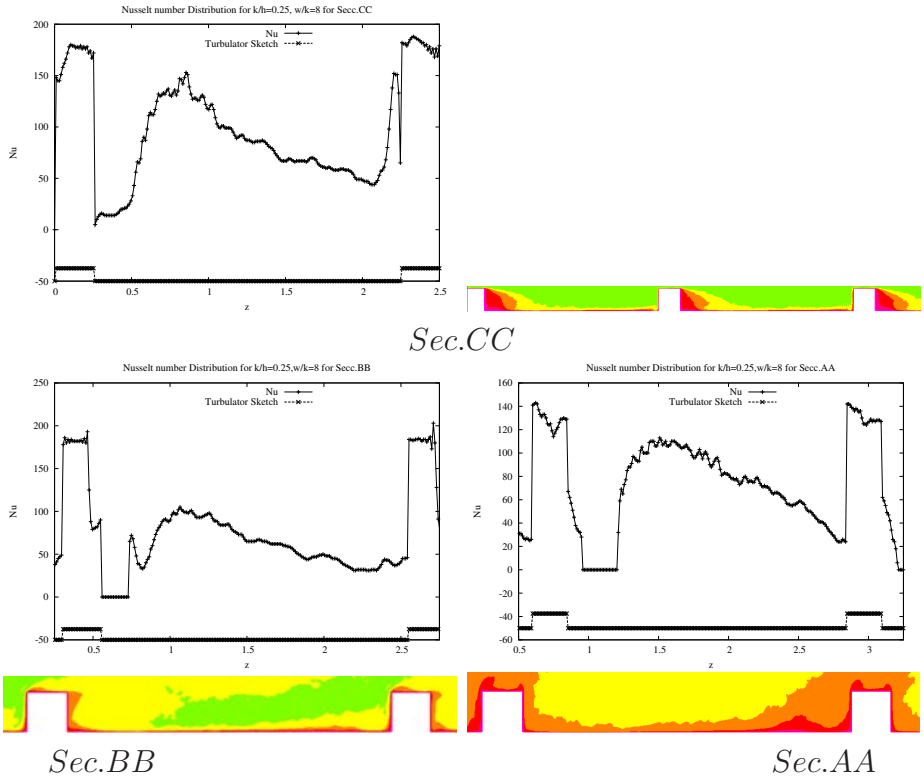

Figure 8–44: Skin frictional drag distribution and streamwise velocity contours along streamwise direction for $k/h = 0.25$ and $w/k = 8$.

An oscillatory transition of the maximum value for the Nusselt number at the crest plane is observe in Section BB of 8–45 and 8–46. As the streamwise distance increase, the spanwise vortex dissipates and is substitute for an ejection/injection motion at the trailing edge of the turbulators. This secondary motion produces the oscillatory motions of the transition from the crest plane to the cavity. As the streamwise distance increases Nusselt number increases similar to the $w/k = 8$ and decreases it reaches the leading edge of the next turbulator.

The reduction of the oscillatory transition is reduced as the spanwise distance increases until it reaches the side walls in section AA. At this location an increase in the Nusselt number within the cavity of the turbulator is observed in figure 8–45 and 8–46. For high w/k ratios the intensity of the ejections decreases, but the interaction of the side walls and ejection flow produces high temperature gradient in

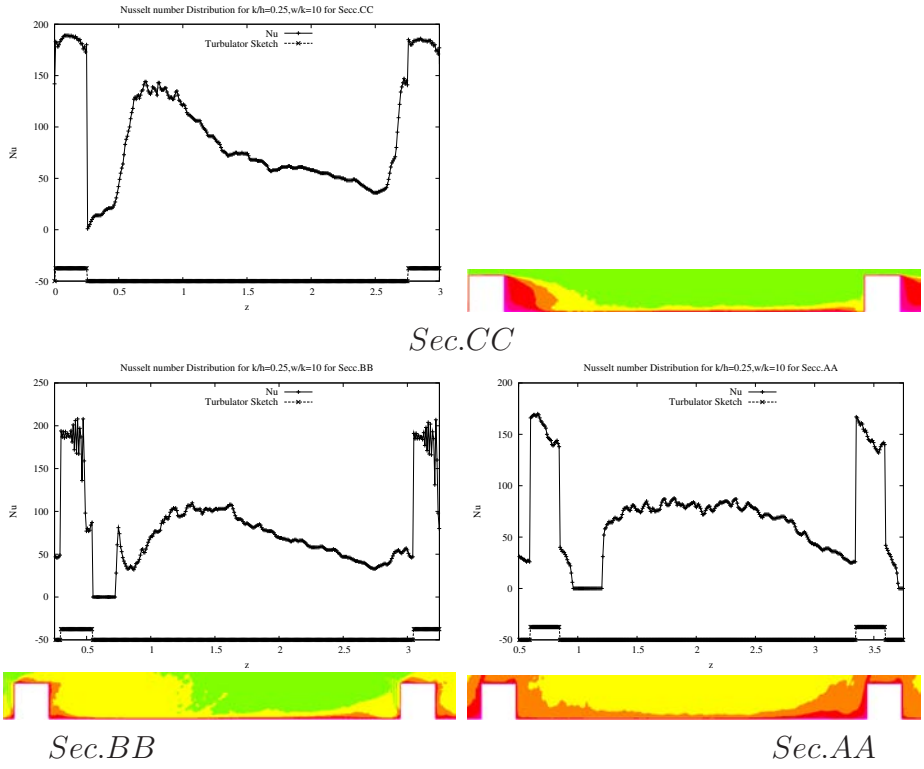

Figure 8–45: Skin frictional drag distribution and streamwise velocity contours along streamwise direction for $k/h = 0.25$ and $w/k = 8$.

the cavity of the turbulators which decreases as the streamwise direction increases. This behavior is characteristic in previous w/k ratios of $k/h = 0.25$

8.8 AUGMENTATION

It has been demonstrated that the secondary motions are the mechanisms that promotes heat transfer. The advantages of the geometrical configuration of the V-shape turbulators allows additional features on the channel which makes it a reliable candidate for a heat transfer enhancement. In order to obtain a quantitative evaluation on the augmentation of the V-shape turbulators against another type of geometrical configuration, an analysis of the augmentation of total heat flux is calculated for the smooth wall and square bars turbulators.

As previously mentioned, Direct Numerical Simulations of the channel flow with smooth walls were performed as a preliminary study to understand the dynamics of the flow before introducing a rough wall. Turbulent heat flux and molecular

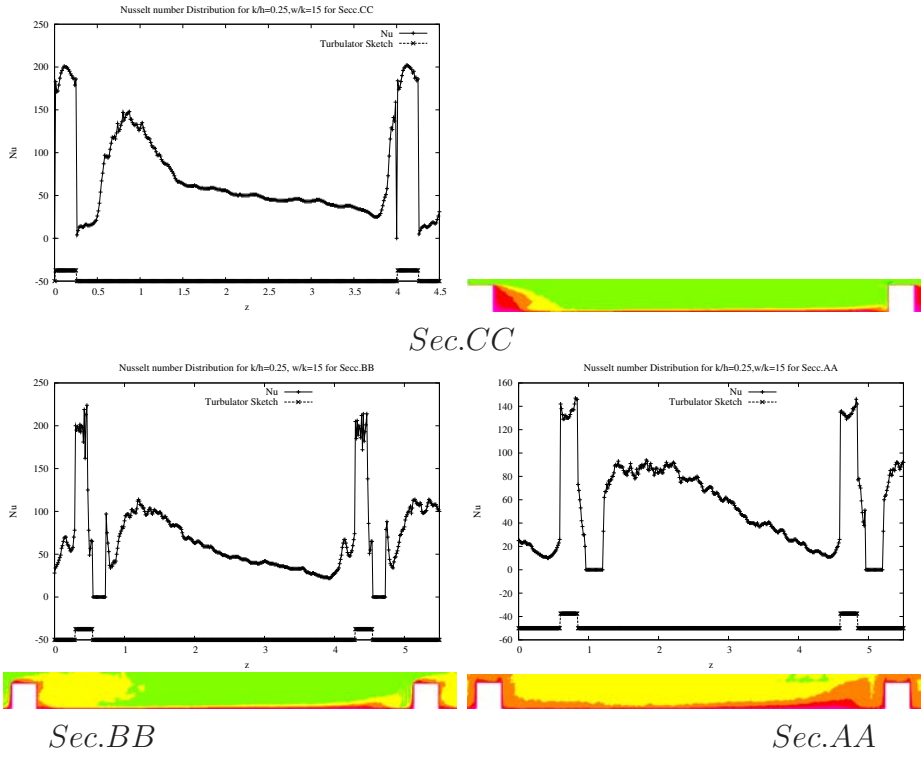

Figure 8–46: Skin frictional drag distribution and streamwise velocity contours along streamwise direction for $k/h = 0.25$ and $w/k = 8$.

conduction where calculated for the channel flow to compared with the V-shape turbulators.

The augmentation of total heat flux of the V-shape turbulators against the channel flow is showed in figure 8–47. From $k/h = 0.25$ can be observe that the augmentation in terms of heat transfer rise up to 7 times the channel flow for $w/k = 3$ which in the previous chapters shows the more intense secondary motions. As the w/k increases the augmentation with respect to the channel flow decreases which follows the behavior of the heat flux for the V-shape turbulators. For the lowest augmentation of the heat flux it can be shows that even up to 5.6 times in augmentation is obtain for higher values of pitch to height ratio.

In terms of the $k/h = 0.1$, augmentations of 3.3 are observed for small pitch to height ratios which still a significant enhancement against the smooth wall. As the w/k ratio increases the augmentation decreases which is the trend observed in the

ht

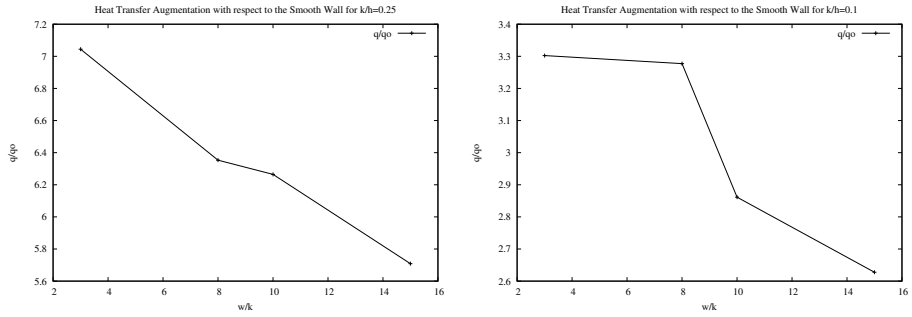

$k/h = 0.25$ $k/h = 0.1$

Figure 8–47: Total heat flux augmentation with respect to the channel flow for $k/h = 0.25, 0.1$ for $w/k = 3, 8, 10, 15$

ht

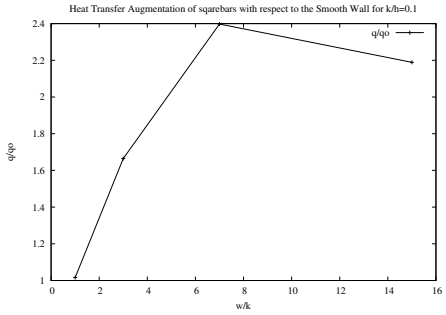

Figure 8–48: Total heat flux augmentation with respect to the channel flow for $k/h = 0.25, 0.1$ for $w/k = 3, 8, 10, 15$

heat transfer chapter for the heat flux. For lower ratios up to 2.6 in augmentation against the smooth wall was obtained.

In order to compare with other type of roughness, augmentation analysis was performed for square bar roughness which where previously study. Figure **??** shows the total heat flux for square bar roughness with $k/h = 0.1$ for $w/k = 1, 3, 7, 15$. Augmentation values of 2.4 are found for $w/k = 7$ which is the configuration that produces the maximum heat transfer as found in the square bars chapter. In the lower range, augmentation of 1.2 are found for $w/k = 1$ which is the configuration closest to the smooth wall. In overall, the square bars produces and increase in the total heat flux for a maximum of 2.1 which makes it a candidate for an effective heat transfer enhancement configuration.

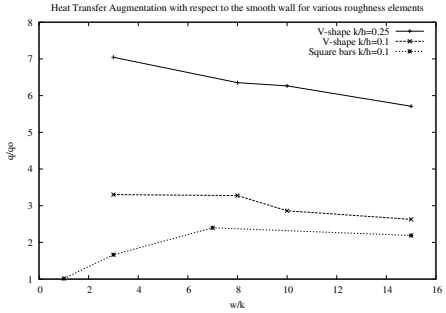

ht

Figure 8–49: Total heat flux augmentation with respect to the channel flow for Square bars and V-shaped turbulators

The combination of all the plots together is showed in figure 8–49. In overall, V-shaped turbulators produce more augmentation with respect to the smooth wall than the square bars turbulators. For the parameters under study the configuration that has the maximum augmentation is $k/h = 0.25$ for all ratios of w/k with a peak for $w/k = 3$. As the w/k is reduced the augmentation reduces which follows the same behavior of the turbulent heat flux. For the case of square bars a peak in augmentation is reached at $w/k = 7$ for $k/h = 0.1$ which follows a different behavior than the V-shape. In the comparison of the V-shaped and square bars turbulators for the same $k/h = 0.1$, it is shown that the angle of the turbulators provides the flow characteristics necessary to enhance the heat transfer at a greater scale than a transverse square bar. The advantage of the angle from V-shape turbulator produces secondary motion that are not present in the square bar turbulator, which makes the V-shaped turbulator the optimum design for total heat flux augmentation.

CHAPTER 9
CONCLUSION

Numerical results show that V-shape square ribs are more efficient than square ribs in maximizing the heat transfer. The increase in the heat transfer is due to a secondary motion which is generated by the V-shape turbulators. The transverse vortex generated in the cavity of the turbulator transports the heat along the spanwise direction creating a temperature gradient at the top and bottom wall. Due to continuity, at the location of the side wall the flow is ejected into the mean stream. Ejections at the location of the sidewalls transport the heat out of the cavity of the turbulators to the crest plane increasing the normal velocity (see. Fig. 8–4). The interaction between the ejected flow and the mean stream at the center of the channel generates two counter rotating which are extended through the streamwise direction as shown in Fig. 8–4. The effects produced on the mean flow analysis promotes the generation of flow structure which have a direct effect of the heat transfer.

These secondary motions produces high temperature gradient at the side walls of the cavity which is reflected on the turbulent intensities of the temperature. In the normal direction, ejections produces increases in the RMS values of the velocities at the location of the side walls. Due to continuity fluctuation along the normal directions produces fluctuations along the streamwise direction which are related with the generation of the large scale vortices at the top of the crest plane. These large scale vortex increase in the mixing of flow particles along the streamwise direction removing hot particles from the cavity to the center of the channel. The

combination of the ejections and large scale vortices is the mechanism that enhance the heat transfer of the turbulators.

Increases of the w/k ratio reduces the generation of secondary motion. Weaker ejections and reattachment of the flow reduces the mixing of flow particles reducing the heat transfer in the channel. As the w/k distance increases, longer reattachment zones are obtained and back flow at the sidewalls are produced. Smaller w/k ratios confines the flow in a region where the transport of flow particles is produce by other directions than than the streamwise.

As compared with square bar turbulators, the angle of the Vshaped turbulator is a key element to produce mixing of the flow in different direction. Higher velocity gradients in all directions where obtained with an angle in the geometry which produces a non-uniform spanwise velocity as compared with the transverse square bars. Side wall ejections is not observed in transverse square bars due to the lack of an angle that redirects the flow. Once again the redirection of the flow into two spanwise streams is a key factor that promotes secondary motions in the flow.

Different sections in the spanwise direction where analyze to the study the changes in velocity and temperature.The interactions of the flow at the crest plane of the turbulators produced the highest velocity and temperature gradient. At this locations the highest Nusselt number and skin friction coefficient where obtained due to the interaction of the ejected flow and the mean stream flow at the center of the channel.

The augmentation of the total heat flux with respect to the smooth wall is an important factor to compared the total heat transfer with other type of roughness. For all the V-shaped turbulators configuration, higher augmentations where obtain as compared with the transverse square bars. The configuration that generates the

maximum total heat flux is $w/k = 3$ for $k/h = 0.25$. The high values of augmentation for the V-shaped turbulators and the comparison with other roughness types identifies this system the optimum configuration that enhances the heat transfer.

APPENDICES

APPENDIX A
STATISTICAL CONVERGENCE

A.1 Turbulent Heat Flux Convergence for k/h=0.25

A time convergence analysis of the turbulent heat flux $< vT >$ was performed in order to analyze the variations of the solutions in time until a steady state of the energy equation was obtained. For the case of $k/h = 0.25$ the convergence for the w/k cases is presented in figure A–1. Statistical average of various set of times (around $40 - 50$ times) show the history of the solution as it approaches steady state. Due to the symmetry of the geometry, a symmetry in the distribution of the turbulent heat flux is expected as the solution reaches steady state. In Fig A–1 the $w/k = 15$ ratio achieve convergence for the last range of time. For this ratio the solution of previous times shows a non-symmetric configuration. As the simulation time increases, the solution stabilize until an increase the results does not showed a significant difference in the results. In addition, the plot for the complete set of time (dash line) is not symmetric because the variations of the previous sets of time are large. For the other cases of w/k, the fluctuations in time are not as large as in the $w/k = 15$ and the average of all times can be used.

A.2 Turbulent Heat Flux Convergence for k/h=0.1

Turbulent flux convergence plots are presented in Fig A–2 for $k/h = 0.1$. High fluctuations in time for $w/k = 3, 8, 10$ proves that convergence has not been achieved and more simulations are required. The high jumps of the plots in time indicates that the system is far from convergence for these ratios. In the case of the $w/k = 15$, fluctuations of the latest times are approaching a convergence. This is consistent

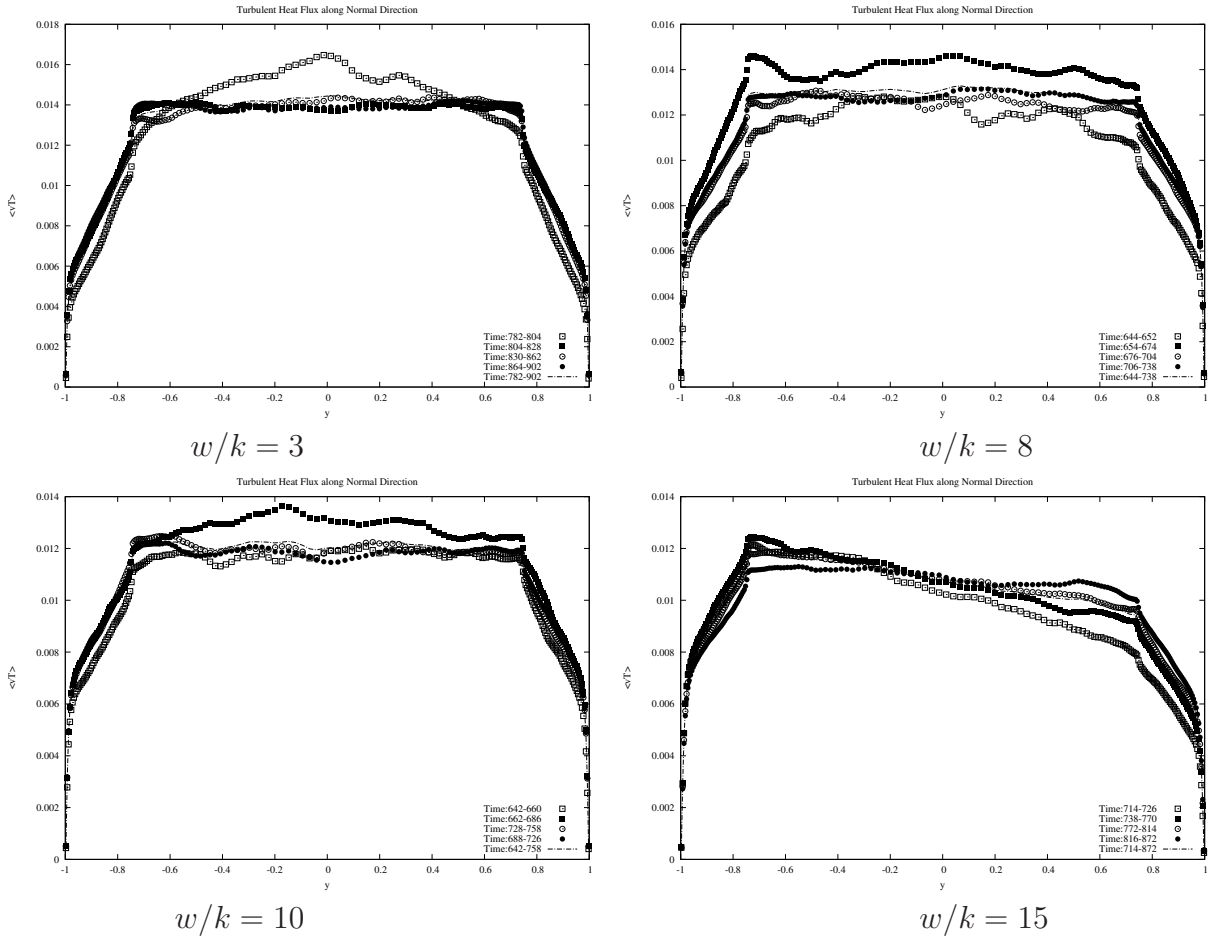

Figure A–1: Turbulent Heat flux for all ratios of w/k all ratios of $k/h = 0.25$ with the symmetry found in the velocity contours for the ratios $k/h = 0.25$. This configuration (w/k=15) seems to be the more stable for both k/h ratios in terms of symmetry of the velocity contours.

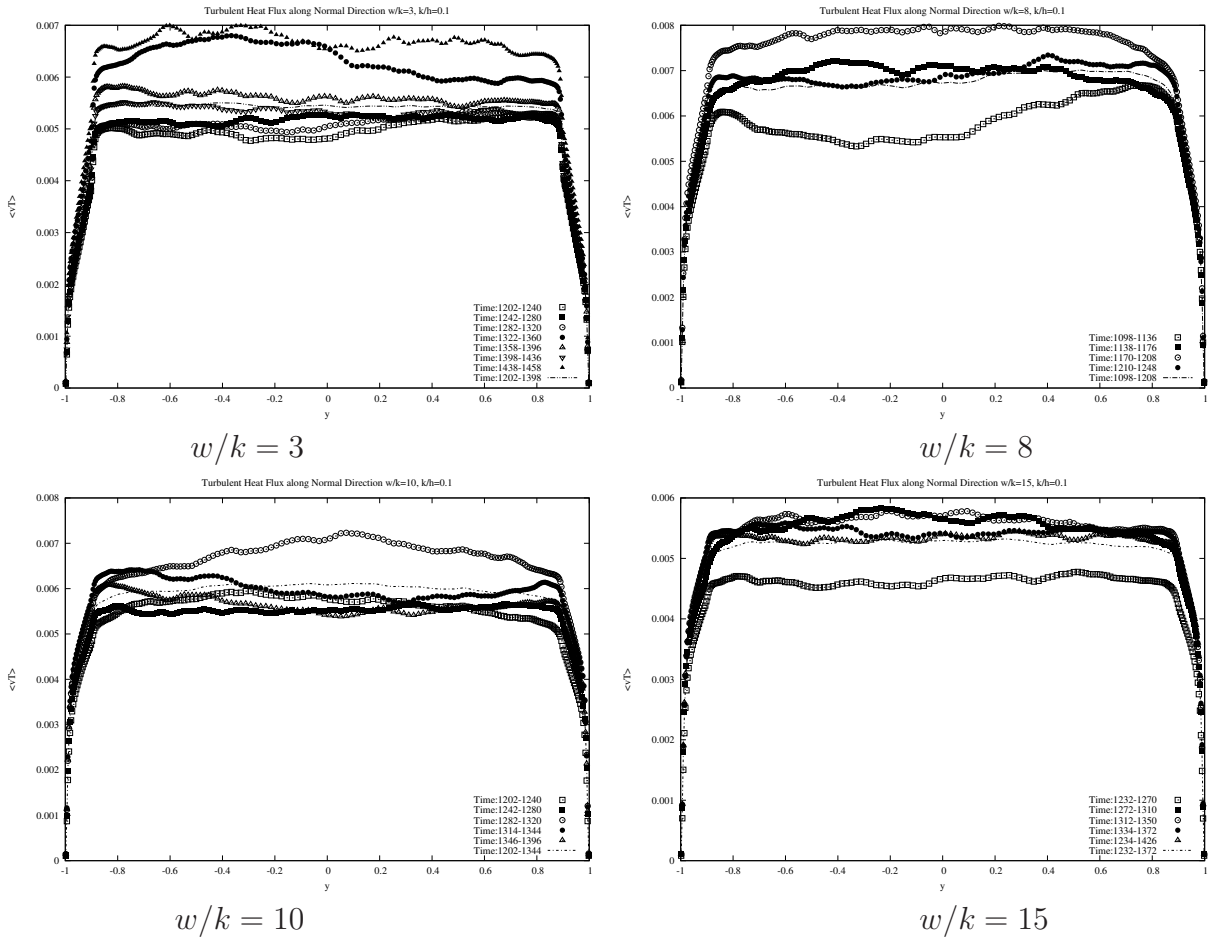

Figure A–2: Turbulent Heat flux for all ratios of w/k all ratios of $k/h = 0.1$

REFERENCE LIST

[1] Han J.C., Dutta S., and Ekkad S. *Gas Turbine Heat Transfer and Cooling Technology.* Taylor and Francis, 2000.

[2] Y. Furuya and H. Fujita. Turbulent boundary layers on wire-screen roughness. *Bulletin of JSME*, 37:77–86, 1967.

[3] A.E. Perry and P.N Joubert. Rough-wall boundary layers in adverse pressure gradients. *J. Fluid Mech*, 17:193–211, 1963.

[4] F.A. Dvorak. Calculations of turbulent boundary layers on rough surfaces in pressure gradient. *AIAA Journal*, Vol. 7, No.9:1752–1759, 1969.

[5] P.R. Bandyopadhyay and R.D. Watson. Structure of rough-wall turbulent boundary layers. *Phys. Fluids*, 31 (7):1877–1883, 1988.

[6] Miyake Y., Tsujimoto K., and Nakaji M. Direct numerical simulation of a rough–wall heat transfer in a turbulent channel flow. *J. Heat Fluid Flow*, 22:237–244, 2001.

[7] L. Wang, M.M.J.F Verbeek, S.S. Burgers, and B. Sudén. Experimental investigacion of flow fields in a square channel roughned with various ribs on one wall. *2006 ASME International Mechanical Engineering Congress and Exposition Novemner 5-10, Chicago, Illinous, USA*, 2006.

[8] Orlandi P. and Leonardi S. (2006). Dns of turbulent channel flows with two- and three-dimensional roughness. *Journal of Turbulence*, 7, 2006.

[9] Leonardi S., Orlandi P., and R.A. Antonia. Heat transfer in a turbulent channel flow with roughness. *5th International Symposium on Turbulence and Shear Flow PhenomenaTU Munich 2729 August 2007.*, 2007.

[10] A. Ashrafian, H. Andersson, and M. Manhart. Dns of turbulent flow in a rod-roughened channel. *Int. J. Heat and Fluid Flow*, 25:373–383, 2004.

[11] Leonardi S., P. Orlandi, Smalley R.J., Djenidi L., and Antonia R.A. Direct numerical simulations of turbulent channel flow with transverse square bars on one wall. *J. Fluid Mech.*, 491:229–238, 2003.

[12] Mittal M.K., Varun Saini R.P., and Singal S.K. Effectvie efficiency of solar air heaters having different type of roughness elements on the absorber plate. *Energy*, 32(5):739–745, 2007.

[13] K. Kim and Y.Lee. Design optimization of internal cooling passage with v-shaped ribs. *Numerical Heat Transfer, Part A*, 51:1103–1118, 2007.

[14] Han J.C., Zhang Y.M., and Lee C.P. Augmented heat transfer in square channels with parallel, crossed, and v-shaped angled ribs. *ASME J. Heat Trans.*, 113(3):590–596, 1991.

[15] Choi C., Rhee D.H., and Cho H.H. Heat/mass trasnfer and pressure drop in a square duct with v-shaped ribs. *Trans KSME B*, 26(11):1542–1551, 2002.

[16] D.H. Lee, D.-H. Rhee, K.M. Kim, H.H. Cho, and H.K Moon. Detailed measurement of heat/mass transfer with continous and multiple v-shaped ribs in rectangular channel. *J. Energy*, 34 (11):1770–1778, 2009.

[17] R. Jia and M. Faghri B. Sudén. Computational analysis of heat transfer enhancement in square ducts with v-shaped ribs: Turbine blade cooling. *J. Heat Transfer*, 127:425–433, 2005.

[18] S.W. Chang, T.-M. Liou, K.F Chiang, and G.F. Hong. Heat transfer and pressure drop in rectangular channel with compound roughness of v-shaped ribs and dependent scales. *Internat. J. Heat and Mass Transfer*, 51:457–468, 2008.

[19] S. Gavrilakis. Numerical simulation of low-reynolds-number turbulent flow through a straight square duct. *J. Fluid Mech.*, 244:101–129, 1992.

[20] A. Huser and S. Birigen. Direct numerical simulation of turbulent flow in a square duct. *J. Fluid Mech.*, 257:95–95, 1993.

[21] R.F. Blackwelder and R.E. Kaplan. On the wall of the turbulent boundary layer. *J. Fluid Mech.*, 76:89–112, 1976.

[22] P.Moin and J. Kim. The structure of the vorticity field in turbulent channel flow. part1. analysis of instantaneous fields and statistical correlations. *J. Fluid Mech*, 155:441–464, 1985.

[23] J. Jeong and F. Hussain. On the identification of a vortex. *J. Fluid Mech.*, 285:69–94, 1995.

[24] Orlandi P. *Fluid flow phenomena, a numerical toolkit.* Kluwer Academic Publishers, 2000.

[25] Fadlun E. A., R. Verzicco, Orlandi P., and Mohd-Yusof J. Combined immersed boundary finite-difference methods for three-dimensional complex flow simulations. *J. Comput. Phys.*, 161:3560, 2000.

[26] Frank M. White. *Viscous Fluid Flow.* McGraw-Hill, Inc., 2nd edition, 1991.

[27] H.T. Kim, S.J. Kline, and W.C. Reynolds. The production of turbulence near a smooth wall in a turbulent boundary layer. *J. Fluid Mech.*, 50:133–160, 1971.

[28] Stephen B. Pope. *Turbulent Flows.* Cambridge University Press, 1st edition, 2000.

[29] Munson B. R., D. F. Young, and Okiishi T. H. *Fundamentals of Fluid Mechanics.* John Wiley and Sons, Inc., 2002.

[30] Pijush K. Kundu. *Fluid Mechanics.* Academic Press, 1990.

[31] F. P. Incropera and DeWitt D. P. *Fundamentals of Heat and Mass Transfer.* John Wiley and Sons, Inc., 2002.

DIRECT NUMERICAL SIMULATION OF TURBULENT CHANNEL FLOW WITH V-SHAPE TURBULATORS

Jaime A. Toro Medina
(787) 235-9757
Department of Mechanical Engineering
Chair: Stefano Leonardi
Degree: Master of Science
Graduation Date: May 2010